Characterization of Fibre Reinforcements for Non-structural Composite Parts

by

Yousef Badripour

Thesis submitted to the
Faculty of Graduate and Postdoctoral Studies
In partial fulfillment of the requirements
For the M.A.Sc. degree in
Mechanical Engineering

Department of Mechanical Engineering
Faculty of Engineering
University of Ottawa

Abstract

Fibre reinforced composite materials have attracted attention from industry and academia due to their high specific stiffness and strength. Commonly used manufacturing processes include the Liquid Composite Moulding (LCM) group of processes, where a liquid polymer resin impregnates a dry preform that is prepared in advance. The consistency of the resin infusion process and properties of the final composite are highly dependent on preform quality and reproducibility. Preform quality, in turn, depends on a process called draping. This work aims at understanding and developing quantitative knowledge of key elements of reinforcement behaviour during preforming.

Testing characterization methods for dry fabrics are introduced and discussed. Moreover, the thesis probes relations between fabric properties such as their architecture and fibre type, and elements of their draping and preforming behaviour such as bending stiffness and in-plane shear properties of the dry fabrics.

Most materials used in this work were selected by the industrial partner, Hutchinson Aerospace and Industry, based in Montreal. Some experiments were conducted using Hutchinson's characterization devices, which are introduced in the relevant chapters.

Table of contents

List of figures

List of tables

Acknowledgements

I would like to thank my thesis supervisor, Dr. François Robitaille for giving me guidance with my research, passing his invaluable knowledge to me and challenging my writing skills throughout my master's program.

I would like to express my gratitude to my father, who has supported me throughout thick and thin and has always encouraged me to develop myself.

I would like to thank Sébastien Gagné and Hutchinson for giving me the opportunity to experience ongoing research and development of composite materials conducted by industry. Much appreciation goes to Louis Grou and Corentin Rannou at Hutchinson for their cooperation.

I would like to thank my colleagues in our office in Colonel By at the University of Ottawa, specially Mohmmad Rafiee for helping me with all my questions. I would also like to thank Mohammed Yandouzi for his assistance with the digital microscope.

Chapter 1

Introduction

1.1 Background

Polymer matrix composite materials have become mainstream choices for many applications in the automotive and aerospace sectors. Notable improvements were achieved in terms of mechanical, thermal and electrical properties amongst others. Major reductions in weight probably constitute a major advantage of composite materials, especially when it comes to aircrafts. Higher Young's modulus, larger number of cycles during the lifetime of a structural part, significantly higher fatigue resistance and higher corrosion resistance are other important benefits that composites have enabled [1,2]. Although numerous metallic alloys are available, there are limitations to conducting smart design when using metals. Ongoing research is being devoted to the replacement of metallic alloys with materials showing better performance. As a result, composite parts are being manufactured as a superior alternative to metallic parts in order to obtain higher specific strengths and stiffnesses.

The preforming of fibre reinforcements is a critical operation in out-of-autoclave composite manufacturing processes. Reducing defects in the final parts, implementing faster processes,

reducing handling operations of dry fabrics as well as lowering manufacturing costs cannot be achieved without a clear understanding and a capability for prediction of the preforming process as it is done in industrial settings. Different parameters affect this influential process such as fabric type (carbon, glass etc.), fabric architecture (plain, twill, satin etc.), fabric properties (shear, flexural stiffness, springback etc.), mould geometry, and the composite manufacturing process used, such as vacuum assisted resin transfer moulding (VARTM), resin transfer moulding (RTM) and resin film infusion (RFI). Figures 1.1 and 1.2 illustrate the VARTM and RTM processes respectively.

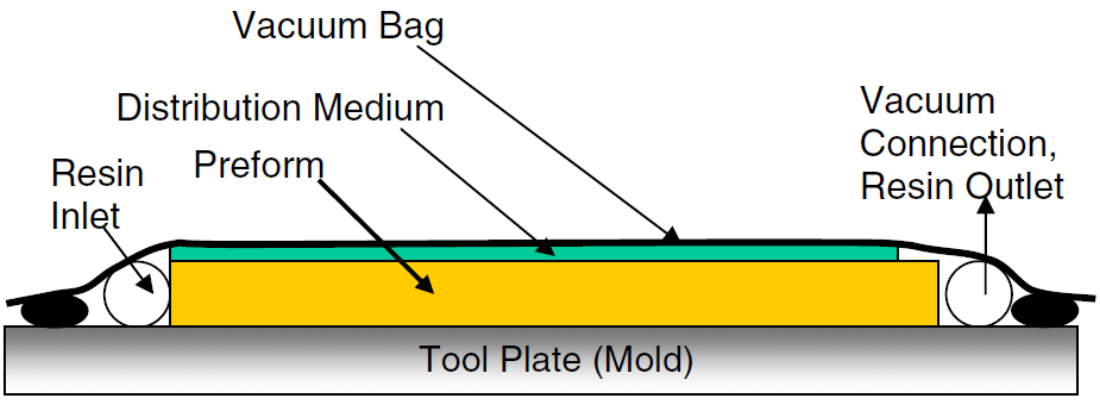

Figure 1.1. VARTM set-up for manufacture of flat plate [3]

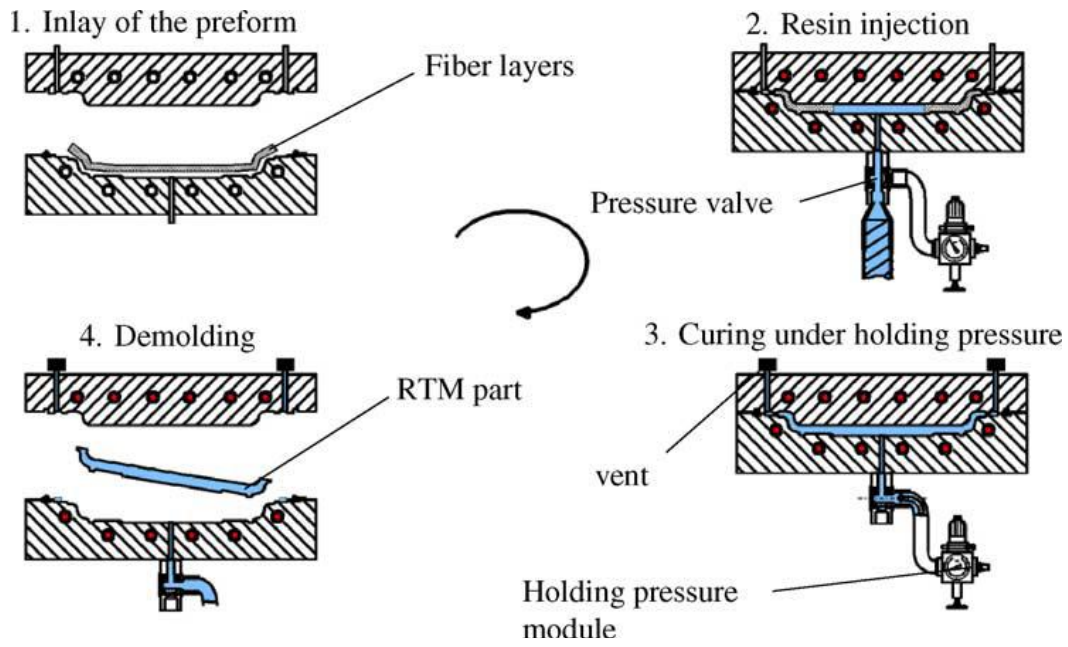

Figure 1.2. The RTM process [4]

Major aerospace OEMs such as Boeing, Airbus and Bombardier are increasingly adopting composite materials throughout airframes and aircrafts, in place of the traditional use of aluminium alloys. The reason is that carbon fibres provide superior stiffness, strength and fatigue properties while reducing mass, when compared with metals. Lower weight in aircrafts results in lower fuel consumption, longer service life and other advantages. Prominent examples include Boeing's 787 Dreamliner and Bombardier's C series, where more than 50 percent materials by mass in the airframe are composites [5]. Figure 1.3 shows an example of a wing rib element in an aircraft.

Figure 1.3. Aircraft wing rib element produced by RTM [6]

Interior non-structural parts are also increasingly made from composites as the materials reduce noise, vibration and harshness (NVH) in aircraft, and they are economical to produce. Even in small series, interior fairings and other components are made using glass fibres primarily. However, there is undoubtedly more work to be done with regards to understanding out-of-autoclave composite manufacturing processes, aiming at lowering production costs and enhancing manufacturing practice every day, especially with the goal of making manufacturing more predictable and more reproducible. The draping and preforming of fabrics are key in attaining better quality and productivity, though procedures that are better documented and optimized.

Numerous studies have been done on the behaviour and draping of textiles reinforcements. Most previous work tends to be theoretical in nature, somewhat simplistic, and fairly disconnected from industrial reality and practice.

1.2 Objectives

The overall objectives of the thesis were to investigate targeted characteristics of reinforcement fabrics that influence the draping process in different ways; to query some of the existing testing methods applicable to dry fabrics that aim at predictive approaches to the draping process; and to develop and deliver pragmatic and readily applicable testing methods and data towards making the draping process more predictable. This work aims at better connecting technical knowledge with industrial production. Specific objectives are listed as follows:

- Studying key deformation modes in single plies and multi-layers;
- Studying target characteristics of fabrics that impact the preforming process such as in-plane shear, bending, fraying and friction;
- Analyzing the relation between fabric parameters such as fibre type, architecture, surface density, yarn count, crimp, cover factor, surface contact area and thickness, and fabric behaviour;
- Developing more reproducible and more accessible testing methods for measuring target characteristics such as fraying.

This thesis is organized in 8 chapters. The first chapter provides a general introduction to the subject and focus of the thesis. It also outlines the objectives and contributions of this work.

The second chapter provides a review of the literature pertaining to two main areas. It reviews deformation modes in fibres, yarns, single ply, as well as 2.5-D and 3-D fabrics. The second subject that this chapter discusses is the existing testing methods for textiles characterization such as bending, shear and friction.

Chapter 3 introduces the materials studied in this work, including 3 glass fibre fabrics and 8 carbon fibre fabrics. This chapter attributes a specific number to each textile and documents textiles parameters such as fibre type, architecture, surface density, yarn count, crimp, cover factor, surface contact area and thickness. Finally, photos of all textiles as well as topographic images are presented.

Chapter 4 starts with an introduction pertaining to the shear test and the tested textiles. The next section presents the apparatus and methodology used in the tests including tool specifications and dimensions. Measured maximum shear extensions are reported. The analysis section investigates existing correlations between fabric parameters and test results. The discussion section elucidates any relationship between observed data and textiles attributes.

Chapter 5 starts by highlighting the importance of the friction test. There are two testing configurations for this test: friction between reinforcement plies, and friction between a single reinforcement ply and aluminium as a mould material. The apparatus and methodology are defined for both configurations in the second section of the chapter. Friction test results as well as average friction force for each textile are presented in the results section. There are two analysis sections, one for each testing methods. Finally, a discussion section compares and contrasts the correlations and trends identified in the analysis sections.

Chapter 6 presents the bending test, where specimens with specific dimensions are bent under their own weight. The introduction section discusses the importance of such test, and a brief history. The apparatus and methodology are detailed in the next section of this chapter, followed by the results section which presents the raw data from the tests as well as calculated bending stiffnesses of textiles. Next section is the analysis of results, which correlates fabric parameters and the bending stiffnesses of reinforcements fabrics. Reasons behind the existence or not of trends are discussed. Finally, a discussion covers the justifications for differences in bending stiffness for different textiles, as well as findings highlighted in an analysis.

Chapter 7 introduces a new testing method for fraying, developed in this thesis. This test aims at quantifying yarn loss in textiles subjected to draping. The chapter starts by stressing the significance of the fraying phenomenon, and the complications that it brings to the draping process in an industrial context. Two measurement methods are introduced, and results for each are presented in the results section. The analysis section of this chapter investigates the correlation between fabric attributes and yarn loss results. The discussion section discusses the reasons for higher or lower amount of fraying observed with different textiles.

Chapter 8 presents a brief conclusion and recommendations highlighting the major findings of this thesis and suggested direction for future work.

1.3 Contributions

The most original contribution of this thesis is the collective analysis of fabrics where numerous fabric parameters and test results are correlated. This model of analyzing a group of industrial

fabrics and investigating their draping behaviour based on their manufacturing parameters is almost non-existent in current literature, especially in the extent done in this work. The analyses offered in the thesis consider each fabric parameters and its correlation with a test result, as well as the variability of test results.

Another contribution is the development of a new fraying testing method, highlighted in Chapter 7. The fraying test was introduced and conducted with satisfying reproducibility. The work covered in chapter 7 was presented at the Canadian Society of Mechanical Engineering Conference 2018 (CSME 2018) and published in the conference proceedings. The test method enables the measurements of one of the most problematic elements of draping behaviour upon preforming.

Chapter 2

Literature review

2.1 Introduction

This chapter introduces deformation modes in textiles, starting from a single fibre to a yarn and a single ply. In section 2.3.1, common weaves are introduced, along with three basic knits in section 2.3.2. In section 2.3.3, 2.5-D and 3-D textiles are discussed. Finally, in section 2.4, existing testing methods are discussed for shear, friction, bending and fraying.

2.2 Deformation modes in textiles

Deformation modes can be analyzed at different scales, from the microscopic scale in fibres, mesoscopic scale in yarns, and macroscopic scale in weaves. Upon preforming, the handling and draping of dry fabrics cause different deformations. These deformations from the microscopic scale to macroscopic scale are reviewed.

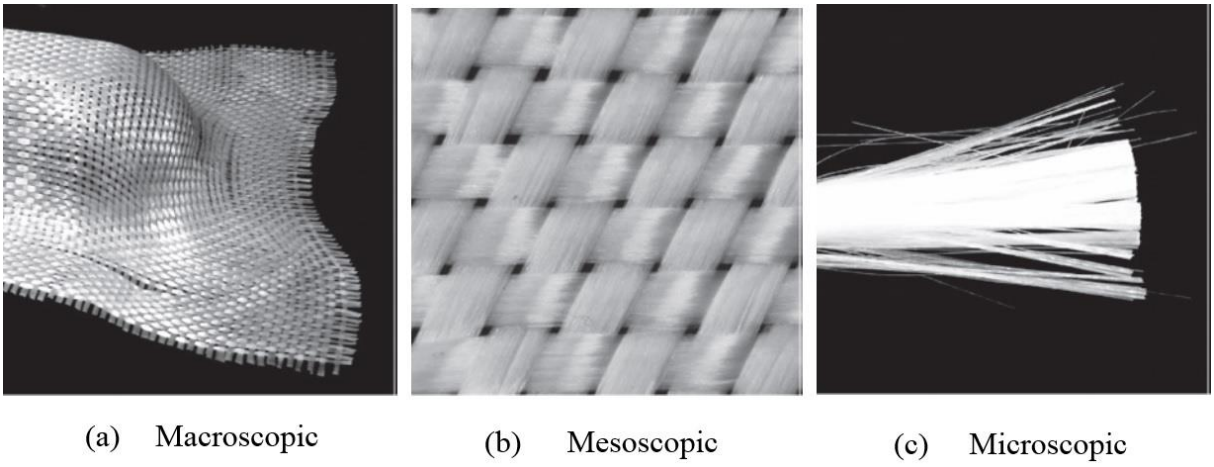

Figure 2.1. Different scales of a fabric [7]

2.2.1 Fibre

Glass and carbon fibres used in reinforcements for composites are essentially continuous cylindrical filaments with diameters ranging from 8 μm to 15 μm. Reinforcement fibres can be assessed at the microscopic scale. Most approaches consider each fibre as a three-dimensional beam interacting with other fibres around it. Deformation modes applicable to single fibres include axial tension A1, axial compression A2, bending A3 and torsion A4.

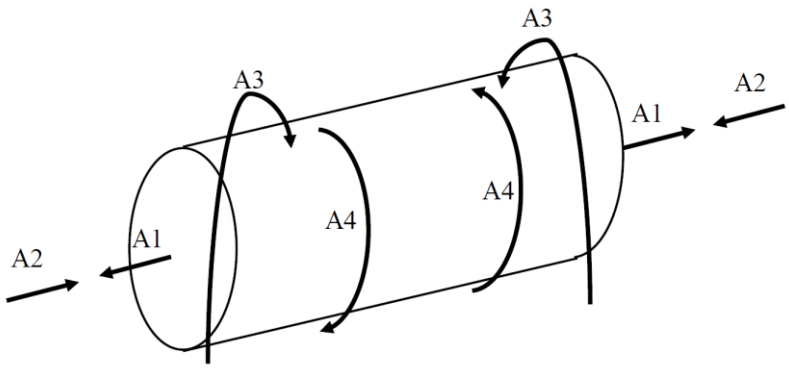

Figure 2.2. Deformation modes in a fibre [8]

Regarding the effects of an applied axial tension, tensile forces applied on textile reinforcements during draping and preforming are not substantial. Hence, tension does not cause considerable deformation in individual fibres.

In reality, fibres are slightly to moderately curved; typical arch length over height *L/a* is assumed to be greater than 100. It will be presumed that the shape of a fibre may be described by the following equation:

$$y = \frac{a}{2}(1 - cos\frac{2\pi x}{L}) \tag{2.1}$$

Regarding axial compression and bending, a fibre can be deformed by axial load P_x or transverse load P_y. Resulting deflections are obtained along the *x* and *y* directions. In order to calculate the displacement Δ, Equation 2.2 is used. N_u and M_u are the axial force and bending moment respectively, while N_e and M_e correspond to the real loads P_x and P_y. *E*, *A* and *I* are the cross section and second moment of area of the fibre beam [9].

$$\Delta = \int_0^L \frac{NuNe}{EA}\,dx + \int_0^L \frac{MuMe}{EI}\,dx \tag{2.2}$$

Solving this equation for the fibre shape given by Equation 2.1 leads to the following equations for displacements Δ_x and Δ_y:

$$\begin{Bmatrix} \Delta x \\ \\ \Delta y \end{Bmatrix} = \begin{bmatrix} \frac{a^2 L}{8EI} + \frac{L}{EA} & -\frac{a2L^2}{4\pi^2 EI} \\ \frac{-aL^2}{4\pi^2 EI} & \frac{L^3}{192EI} \end{bmatrix} \begin{Bmatrix} Px \\ \\ Py \end{Bmatrix} \tag{2.3}$$

Figure 2.3 illustrates the shape of a fibre when subjected to bending or buckling.

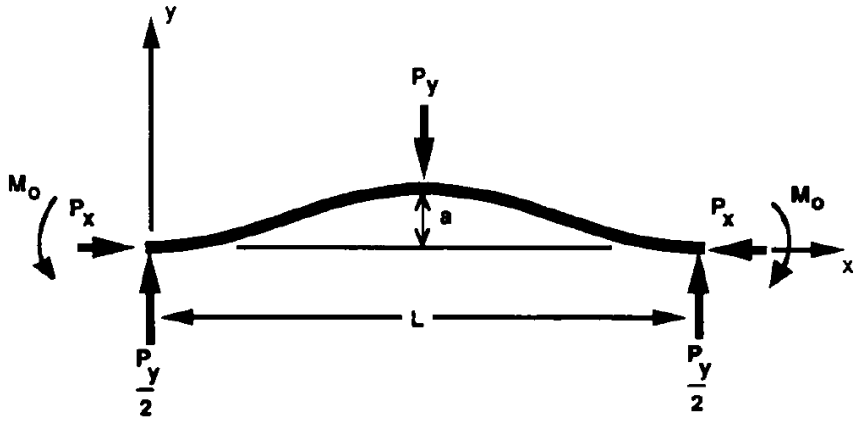

Figure 2.3. Representative curved fibre [9]

Reinforcement fibres mostly have high elastic moduli and consequently high flexural stiffnesses. Bending moment *M*, curvature radius ρ, second moment of inertia *I* and the Young's modulus *E* are related by the following equation:

$$\frac{1}{\rho} = \frac{M1}{EI\rho} = \frac{M}{EI} \tag{2.4}$$

Strain can be calculated using Equation 2.5, where l_d is the deformed length and l_o is the initial length.

$$\varepsilon = \frac{l_d - l_o}{l_o} = \frac{l_d}{l_d} - 1 \tag{2.5}$$

A bent fibre is illustrated in Figure 2.4 where r_f is the fibre radius and r_c is the fibre curvature radius.

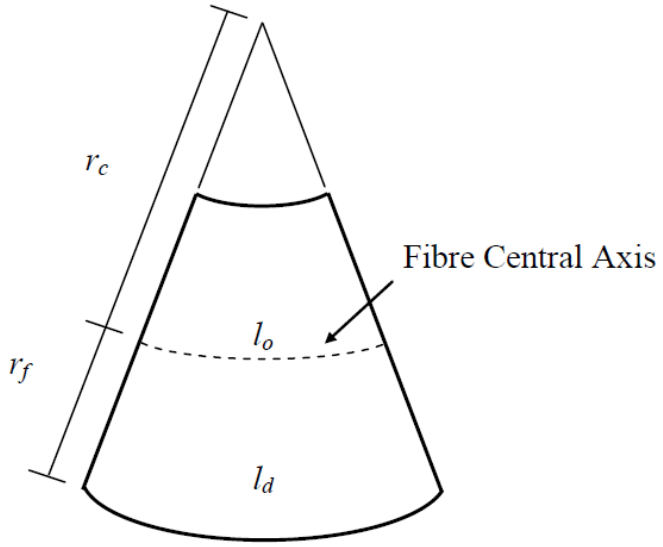

Figure 2.4. Illustration of a bent fibre [8]

If the shape is simplified to a triangle, the following equation is obtained:

$$\frac{l_d}{l_o} = \frac{r_c + r_f}{r_c} = \frac{r_c}{r_f} + 1 \tag{2.6}$$

Inserting Equation 2.4 into Equation 2.5 simplifies to Equation 2.7:

$$\varepsilon = \frac{r_c}{r_f} \tag{2.7}$$

Finally, the presence of torsion moments applied to individual fibres is not significant and can be neglected at the microscopic scale.

2.2.2 Yarn

A number of fibres assembled and generally aligned constitute a yarn. The number of fibres in yarns used as reinforcement in composite materials normally varies from 1000 to 24000 fibres per yarn. Yarn size can affect many characteristics of a reinforcement fabric [10].

Upon draping and preforming, deformations applied to yarns can be categorized into axial stretching (B1), axial compression (B2), bending (B3) and torsion (B4). Furthermore, other deformations such as transverse compression (B5), transverse tension (B6) and intra-yarn shear (B7) can be present. Figure 2.5 schematically shows these deformation modes.

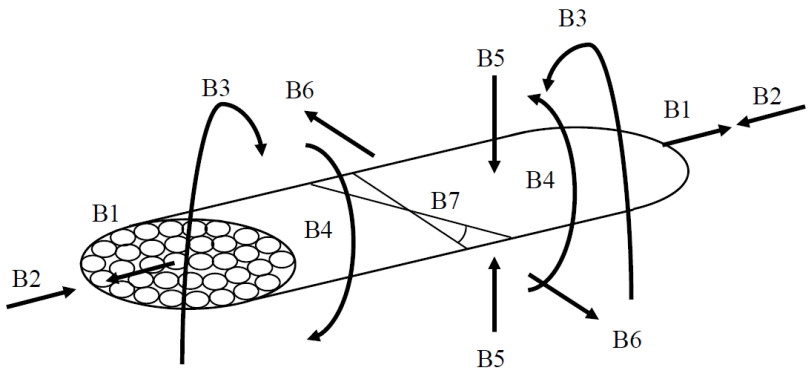

Figure 2.5. Deformation modes in a yarn [8]

In the case of yarns as for fibres, axial forces during draping are trivial, and thus B1 is negligible. Furthermore, it is undesirable for a single yarn to buckle. However, a group of yarns can buckle as a fabric is subjected to compression. During textile handling, inter-yarn friction and compression have a significant impact on fabric deformation [11].

Due to the presence of crimp in weaves as well as upon general handling, bending forces are inevitably present in yarns. Studies have investigated the bending stiffness of single yarns. Two of the testing methods established for measuring the bending stiffness of yarns are the Fabric Assurance by simple testing [12] and Kawabata Evaluation System [13].

The bending stiffness stems from Young's modulus and the second moment of inertia *I*. This moment of inertia is the sum of each fibre's moment of inertia. An assumption of a 10-μm diameter for filaments is held. The second moment of inertia I_d is calculated using Equation 2.8:

$$I_d = N_f \frac{\pi {r_f}^2}{4} \tag{2.8}$$

where N_f is the number of fibres in a yarn and r_f is the radius of the fibre.

2.3 Single ply

A single ply of textile reinforcement can deform in shear, bending, buckling, intra-yarn slippage and compaction. Moreover, the architecture of textiles such as weaves, braids, stitched or knits can impact their response to such deformations, whilst textile architecture also controls the

range of the deformations. Each fabric can feature different fibre type (glass, carbon etc.), surface density, yarn count, crimp, cover factor and thickness leading to a complex relationship between textile construction and its response to deformations.

Different applied forces can cause different deformation modes in textile reinforcements during the draping process. Figures 2.6 and 2.7 illustrate these deformation modes, namely in-plane shear (C1), intra-ply yarn slippage (C2), buckling (C3) and bending (C4).

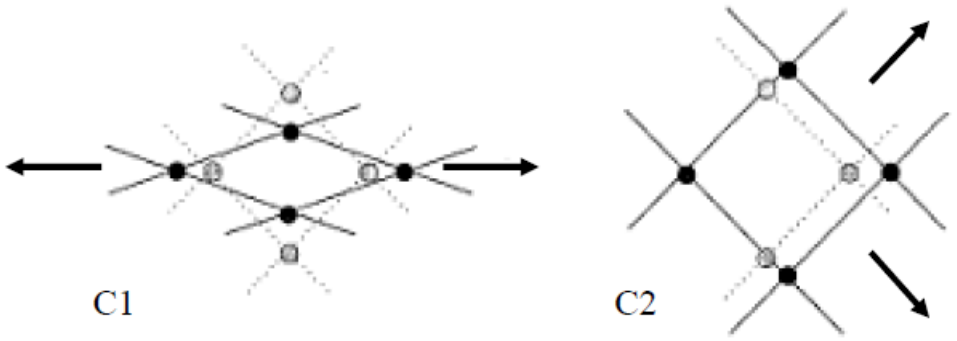

Figure 2.6. Deformation modes C1 and C2 [8]

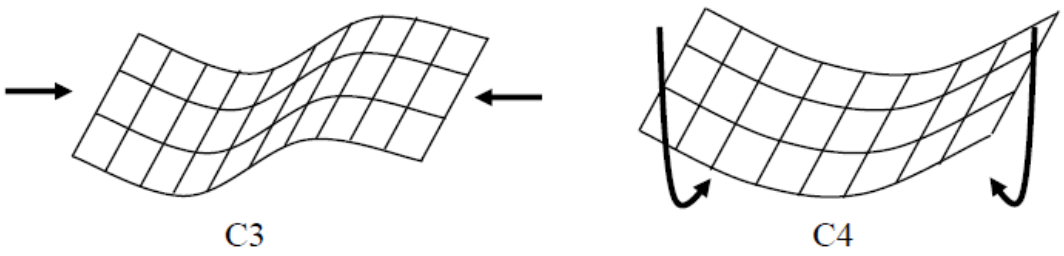

Figure 2.7. Deformation modes C3 and C4 [8]

In-plane shear (C1) occurs frequently in the draping process. In the large majority of experimental and simulation analyses, it is assumed that the shear behaviour does not depend on the tension in yarns [21]. This deformation mode is discussed more thoroughly in section 2.4.1. Intra-ply yarn slippage (C2) is the lateral movement of the yarns at their crossovers and it occurs prevailingly when the fabric reaches its locking angle. When single layers are subject to a compressive force, the buckling phenomenon (C3) can occur in the textile. When draped on a single or double curvature mould, textiles undergo bending (C4). Other deformation modes can occur in a textile such as compaction or yarn stretching, but as they are not prevalent in the draping process, they are not discussed further in this thesis [22].

2.3.1 Woven architectures

A woven fabric can be assembled in the form of plain, twill, satin weaves as well as other interlacing patterns. All these weaves are assembled from two sets of yarns: warp and weft. Figures 2.8 to 2.13 illustrate weaves.

Figure 2.8 shows a 2-D plain weave structure made of interlacing warp and weft yarns.

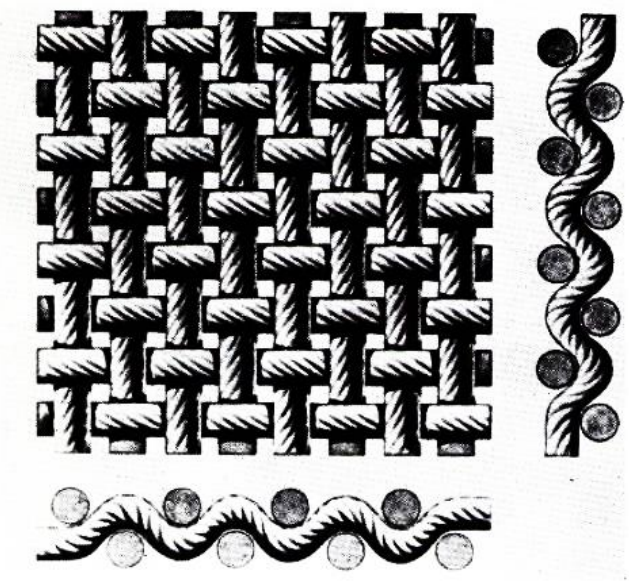

Figure 2.8. Plain weave [14]

Figures 2.9 and 2.10 illustrate twill and satin woven structures respectively. The satin weaves typically vary from 3-harness to 10-harness structures in composite manufacturing. Satin weaves are modified to have fewer intersections of warps and wefts. The number of harness is the total number of yarns crossing and passing under, before the pattern is repeated.

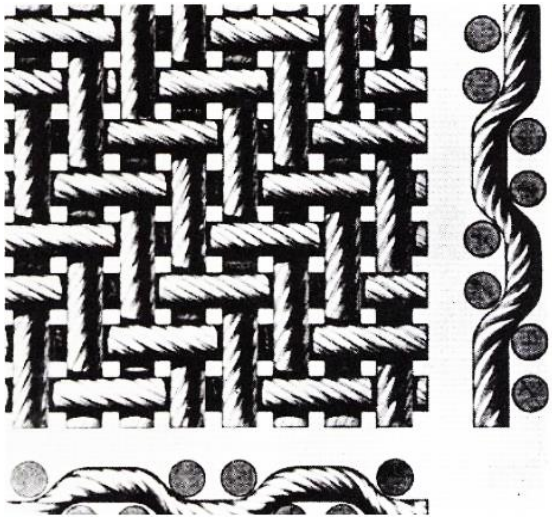

Figure 2.9. Twill weave [14]

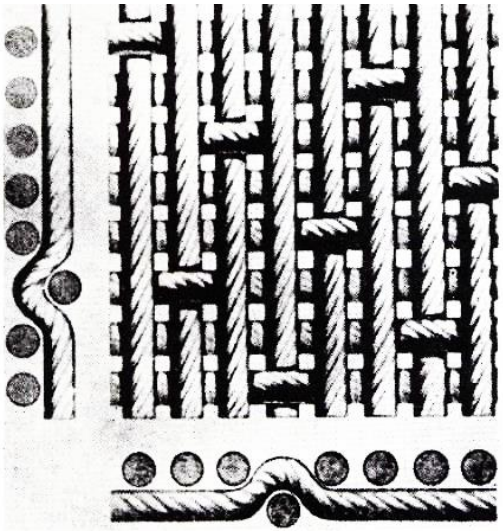

Figure 2.10. Satin weave [14]

Figures 2.11 and 2.12 show the basket weave and rib weave architectures respectively. It can be observed that the warp yarns are thicker in the rib weaves structures illustrated in Figure 2.12. This rib fabric is unbalanced: extending yarns along the warp and weft are different. Unbalanced fabrics are not isotropic and thus do not demonstrate the same mechanical properties along the warp and weft directions.

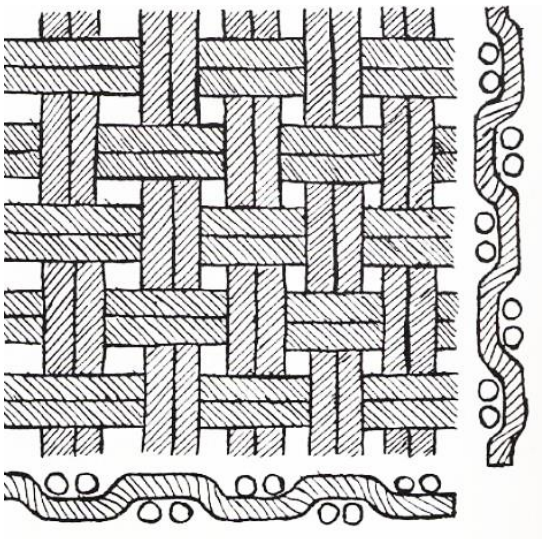

Figure 2.11. Basket weave [14]

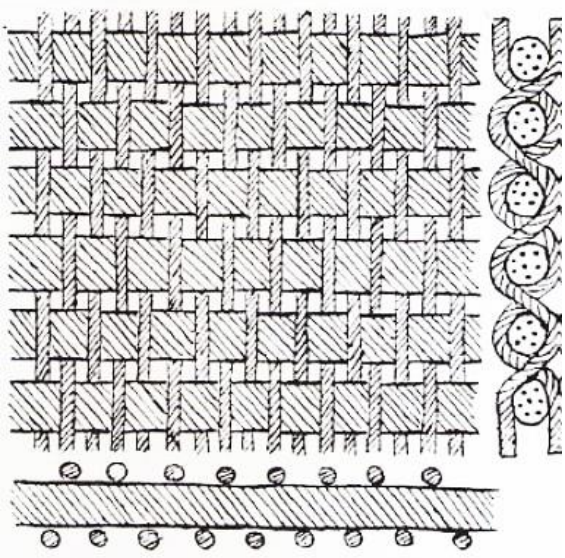

Figure 2.12. Rib weave [14]

Figure 2.13 illustrate the leno weave. It can be observed that this fabric is also unbalanced along both directions.

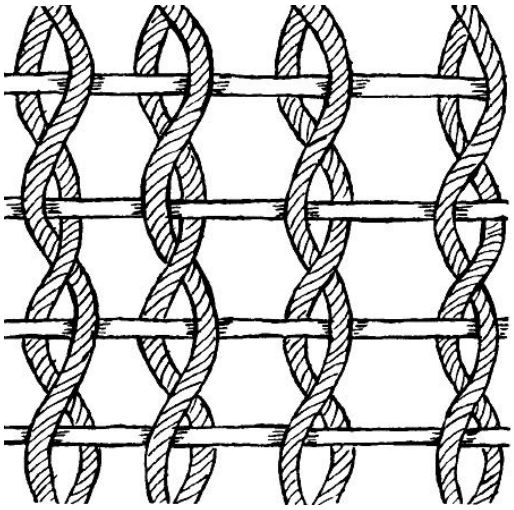

Figure 2.13. Leno weave [14]

2.3.2 Basic knits

Figures 2.14 to 2.16 illustrate some basic knits including the wales loops knit, run-resist circular knit stitch and single warp tricot knit stitch. Figure 2.14 shows the wales loops knit.

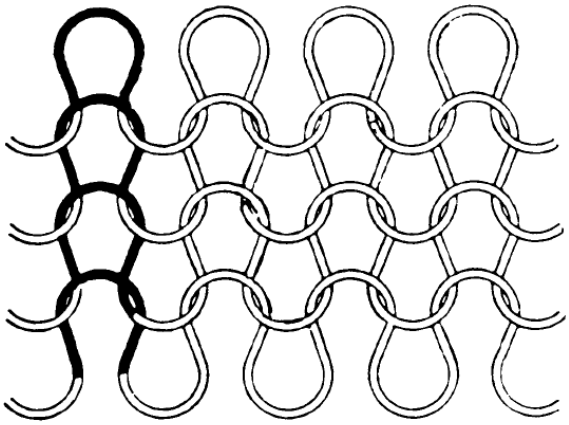

Figure 2.14. Wales loops knit [14]

Figures 2.15 and 2.16 illustrate the run-resist circular knit stitch and the single warp tricot knit stitch respectively.

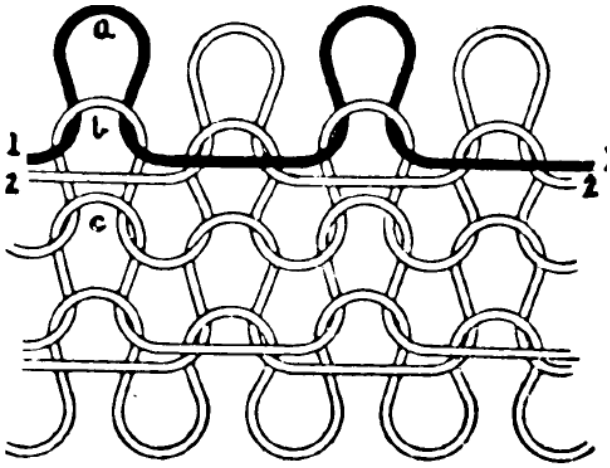

Figure 2.15. Run-resist circular knit stitch [14]

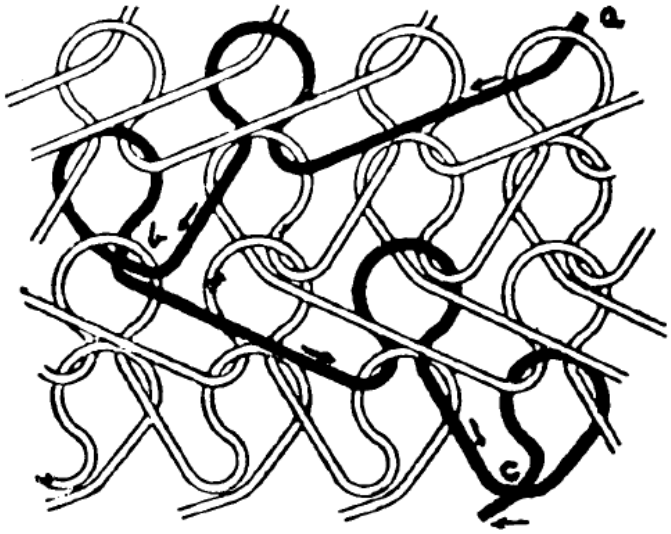

Figure 2.16. Single warp tricot knit stitch [14]

2.3.3 2.5-D and 3-D fabrics

2.5-D textiles are thicker versions of knits or stitched fabrics with in-laid load-bearing yarns [15]. Consequently, 2.5-D fabrics deliver larger bending stiffnesses, higher resistance to fraying, and often smaller shear locking angles and axial extensions compared to their 2-D counterparts.

3-D weaves feature superimposed layers of interlacing yarns, including yarns along the thickness which are labelled z-yarns [16]. Binding is the most common use of the z-yarns [17] followed by a structural function in warp-interlock structures [18]. Such textiles can be transformed into net-shaped preforms with complex geometry, superior delamination resistance and damage resistance [19]. 3-D weaves are available in different types such as layer interlock, orthogonal and multi-axis textiles. The manufacturing of these technical weaves can be done

through standard weaving machinery with minor modifications. Figure 2.17 illustrates an example of warp, weft and binder yarn paths in a simple 3-D weave. In theory, an infinite array of interlacing patterns is possible for 3-D weaving which deliver a range of properties, and thus a specific pattern should be selected carefully for a desired application [20].

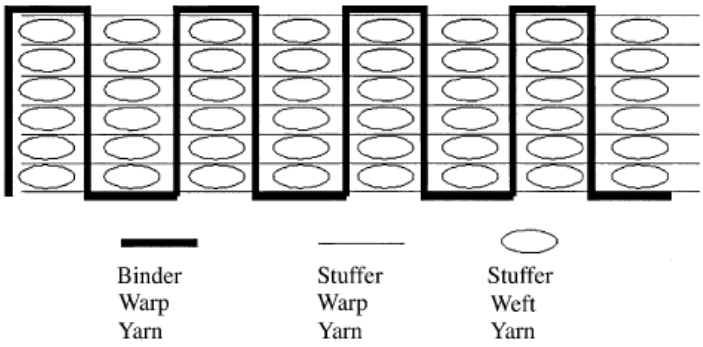

Figure 2.17. Example of yarn path in a 3-D weave [19]

2.4 Testing methods for textiles

2.4.1 In-plane shear testing methods

In-plane shear is defined as the ability of a fabric to deform by relative rotation of its biaxial yarns. The maximum in-plane shear angle which a fabric can withstand is called the locking angle. Beyond this angle, the fabric will wrinkle [23]. The draping of some geometries requires infinite in-plane shear beyond this angle; then, local cutting lines or darting patterns are applied to the textile. However, such cuts will reduce the final properties of the composite.

Another factor that strongly impacts shearing is the initial orientation of the fabric, which should be considered meticulously at the design stage [24]. Draping simulation software can

assist in determining the most effective fabric orientation, to some extent. Two commonly used testing methods are used for quantifying the response of a fabric to in-plane shear: the picture-frame test and the bias extension test.

In the picture-frame test, a textile is clamped in a square frame that is hinged at each corner. Then two opposite corners are displaced during the test. Figure 2.18 shows the set-up for the picture-frame test conducted on a glass fabric. In-plane shear angle can be significant (up to 50°) [21].

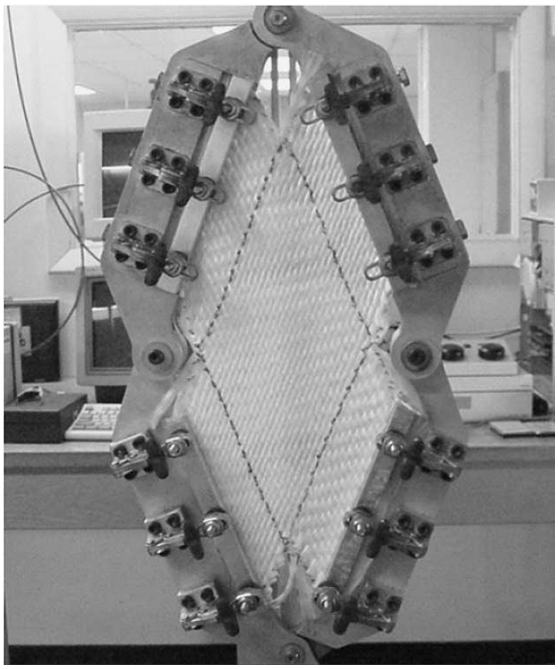

Figure 2.18. Picture frame test [25]

The shear force applied during the test is recorded as the hinges move as a function of displacement of the frame. Using geometrical relations, shear angle can be determined as a

function of the shear force. Figure 2.19 illustrates 3 repeats of the picture frame test at a 162mm/s speed. Variability is often large for the results of such tests.

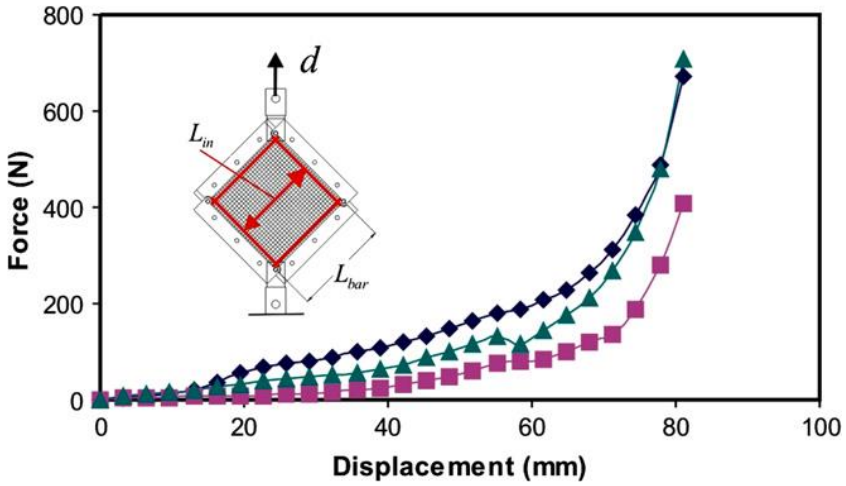

Figure 2.19. Picture-frame test data graph [26]

In the bias extension test, a rectangular textile specimen is clamped from two sides. Different areas are labeled as shown in Figure 2.20. The initial length L_0 and the final length L are measured and the difference is reported as the maximum shear extension. Area A is the only section that deforms purely by in-plane shear. It can be demonstrated that shear angle in region B is half that of region A. Region C remains undeformed during the test.

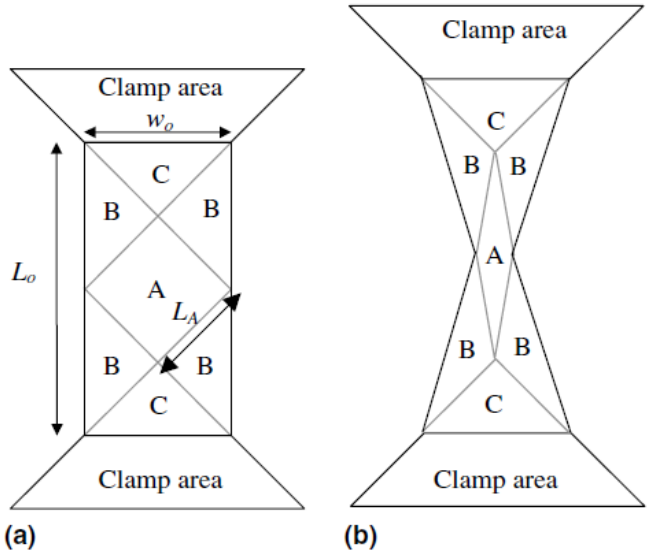

Figure 2.20. Bias extension test, before (a) and after (b) testing [27]

2.4.2 Friction testing method

The most commonly used testing methods for measuring friction between textiles are based on sliding a textile over another and measuring the friction force using a sensor. Figure 2.21 depicts a typical set-up for this test, where the textile is slid over another and a normal load is applied for increasing the friction between those textiles [28].

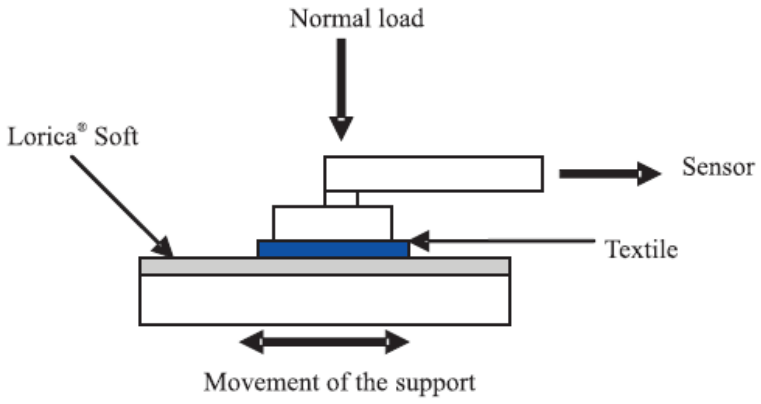

Figure 2.21. Textile friction analyzer [29]

Sample size varies in different works of literature, based on device dimensions. In a specific study [29] conducted to measure the friction between two fabrics, the fabric sample was a circle of 28.55mm diameter. Furthermore, the friction force was measured using a quartz force sensor combined with a charge amplifier. Results of the test lead to the friction force between two fabrics. Tests were repeated 6 times using a new sample each time. The average friction forces for different fabrics were compared, and textiles were ranked based on those forces. Tests were conducted for 20 fabrics in this specific study.

2.4.3 Bending testing methods

A considerable amount of research was done pertaining to the study of bending behavior of fabrics, its effect on preforming, and functional measurement techniques [30]. Although this deformation mode is typically tested in a two-dimensional approach, three-dimensional bending deformation was also measured [31] which also investigates a non-linear strain function for the textile's extension.

The KES-FB2 bending test was originally created to quantify properties in bending [32]. It allows the recording of the evolution of the bending moment per unit width as a function of the curvature, over a cycle of loading an unloading. Specimen dimension is 1 cm along the bending direction and the width is 20 cm. The specimen is clamped between a fixed (A) and a moving (B) clamps. The moving clamp (B) rotates around the fixed clamp (A) to warrant a consistent curvature along the specimen length. The movement is conducted with a curvature rate of $0.5 cm^{-1} s^{-1}$. Figure 2.22 illustrates the KES-FB2 bending test tool.

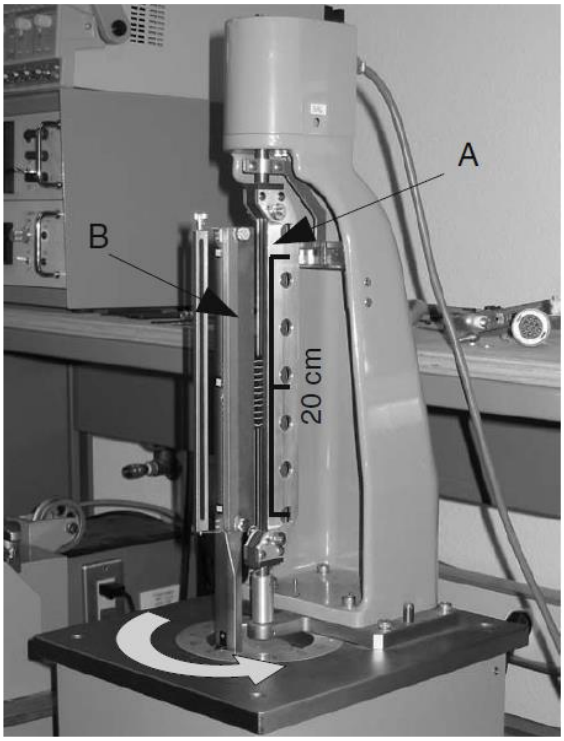

Figure 2.22. KES-FB2 bending test [32]

The bending stiffness G and the bending hysteresis M_0 can be calculated as follows.

Slopes are calculated between k = 0.5 cm^{-1} and k = 1.5 cm^{-1} for s_1, and between k = -0.5 cm^{-1} and k = -1.5 cm^{-1} for s_2 (equation 2.9).

$$\begin{cases} s_1 = \dfrac{\Delta M = M(\kappa = 1.5) - M(\kappa = 0.5)}{\Delta\kappa = 1} \\ s_2 = \dfrac{\Delta M = M(\kappa = -0.5) - M(\kappa = -1.5)}{\Delta\kappa = 1} \\ G = (s_1 + s_2)/2 \end{cases} \tag{2.9}$$

The bending hysteresis M_0, which is the frictional restraint force, is half of the average between the two hysteresis h_1 and h_2 at $k = 1\text{cm}^{-1}$ and $k = -1\text{cm}^{-1}$ respectively (equation 2.10). M_1 and M_{ul} are moments for the load and unload curves respectively.

$$\begin{cases} h_1 & = M_l(\kappa = 1) - M_{ul}(\kappa = 1) \\ h_2 & = M_l(\kappa = -1) - M_{ul}(\kappa = -1) \\ M_0 & = (h_1 + h_2)/2 \end{cases} \tag{2.10}$$

Obtaining the bending stiffness G and bending hysteresis M_0, fabrics can be ranked based on such values. Figure 2.23 illustrates the KES-FB2 test for a fabric along the weft direction as well as the Grosberg's parameters.

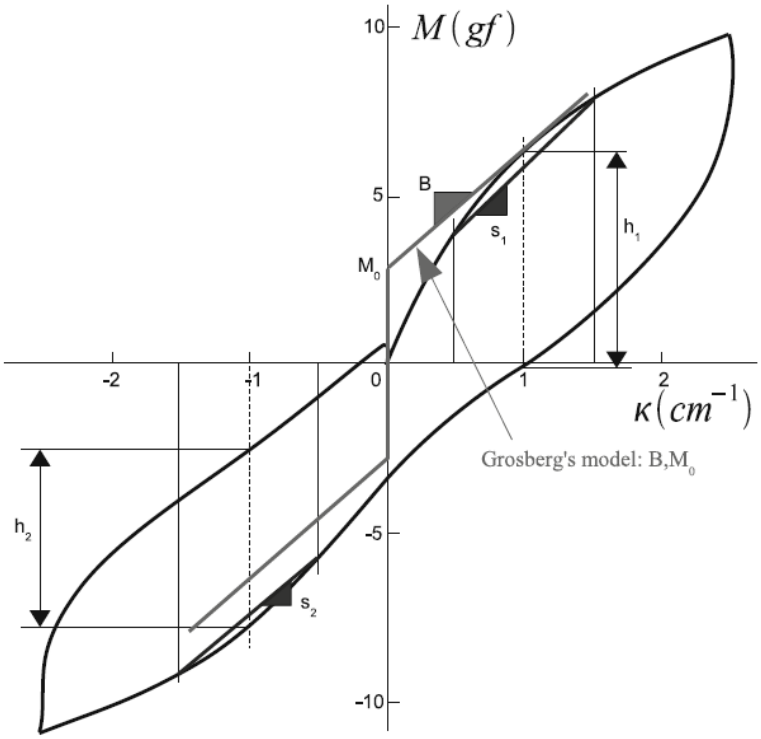

Figure 2.23. KES-FB2 test data for a fabric and Grosberg's parameters [32]

The flexometer is another bending testing method for fabrics [32]. There are two modules in this test: the mechanical module and the optical module. The mechanical module allows the fabric in cantilever configuration to bend under its own weight. The optical module generates photos of the bent sample. The sample can be a yarn, a single ply or a stack of plies. The width is normally around 100 mm. The sample *S* is positioned on a fixed board *F* and a plane *B* comprising laths L_1. For ensuring the embedding condition, a translucent plate is fixed upon he laths and the sample alike. The translation of the drawer *T* enables the laths to successively retract, starting with lath L_1. The test is stopped for a specific length *L* and a repeated for a new length.

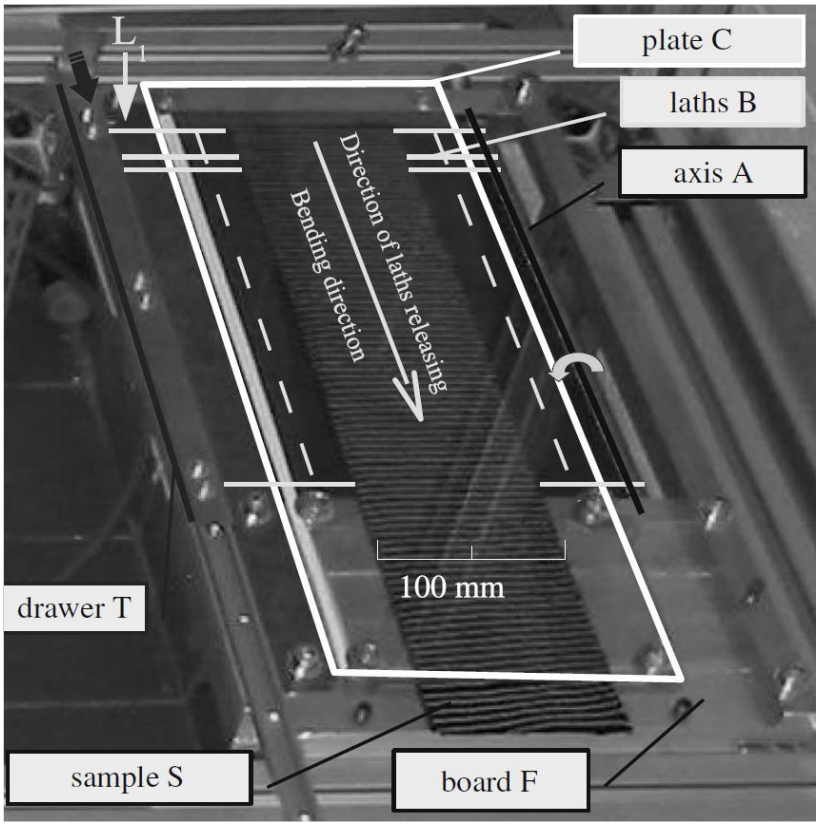

Figure 2.24. Flexometer – mechanical module [32]

In the optical module, a digital camera takes photos of each bent sample. The photos are processed to extract the bent sample shape. Figure 2.25 illustrates the optical module for three lengths.

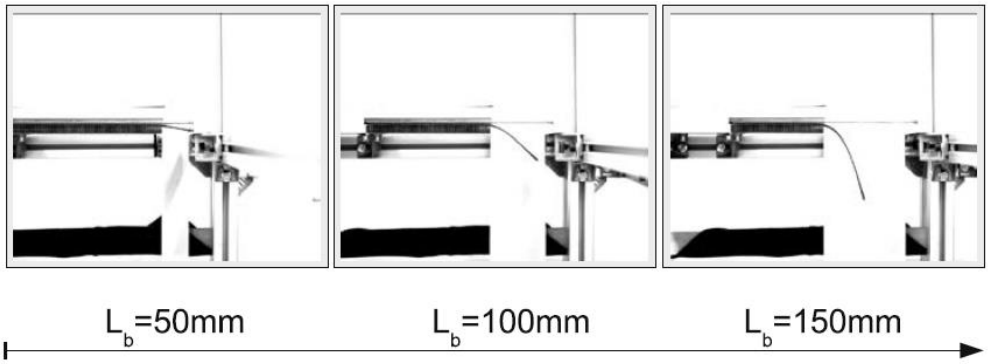

Figure 2.25. Flexometer - optical module for three lengths [32]

Figure 2.26 shows the profile extracted from the photos by image processing for the optical module. Bent shapes are defined by bending length which the deformed shapes have been acquired.

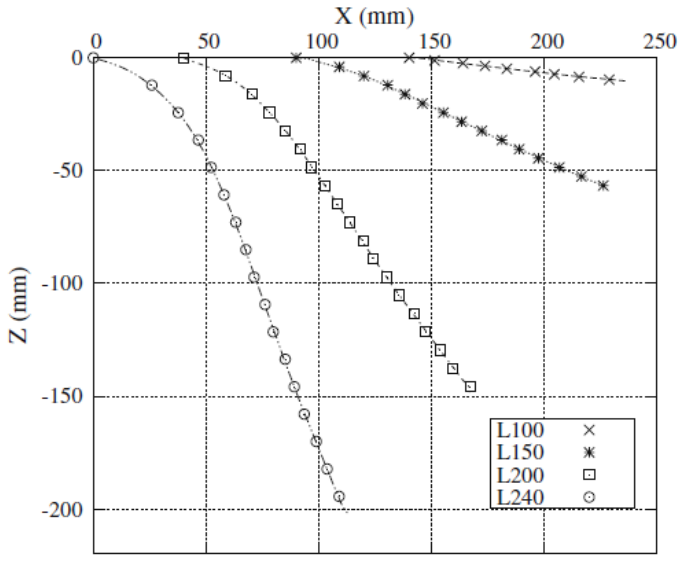

Figure 2.26. Extracted profile using image processing [32]

Using these curves, the curvature as well as the bending moment can be calculated for each distance L_b using the following equation:

$$\kappa = \frac{z''}{(1 + z'^2)^{3/2}} \tag{2.11}$$

where *k* is the curvature and *z"* is the second derivative of the vertical coordinate. The bending moment *M(s)* is calculated by knowing the curvilinear abscissa *s* and the length of the fabric L_b using Equation 2.12:

$$M(s) = W \int_s^{L_b} (u - s)cos(\varphi)\mathrm{d}u \tag{2.12}$$

where *W* is the weight per unit length (*N/m*) and *u* and φ are the Frenet's coordinates of the point *Q* moving toward the shape from *P* to *F*. Figure 2.27 illustrates the bending moment computed along the profile, where *E* is the embedded point and *F* corresponds to the free edge. The moment and the curvature are calculated at general point *P* with curvilinear abscissa *s*.

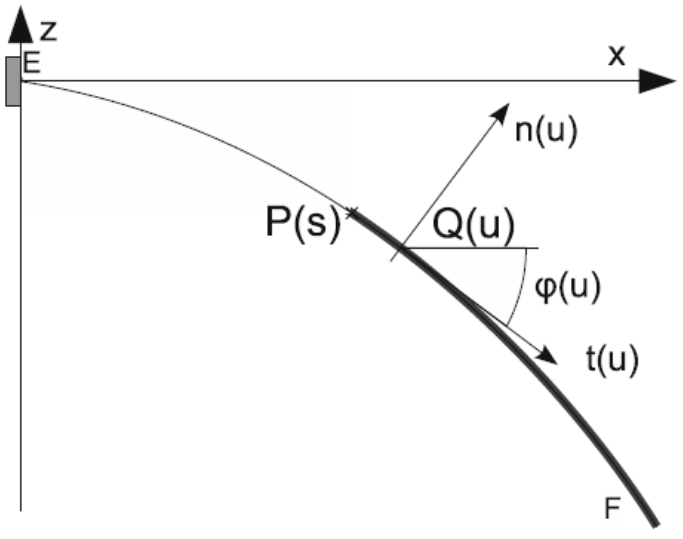

Figure 2.27. Computation of the bending moment along the profile [32]

Figure 2.28 illustrates a flexometer test result. The evolution of flexural stiffness *G* (*N.mm*) with bending length *L* (*mm*) can be observed from the curve. This curve demonstrates a rapid decline in flexural stiffness in the beginning, an increase up to 140mm of length, followed by an overall decline towards the end of the test.

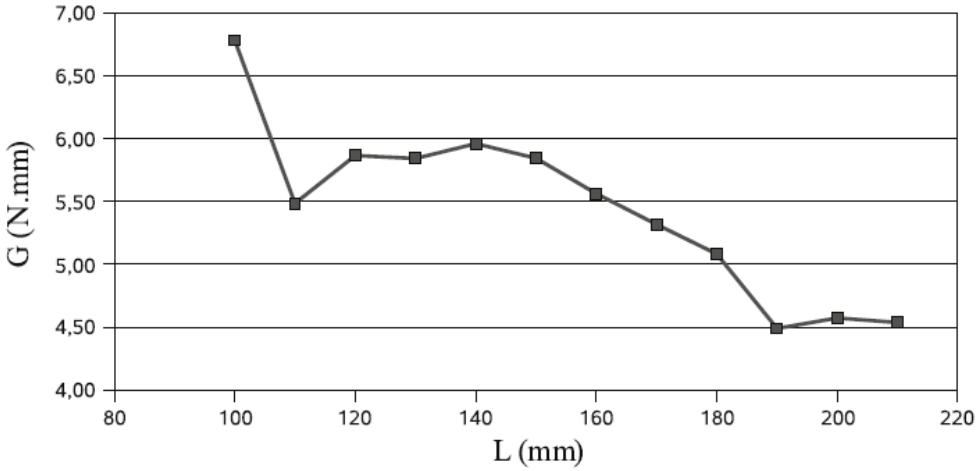

Figure 2.28. Evolution of flexural stiffness with bending length [32]

2.4.4 Fraying testing method

Knowledge of the fraying characteristics of fabric reinforcements upon cutting and handling is important in manufacturing. However, no established testing method exists for assessing it. Although some work was done towards that aim, leading to the yarn pull-out test [33] and the inter-yarn friction test [34], such tests mostly measure friction between yarns subjected to pulling or shear. However, yarns fraying from the edges upon draping on moulds is a recurring phenomenon. The following work was developed by master's candidate Sébastien Gagné at Hutchinson.

The concept of the test is to use controlled airflow to fray the fabric for a certain period of time and measure the yarn loss using image analysis for 5 repeated tests. The fraying tool consists of a chamber and an acrylic plate with dimensions of 304.8mm by 101.6mm. There are 4 holes in the acrylic plate positioned by 4 pins into the chamber. A pressured control valve is connected to the air inlet of the tool, and a manometer is installed after the valve to measure the pressure. The tool also features a drawer to allow the collecting of frayed yarns. The dimensions of samples tested are 76.2mm by 228.6mm with a triangular head of length 152.44mm. The rectangular part of the fabric is held by tapes and thus it cannot fray. The triangular part of the sample can fray, and loss is measured at the end of the test. Figure 2.29 illustrates the fraying test tool.

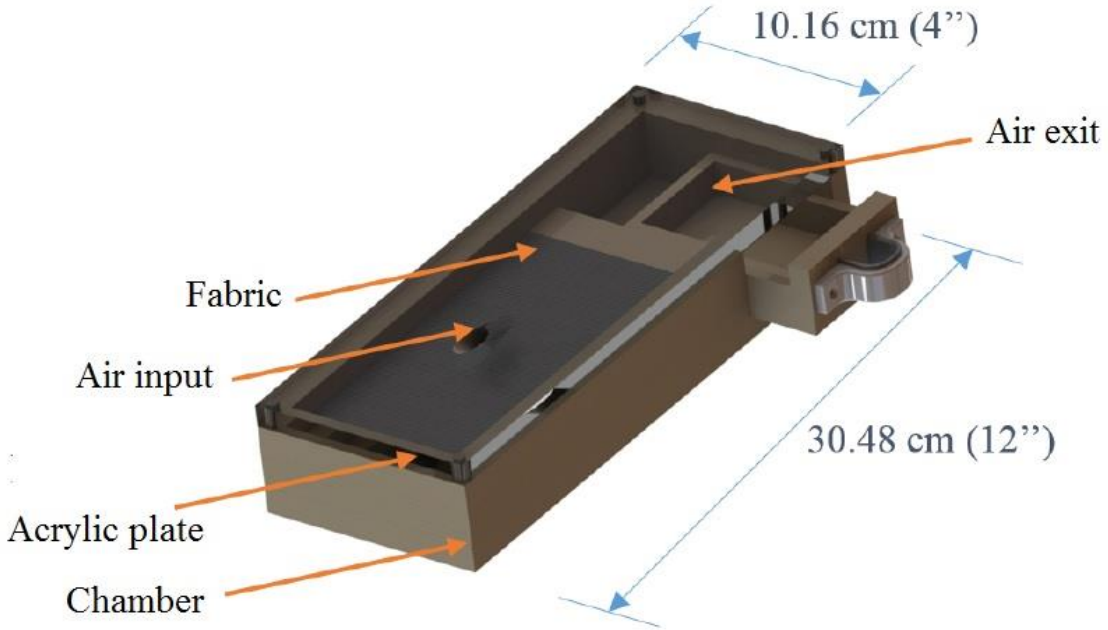

Figure 2.29. Fraying test tool specifications [36]

This test introduces a novel procedure for measurement of yarn loss in fabrics. However, during the test, there is friction between the sample and the chamber applied by the air pressure. Hence, the test does not purely measure the fraying of yarns in fabrics. Moreover, positioning and securing of the fabric into the chamber seems to be time-consuming due to the taping process.

Chapter 3

Materials

3.1 Introduction

This chapter features information pertaining to the reinforcements used in this work including fibre type, architecture, surface density, yarn count, thickness with and without applied pressure, crimp and cover factor. Photographs and topographies of the reinforcements are also included. The information presented in this chapter is referred to extensively in upcoming chapters. Section 3.2 introduces fabric parameters including fibre type, architecture, surface density, yarn count, crimp, cover factor, surface contact area and thickness along with photographs of the fabrics. Section 3.3 features fabric topography images. Section 3.4 features the discussion for this chapter.

3.2 Fabric parameters

Eleven reinforcements were subjected to various characterization tests in this thesis; each test is introduced in an individual chapter, along with the relevant results and their analysis. The reinforcements, labeled fabric 101 to fabric 111, were made of glass or carbon fibres.

The first reinforcement is labeled fabric 101, which is a plain weave glass fibre fabric. This fabric has a surface density of 304 g/m^2, yarn count of 5.5 yarn/cm, crimp factor of 196.5 µm, cover factor of 91.13%, surface contact area of 89.42%, thickness under pressure of 230 µm and thickness without pressure of 280 µm.

Fabric 102 is a twill woven glass fibre fabric with a surface density of 300 g/m^2, yarn count of 6.5 yarn/cm, crimp factor of 192 µm, cover factor of 96.21%, surface contact area of 85.62%, thickness under pressure of 270 µm and thickness without pressure of 340µm.

Fabric 103 is a 8-harness woven satin glass fibre fabric with a surface density of 296 g/m^2, yarn count of 22.4 yarn/cm, crimp factor of 237.2 µm, cover factor of 100%, surface contact area of 71.19%, thickness under pressure of 180 µm and thickness without pressure of 230 µm.

The fourth textile is labeled fabric 104, which is a twill woven carbon fibre fabric featuring a surface density of 408 g/m^2, yarn count of 5.0 yarn/cm, crimp factor of 341.9 µm, cover factor of 98.10%, surface contact area of 90.31%, thickness under pressure of 410 µm and thickness without pressure of 530 µm.

Fabric 105 is the next textile tested, which is a 5-harness satin carbon fabric with binder on the surface on both sides. This textile has a surface density of 368 g/m^2, yarn count of 4.5 yarn/cm, crimp factor of 441 µm, cover factor of 99.2%, surface contact area of 81.14%, thickness under pressure of 400 µm and thickness without pressure of 510 µm.

Non-crimp stitched carbon fibre fabric 106 is the next textile introduced, which features a surface density of 288 g/m^2, yarn count of 2.0 yarn/cm, crimp factor of 0µm, cover factor of

100%, surface contact area of 96.41%, thickness under pressure of 180 µm and thickness without pressure of 250 µm.

Fabric 107 is a woven 4-harness satin carbon fibre fabric featuring a surface density of 188 g/m^2, yarn count of 5.0 yarn/cm, crimp factor of 194 µm, cover factor of 99.34%, surface contact area of 78.29%, thickness under pressure of 220 µm and thickness without pressure of 300 µm.

The next textile listed is carbon fibre fabric 108 with a woven architecture of 5-harness satin. This textile features a surface density of 365 g/m^2, yarn count of 4.6 yarn/cm, crimp factor of 392 µm, cover factor of 100%, surface contact area of 83.63%, thickness under pressure of 400 µm and thickness without pressure of 510 µm.

Carbon fibre fabric 109 has binder on its 2.5-D woven structure, and also featuring a surface density of 624 g/m^2, yarn count of 6.0 yarn/cm, crimp factor of 494 µm, cover factor of 100%, surface contact area of 87.29%, thickness under pressure of 700 µm and thickness without pressure of 1070 µm.

Non-crimp fabric (NCF) 3K carbon fibre fabric 110 has a surface density of 362 g/m^2, yarn count of 6.0 yarn/cm, crimp factor of 0µm, cover factor of 100%, surface contact area of 84.77%, thickness under pressure of 180 µm and thickness without pressure of 250 µm.

The last textile tested in this thesis is NCF 6K carbon fibre fabric 111. This textile shows a surface density of 724 g/m^2, yarn count of 12 yarn/cm, crimp factor of 0 µm, cover factor of 100%, surface contact area of 84.77%, thickness under pressure of 350 µm and thickness without pressure of 480 µm.

Data pertaining to surface density was available from the industrial partner. The numbers were summarily verified and confirmed as follows. A 1cm by 1cm specimen was cut off the fabric roll and weighed on a scale with ±0.001 g accuracy. Then, the weight was divided by the area. Yarn count was simply attained by counting the number of yarns in 10cm length and dividing by 10. Crimp was measured by microscopy, calculating the difference between the minimum and maximum height of yarns. Cover factor was measured using imageJ software, dividing the area occupied by yarns over the whole area, reported as a percentage.

Surface contact area was quantified by looking at the topography of textiles given by the Keyence VHX-6000 series digital microscope processes using the imageJ software. Afterwards, the area with superior height coloured yellow to red by the topography analysis was divided by the whole area of the textile. Thickness without pressure was measured using a caliper. Finally, thickness under pressure was measured using a caliper while two plates were constraining the fabric.

Table 3.1 shows the information pertaining to all fabrics tested, including architecture, surface density and yarn count. Identifier numbers assigned to each fabric will be used forthwith. Supplier information is known by the author but was withheld at the request of the industrial partner. Photographs of the reinforcements appear in Figures 3.1 to 3.11. Such photographs enabled the measurements of the cover factor attribute in fabrics.

Table 3.1. Technical parameters of reinforcement fabrics

Fabric number	Fibre	Architecture	Surface density (g/m^2)	Yarn count (yarn/cm)	Crimp (μm)	Cover factor (%)	Surface contact area (%)	Thickness under pressure (μm)	Thickness without pressure (μm)
101	Glass	Plain	304	5.5	196.5	91.13	89.42	230	280
102	Glass	Twill	300	6.5	192	96.21	85.62	270	340
103	Glass	8-harness satin	296	22.4	237.2	100	71.19	180	230
104	Carbon	Twill	408	5.0	341.9	98.10	90.31	410	530
105	Carbon	5-harness satin with binder	368	4.5	441	99.02	81.14	400	510
106	Carbon	Non-crimp stitched	288	2.0	0	100	96.41	180	250
107	Carbon	4-harness satin	188	5.0	194	99.34	78.29	220	300
108	Carbon	5-harness satin	365	4.6	392	100	83.63	400	510
109	Carbon	2.5-D with binder	624	6.0	494	100	87.29	700	1070
110	Carbon	NCF 3K chain stitch	362	6.0	0	100	84.77	180	250
111	Carbon	NCF 6K chain stitch	724	12.0	0	100	84.77	350	480

Figures 3.1 and 3.2 illustrate the plain weave glass fabric 101 and twill weave glass fabric 102 respectively.

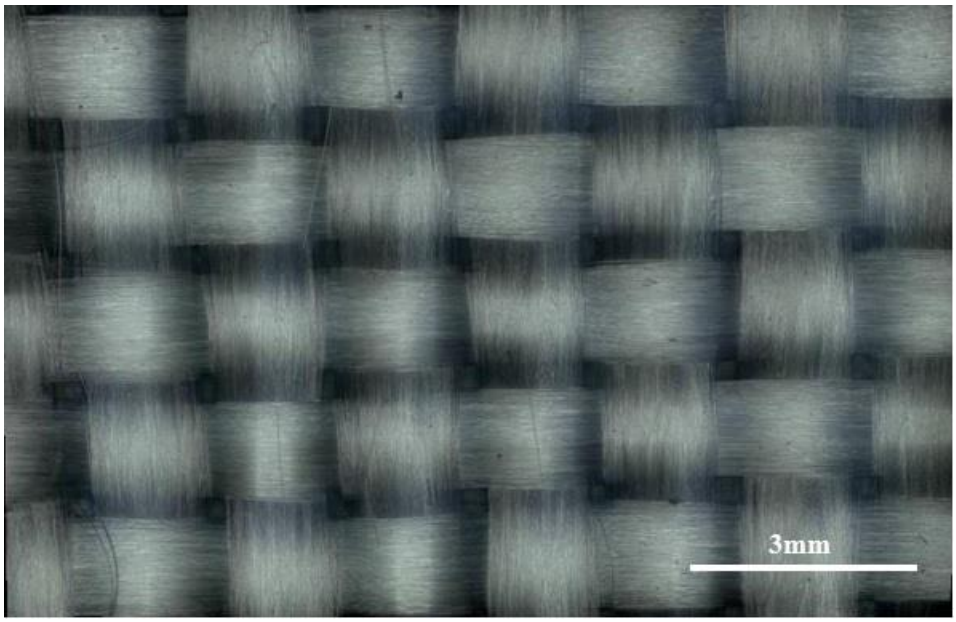

Figure 3.1. Plain weave glass fabric 101

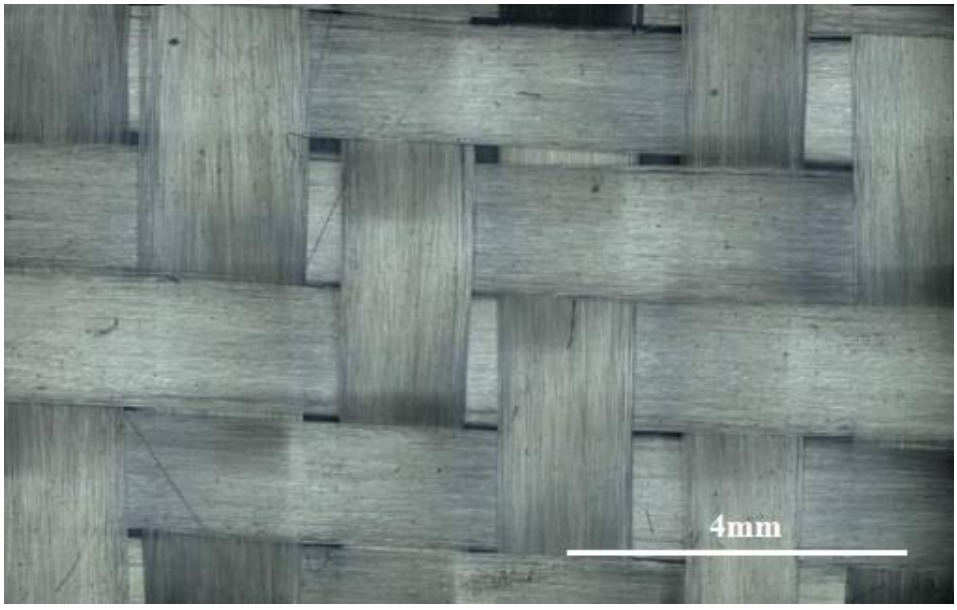

Figure 3.2. Twill weave glass fabric 102

Figures 3.3 and 3.4 illustrate the 8-harness satin weave glass fabric 103 and twill weave carbon fabric 104 respectively.

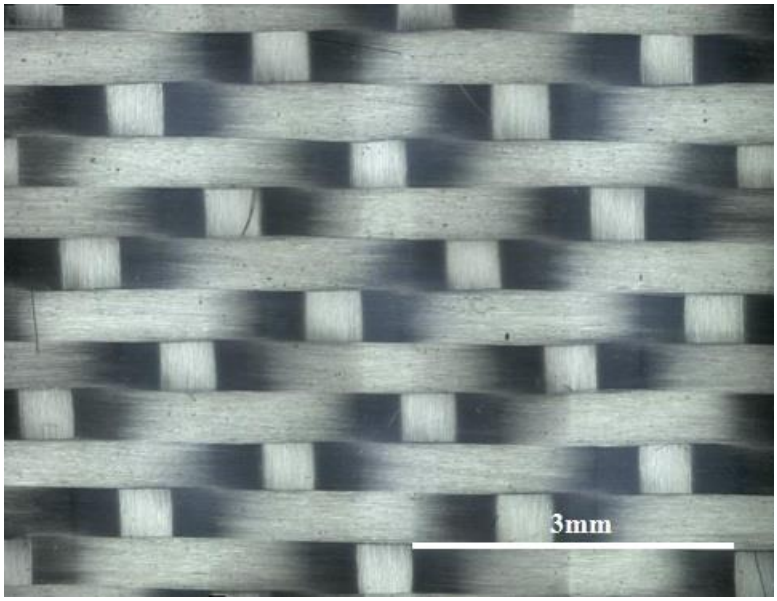

Figure 3.3. 8-harness satin weave glass fabric 103

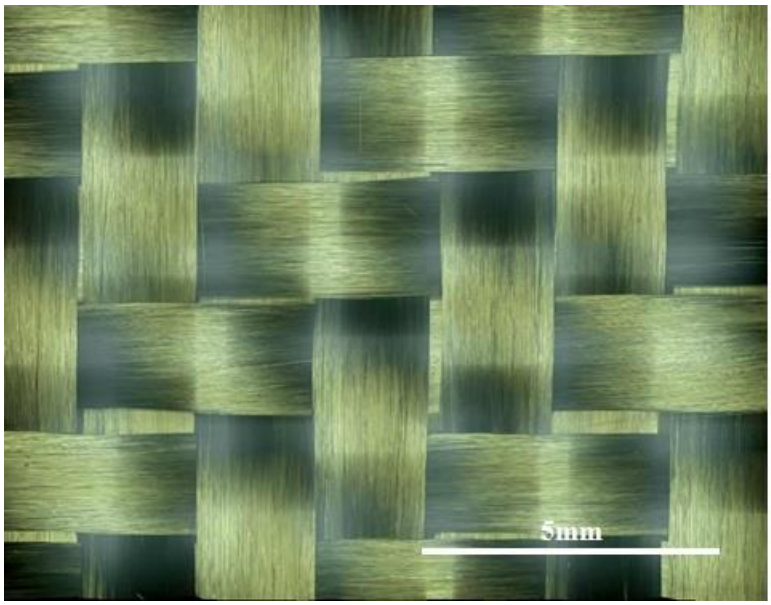

Figure 3.4. Twill weave carbon fabric 104

Figures 3.5 and 3.6 illustrate the 5-harness satin weave carbon fabric 105 and non-crimp stitched carbon fabric 106 respectively.

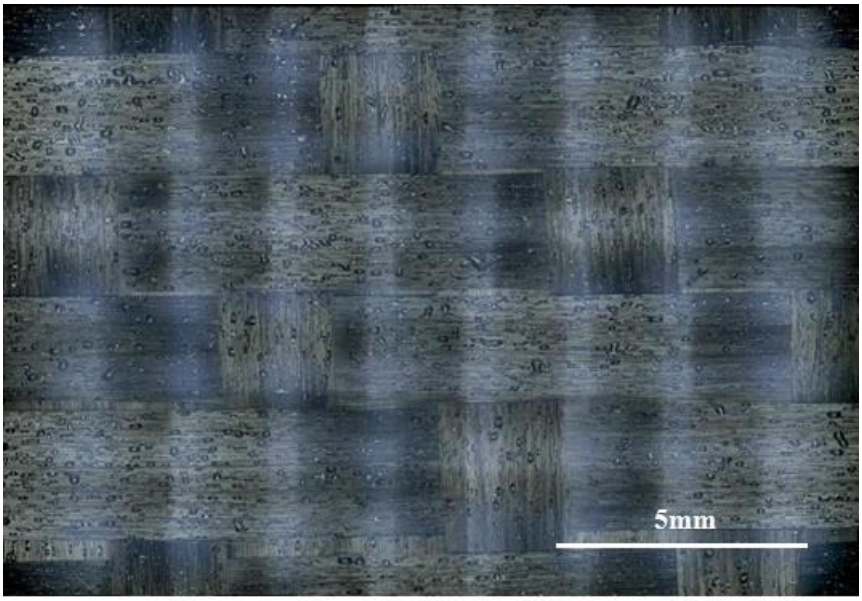

Figure 3.5. 5-harness satin weave carbon fabric with binder 105

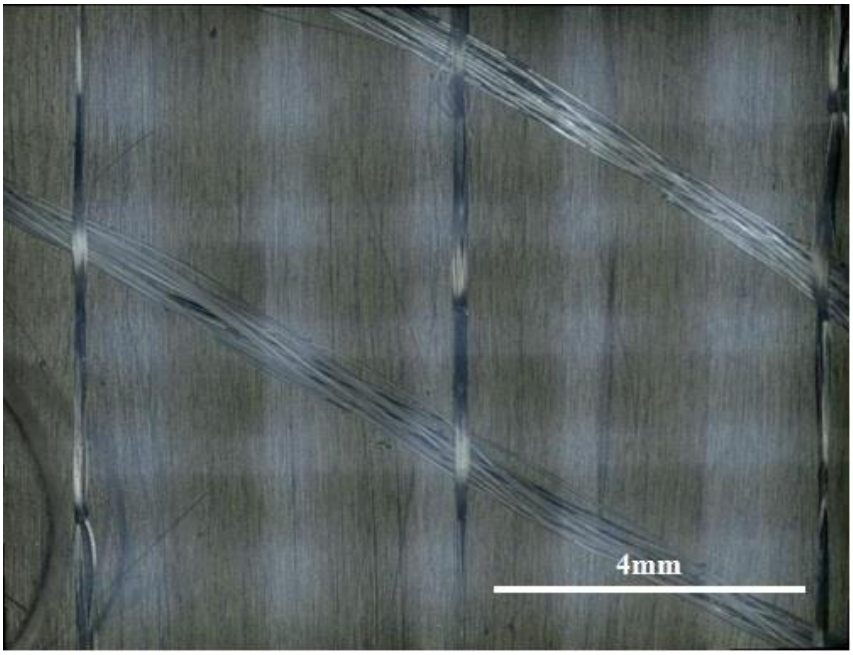

Figure 3.6. Non-crimp stitched carbon fabric 106

Figures 3.7 and 3.8 illustrate the 4-harness satin carbon fabric 107 and 5-harness satin weave carbon fabric 108 respectively.

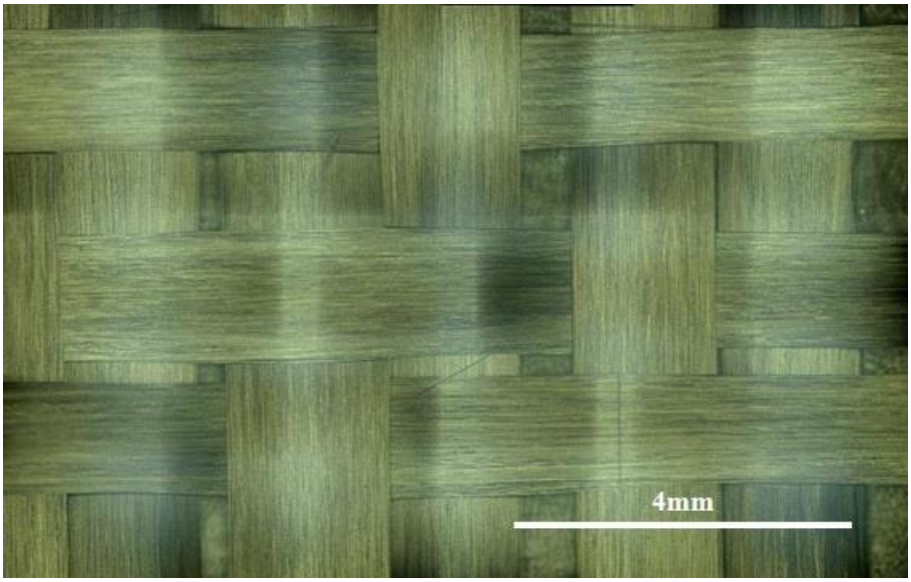

Figure 3.7. 4-harness satin weave carbon fabric 107

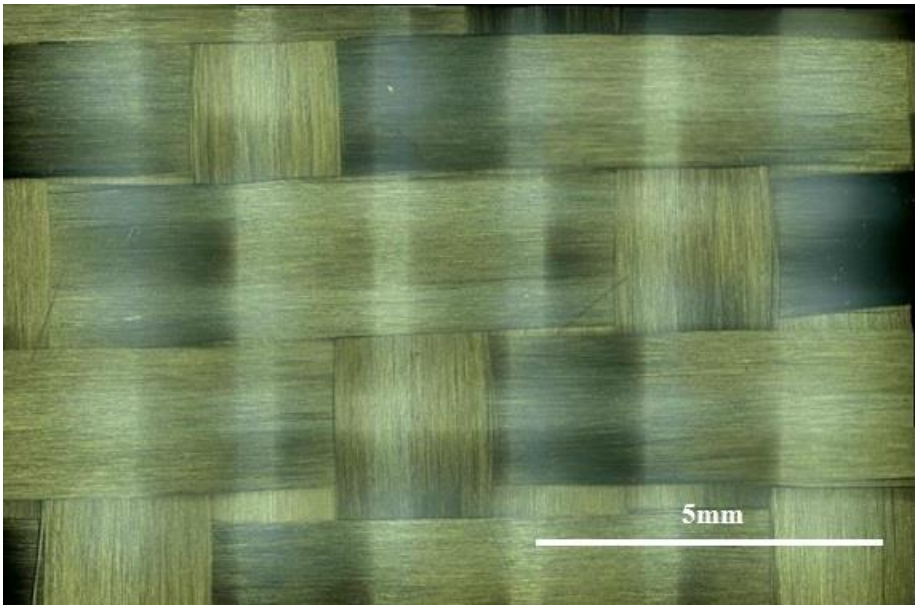

Figure 3.8. 5-harness satin weave carbon fabric 108

Figures 3.9, 3.10 and 3.11 illustrate the 2.5-D weave carbon fabric 109, NCF 3K weave carbon fabric 110 and NCF 6K carbon fabric 111 respectively.

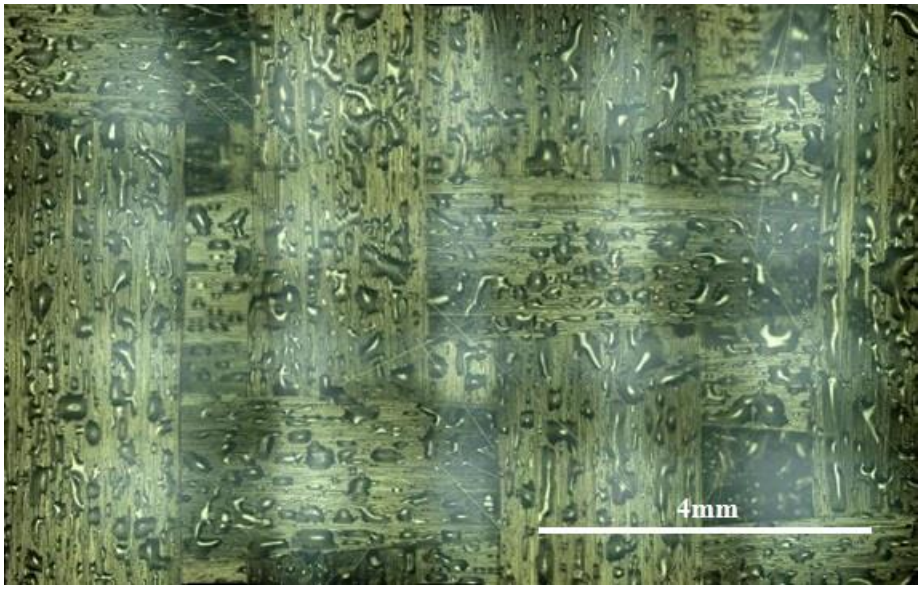

Figure 3.9. 2.5-D weave carbon fabric with binder 109

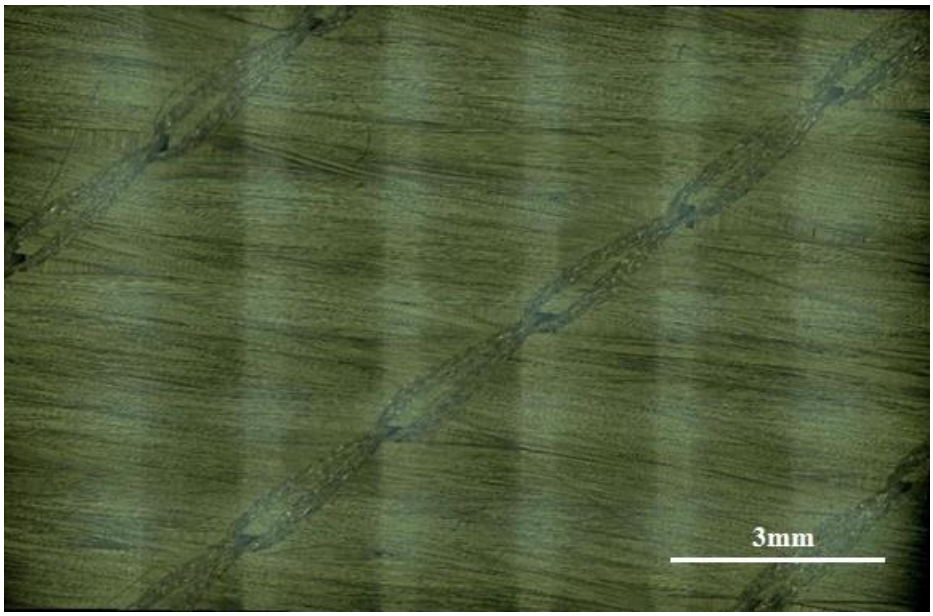

Figure 3.10. NCF 3K chain stitch carbon fabric 110

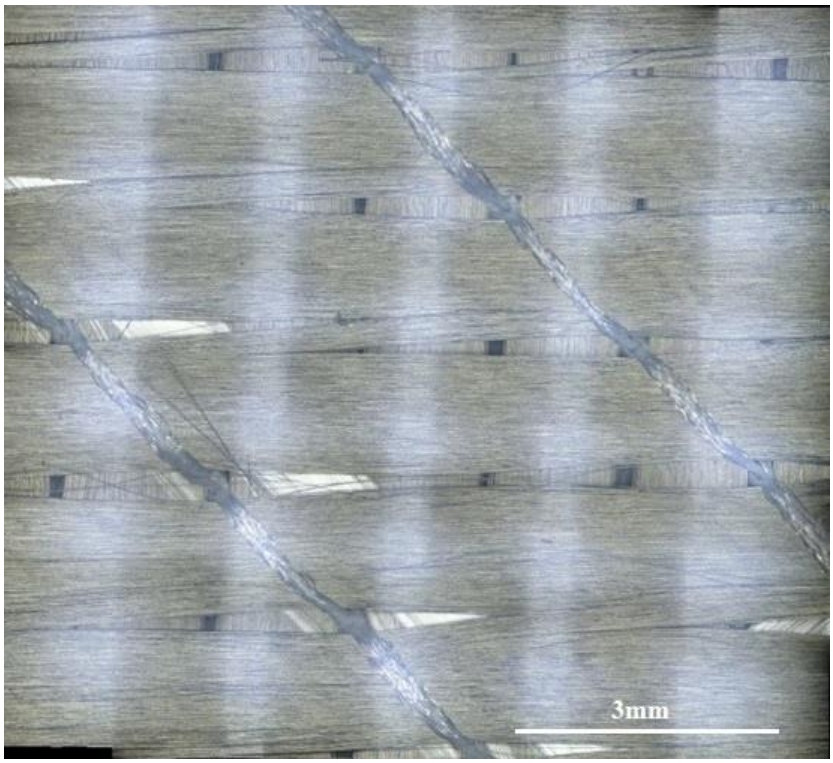

Figure 3.11. NCF 6K chain stitch carbon fabric 111

Fabrics 101, 102 and 103 are glass fibre fabrics. Fabrics 104 to 111 are carbon fibre fabrics. Fabric 101 is a plain weave while fabrics 102 and 104 are twill weaves. Furthermore, fabrics 103, 105, 107, 108 are satin weaves whilst fabrics 106, 110 and 111 are stitched non-crimp fabrics and fabrics 105 and 109 are fabrics with binder.

3.3 Fabric topography

Topographies of fabrics were generated using a Keyence VHX-6000 series digital microscope. Figures 3.12 to 3.22 illustrate these topographies for the fabrics used in this work. The importance of these topographies is highlighted as they enabled the measurements of fabric parameters such as surface contact area and crimp.

Figure 3.12 and 3.13 illustrate the topographies of fabrics 101 and 102 with crimp factor of 196.5 µm and 192 µm respectively. The plain weave structure in Figure 3.12 and the twill woven structure in Figure 3.13 are evident.

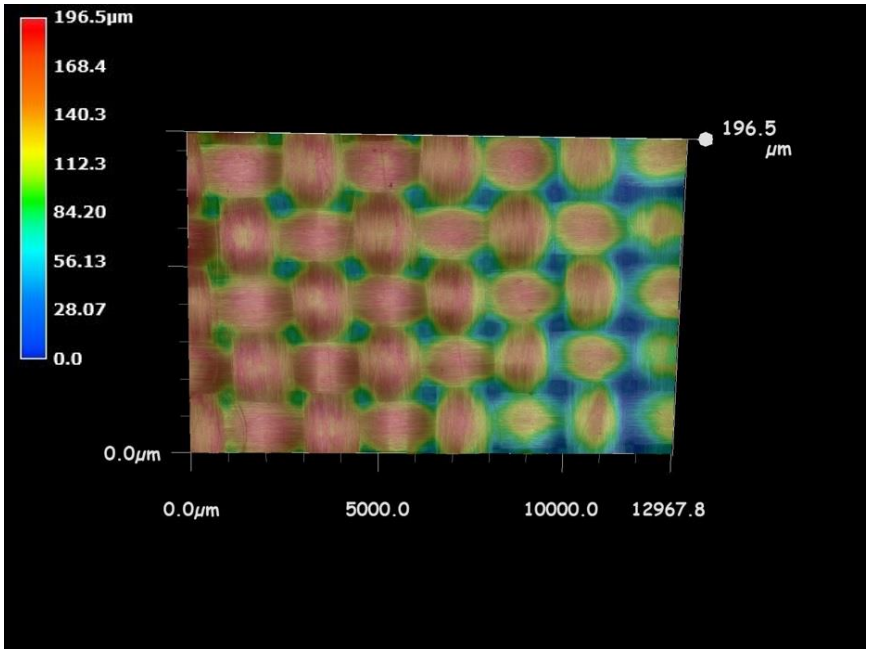

Figure 3.12. Topography of plain glass fabric 101

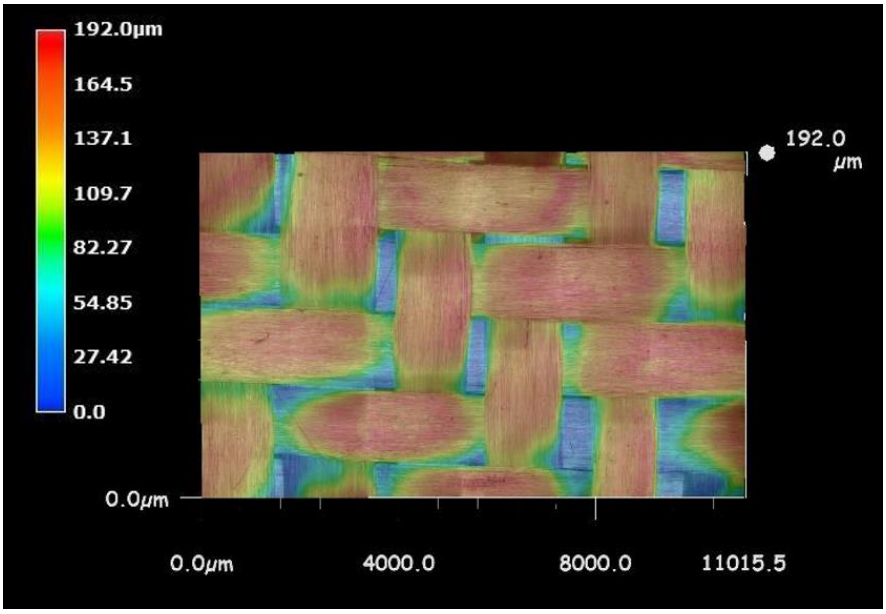

Figure 3.13. Topography of twill glass fabric 102

Figures 3.13 and 3.14 illustrate the topographies of fabrics 103 and 104 with crimp factor of 237.2 µm and 341.9 µm respectively. The 8-harness satin structure as well as the high cover factor in Figure 3.13 and the twill structure in Figure 3.14 can be observed.

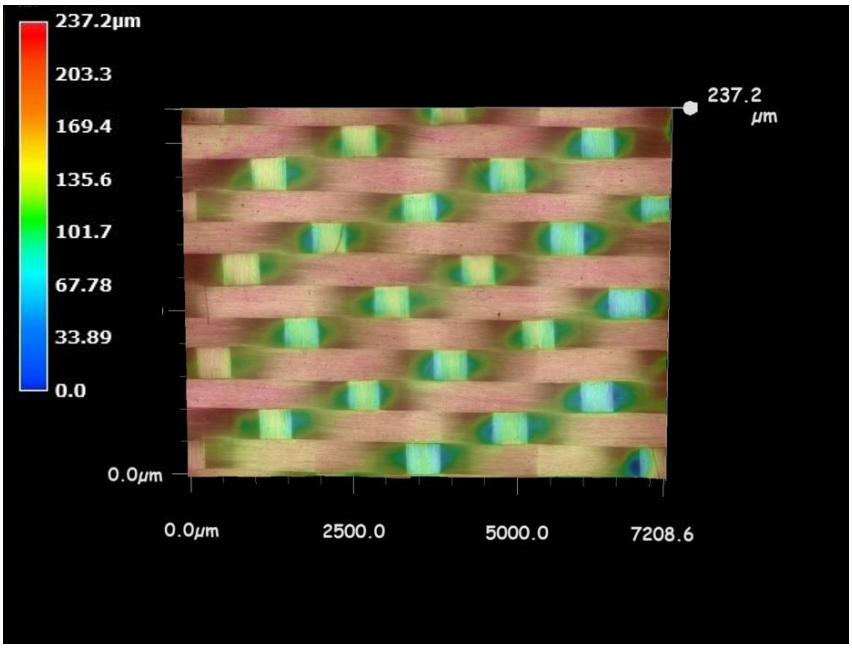

Figure 3.14. Topography of 8-harness glass fabric 103

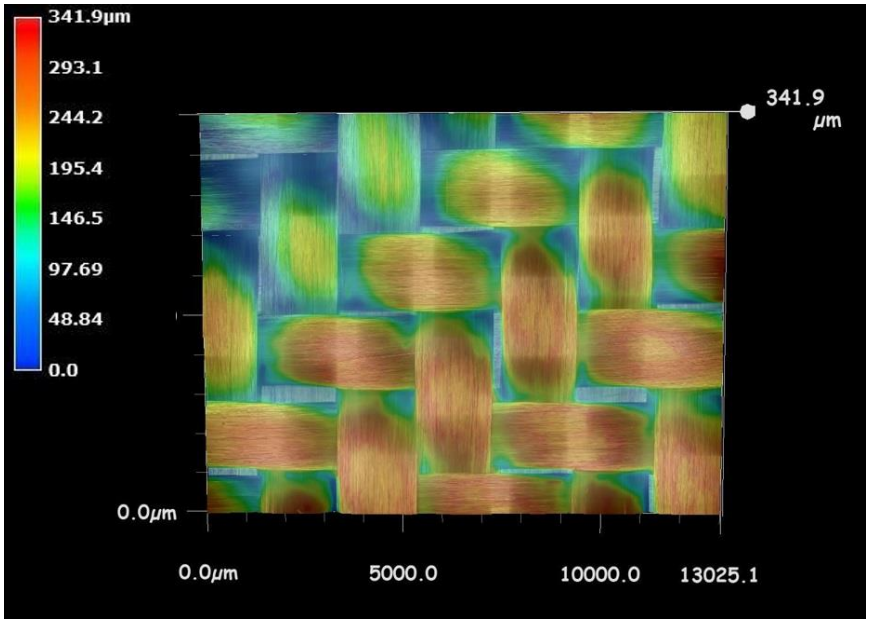

Figure 3.15. Topography of twill carbon fabric 104

Figures 3.16 and 3.17 illustrate the topographies of fabrics 105 and 106 with crimp factor of 441.0 µm and 0 µm (non-crimp fabric) respectively. The 5-harness satin structure and the presence of binder in the Figure 3.16, and the NCF structure as well as the large contact area in Figure 3.17, can be observed.

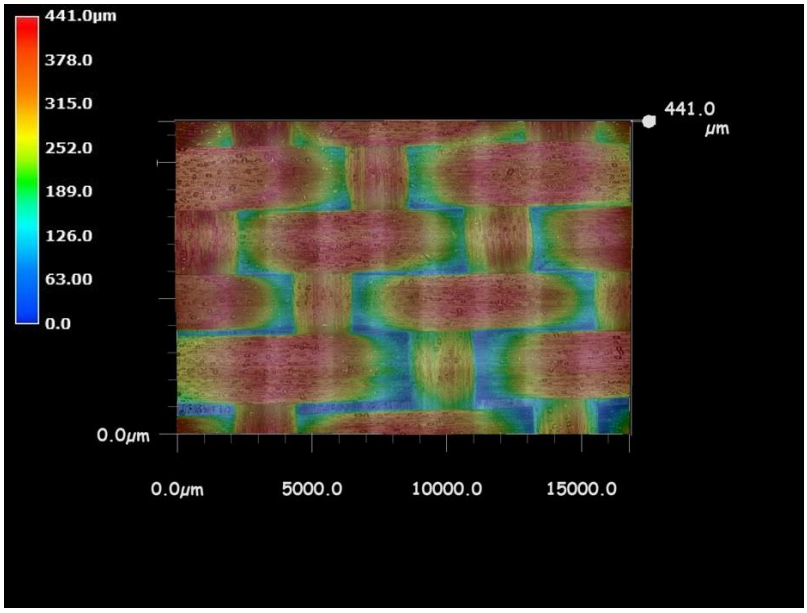

Figure 3.16. Topography of 5-harness carbon fabric 105 with binder

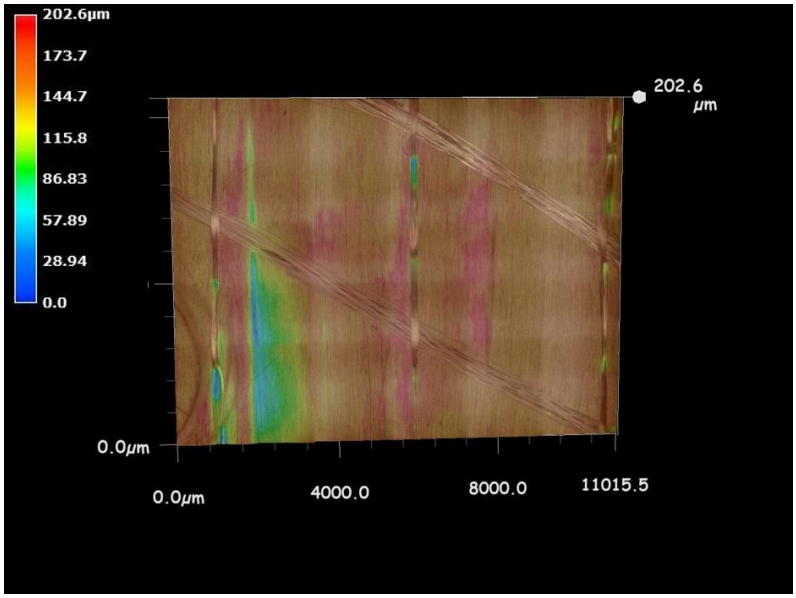

Figure 3.17. Topography of non-crimp stitched carbon fabric 106

Figures 3.18 and 3.19 illustrate the topographies of fabrics 107 and 108 with crimp factors of 194.0 µm and 392.0 µm respectively. The 4-harness satin structure in Figure 3.18, the 5-harness satin structure in Figure 3.19 and the l00% cover factor in both figures can be observed.

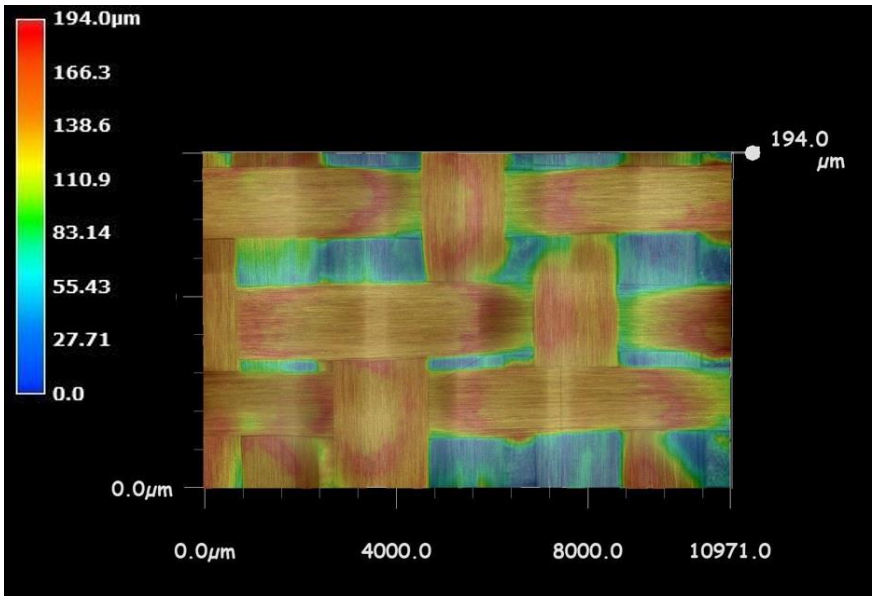

Figure 3.18. Topography of 4-harness carbon fabric 107

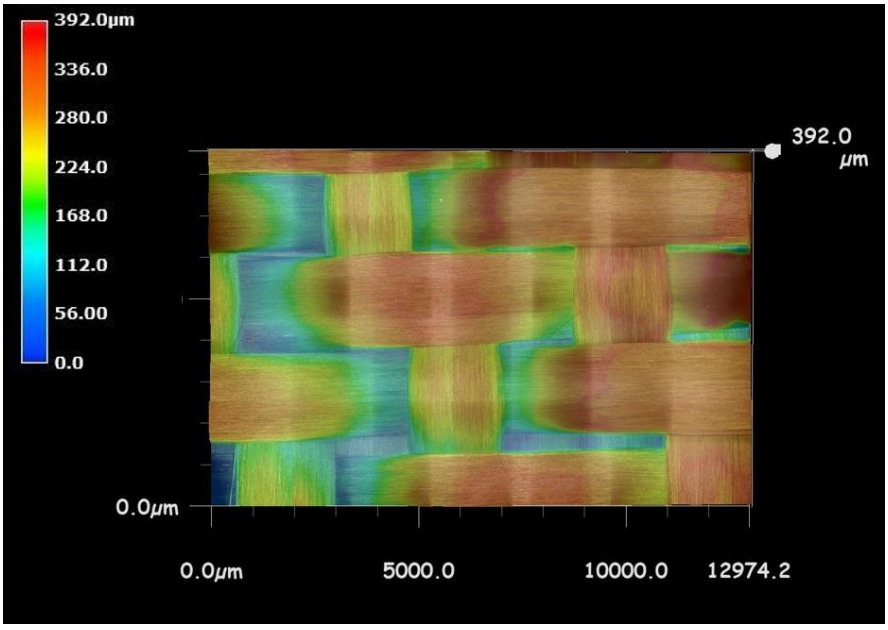

Figure 3.19. Topography of 5-harness carbon fabric 108

Figures 3.19 and 3.20 illustrate the topographies of fabrics 109 and 110 with crimp factors of 494.0 µm and 0 µm (non-crimp fabric) respectively. The presence of binder in Figure 3.20, the NCF structure in Figure 3.21 and the l00% cover factor in both figures can be observed.

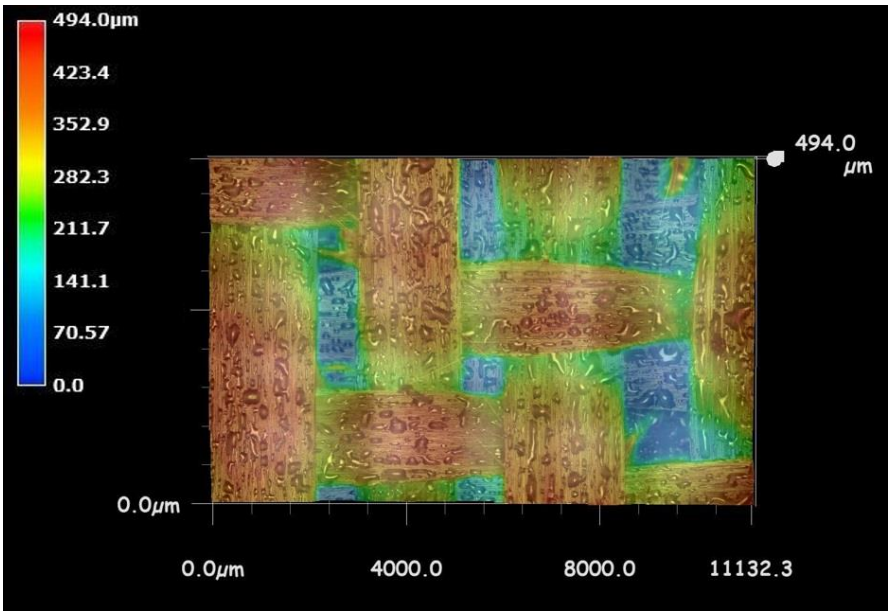

Figure 3.20. Topography of 2.5-D carbon fabric 109 with binder

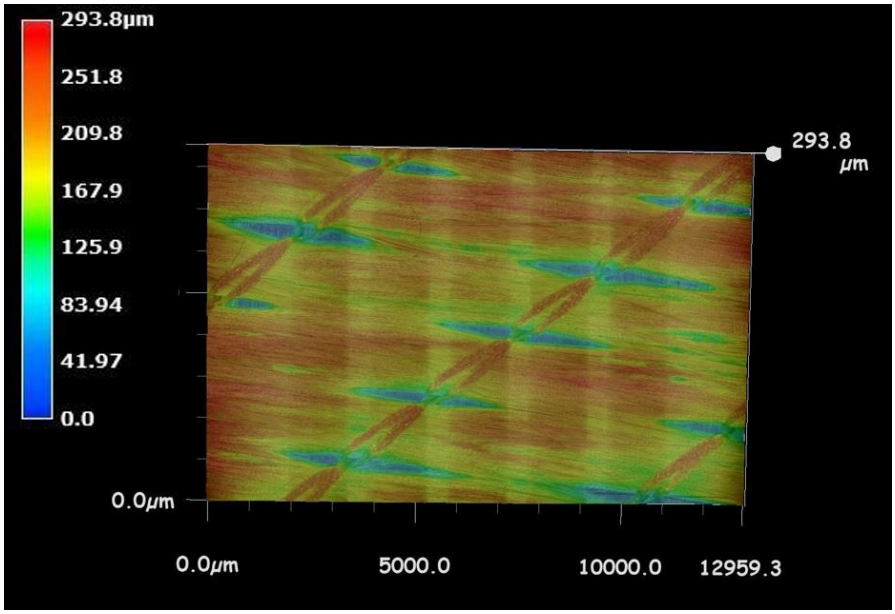

Figure 3.21. Topography of NCF 3K carbon fabric 110

Figure 3.21 illustrates the topography for fabric 111 with crimp factor of 0 µm (non-crimp fabric). The NCF structure in and the l00% cover factor can be observed.

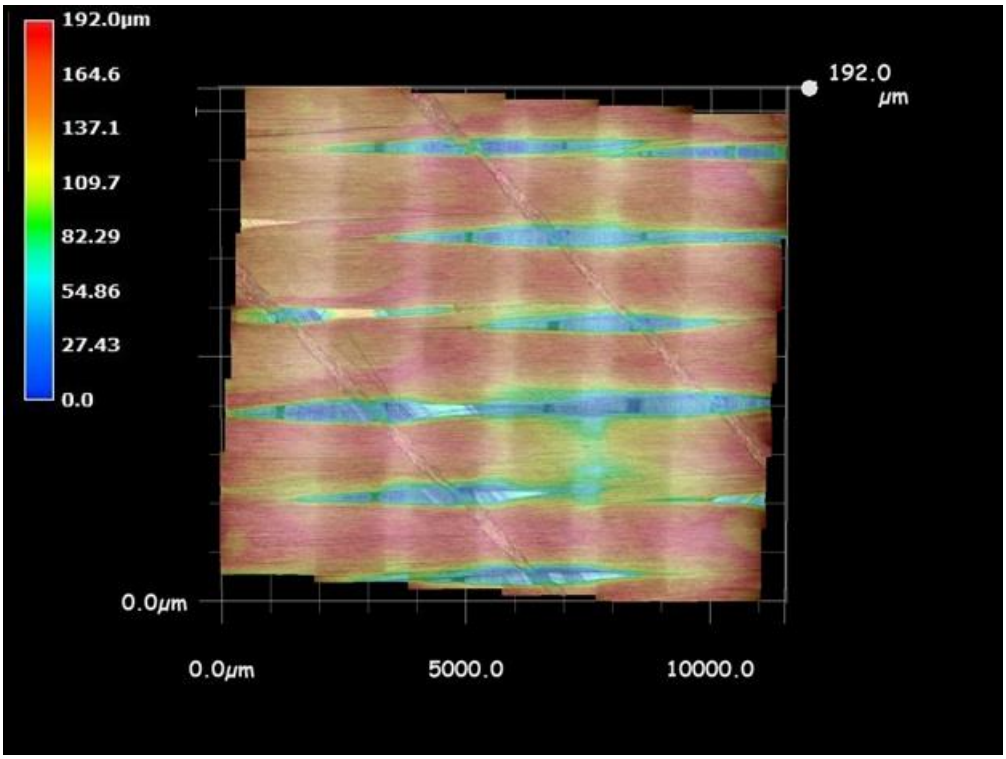

Figure 3.22. Topography of NCF 6K carbon fabric 111

3.4 Discussion

This chapter introduced 11 reinforcement fabrics probed in this work. Section 3.2 introduced textiles parameters, and their measurement methods. This section also featured this data in Table 3.1 along with photographs of all textiles. Furthermore, Section 3.3 illustrated fabric topographies. Eight of the textiles were weaves including plain 101, twill 102 and 104, satin 103, 105, 107 and 108, and 2.5-D 109. Fabrics 106, 110 and 111 were NCF textiles.

Chapter 4

Shear Tests

4.1 Introduction

Results presented in this chapter determine how fabrics performed in bias extension in-plane shear tests [35]. Since shear tests cannot be performed for triaxial fabrics, no results are presented for fabrics 106, 110 and 111. Tests were conducted for all biaxial weaves. Each fabric was tested 3 times, using a different sample with each repeat. Test specifications and procedures are explained in Section 4.2. Section 4.3 presents the shear test results, and Section 4.4 relates them to fabric parameters. Section 4.5 delivers the discussion for this chapter

4.2 Apparatus and methodology

The characterization machine defined below was developed at Hutchinson primarily by Master's candidate Sébastien Gagné. This section offers a brief description of the capabilities and test procedures, as well as the aim of tests. The machine can run 2 tests: the shear tests discussed in this chapter and the friction tests discussed in Chapter 5. The machine consists of a motor, torque sensor, controller, displacement hardware, and a laptop to track and record the data. The machine

can be used to derive characteristics including maximum shear extension, shear force, friction between plies and friction between a single ply and a mould. Figure 4.1 illustrates the components of this machine.

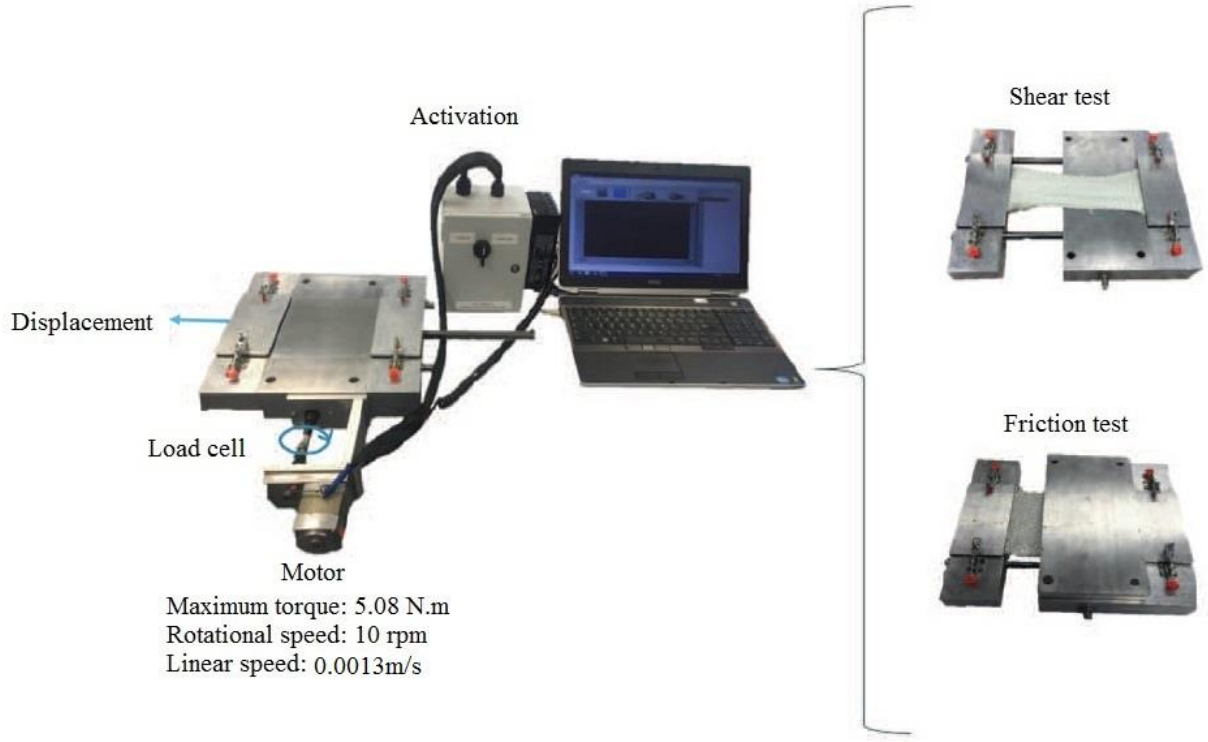

Figure 4.1. Characterization tool [36]

The general concept of the displacement hardware is shown in Figure 4.2. Parts include a fixed and a moving block, an input shaft as well as 4 clamps. Components are all made of aluminium while the shafts and clamps are made of steel. Two clamping plates are held by two clamps each for fixing the tested fabric. The input shaft is connected to a torque sensor for measuring the resistive torque during the test.

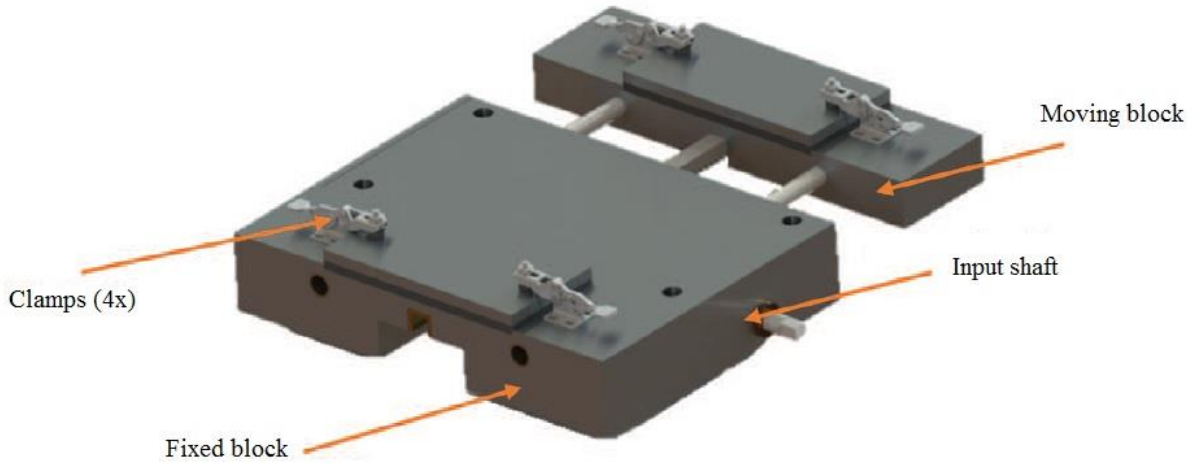

Figure 4.2. General concept of device [36]

Figure 4.3 illustrates a partial view of the components of the displacement hardware including the rack, pinion, input shaft, bearings and guiding rods. The rack is attached to the moving block using screws. The pinion is also attached to the input shaft using screws as well. The moving block and the bearing follow the linear movement of the rack, without vibration.

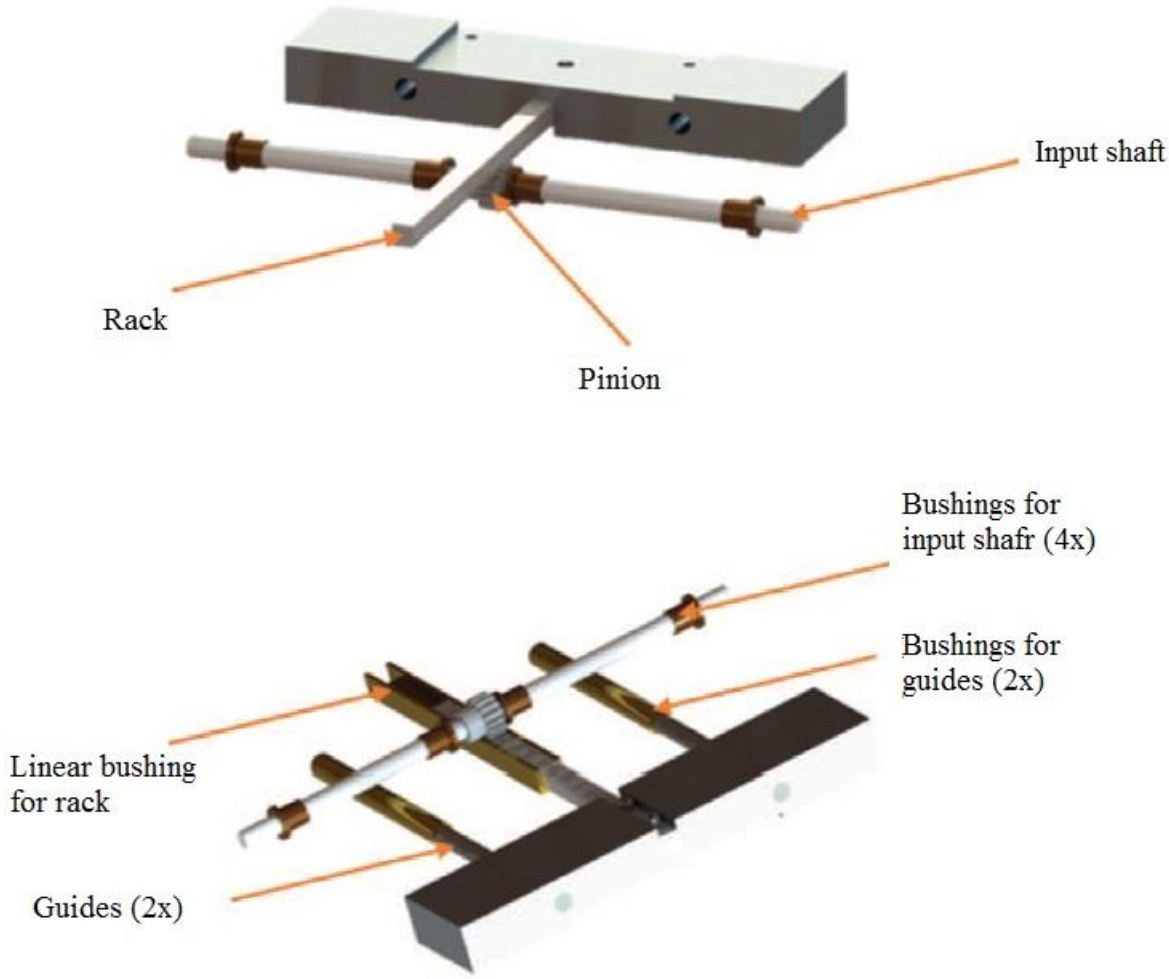

Figure 4.3. Mechanisms of the characterization tool [36]

Figure 4.4 shows the clamping plates, each side used for holding the fabrics. Figure 4.5 illustrates the assembly of each clamping plate and the fabric placement for shear tests.

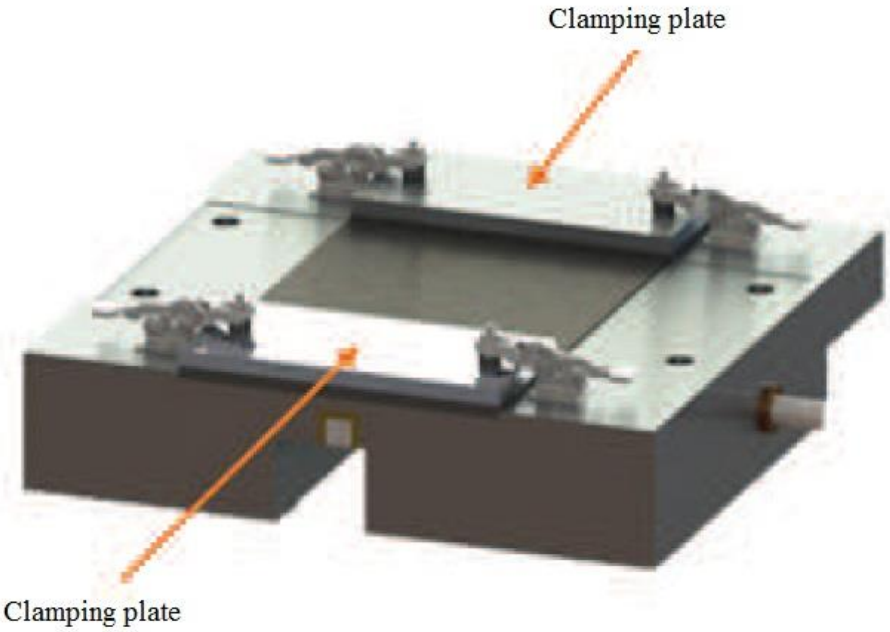

Figure 4.4. Clamping of the tool [36]

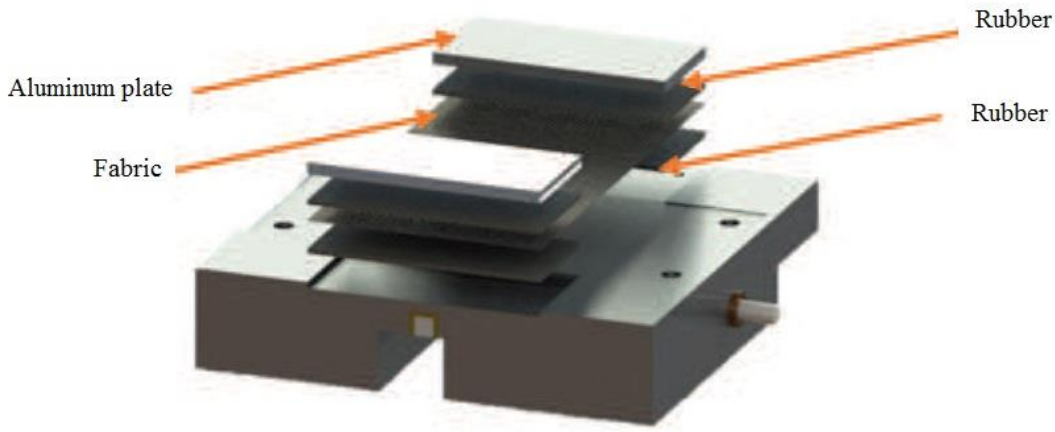

Figure 4.5. Assembly of the clamping plates [36]

Figure 4.6 shows the orientation of fabric samples for the test, which require that the yarns be oriented at -45°/+45° of the displacement direction to enable shear. The figure also indicates the dimensions of the specimen along both directions.

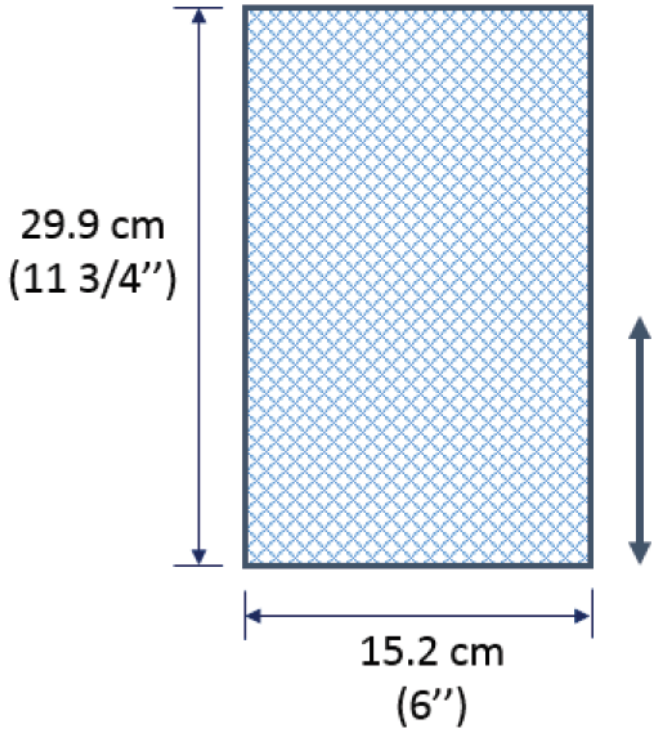

Figure 4.6. Dimensions of in-plane shear test specimen [36]

The maximum shear extension was measured manually upon each test, using a 300 mm ruler. Data are reported in Table 4.1. Figure 4.7 illustrates the clamping of a shear test sample as well as the maximum extension of a fabric, reached after it is locked at the end of the test.

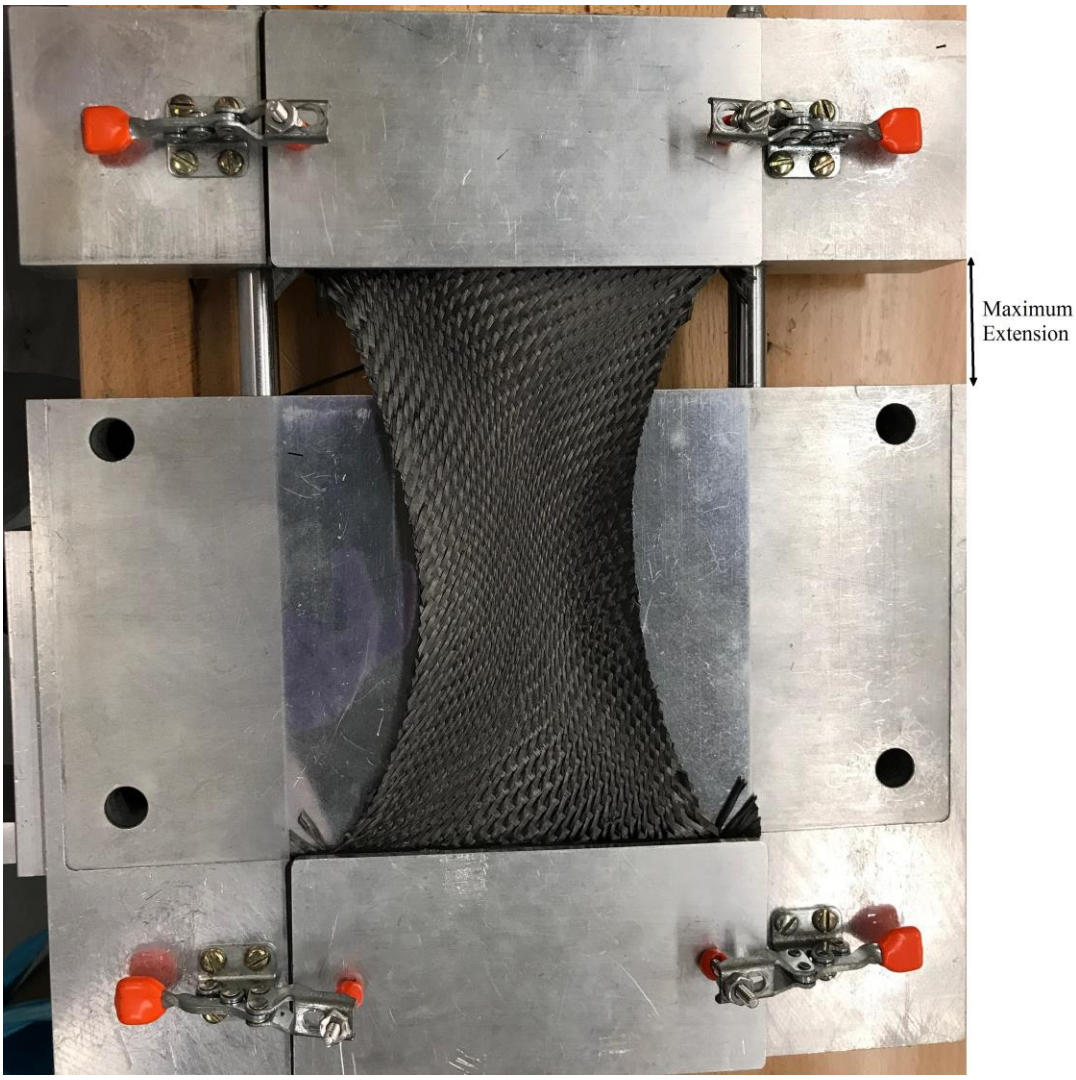

Figure 4.7. Clamping and maximum extension in the shear test

The approximate displacement speed is 1.3 mm/s and the approximate test duration varies from 6 to 10 seconds.

4.3 Results

Bias extension tests were run 3 times for fabrics 101, 102, 103, 104, 105, 107, 108 and 109. The normalized force (N) is plotted as a function of time (s) [37] for fabric 101 as an example of

typical results, Figure 4.8. The reason for reporting time is that each data point is obtained every 0.1 second by the data acquisition system of the machine. For most tests conducted, fabrics reached locking angle and the machine stopped. Figure 4.8 demonstrates good reproducibility for the tests conducted. The existence of jumps in the plotted data is because of the resolution of the load cell used in the device.

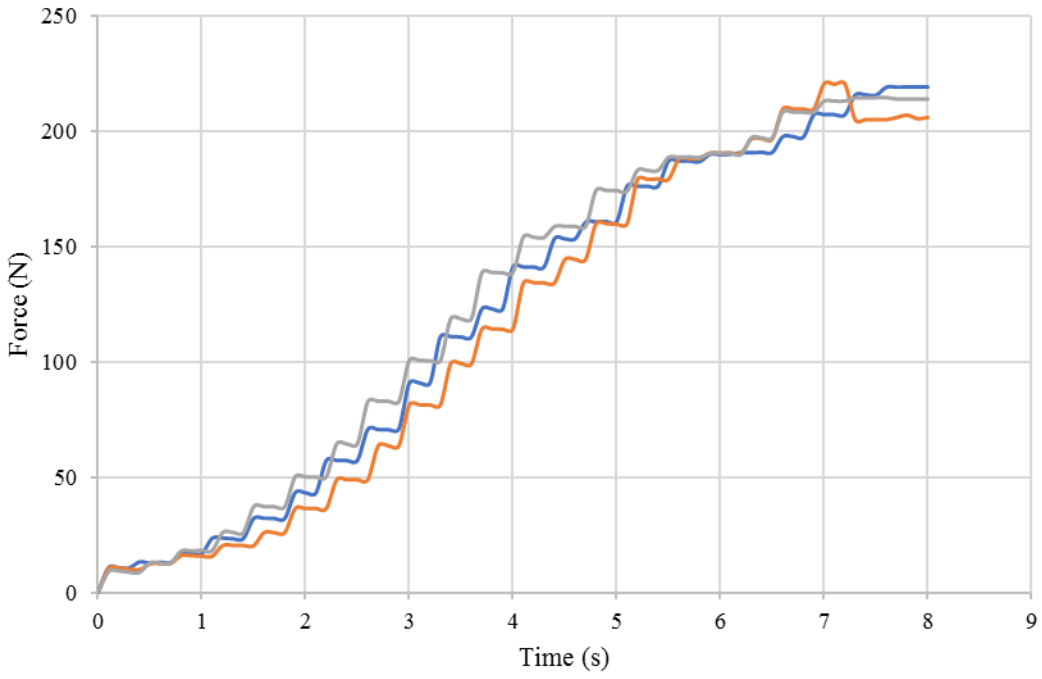

Figure 4.8. Shear tests for fabric 101

Table 4.1 lists the measured maximum shear extension for each tested fabric along with fabric number, fibre type and architecture. The shear tests ended when the fabrics reached its locking angle and wrinkled and the device reached the maximum load. However, fabrics 107 and 108 frayed after reaching their locking angle and the device did not reach maximum loads in those cases.

Table 4.1. Maximum shear extension for fabrics tested

Fabric number	Fibre	Architecture	Shear extension (mm)
101	Glass	Plain	143.05
102	Glass	Twill	104.64
103	Glass	8-harness satin	91.87
104	Carbon	Twill	103.79
105	Carbon	5-harness satin with binder	96.38
107	Carbon	4-harness satin	102.11
108	Carbon	5-harness satin	99.25
109	Carbon	2.5-D with binder	85.52

4.4 Analysis

Shear extension is plotted as a function of different fabrics parameters: fabric type, architecture, cover factor, thickness, surface density and yarn count, as shown in Figures 4.9 to 4.16.

Looking at Figure 4.9, glass fibre fabrics demonstrated a higher average shear extension compared to carbon fibre fabrics. The figure also indicates a lower variability of shear extension for carbon fibre fabrics compared to glass fibre fabrics. However, given the large overall

variability of results within each group, it is not possible to separate the two groups in a statistically significant way.

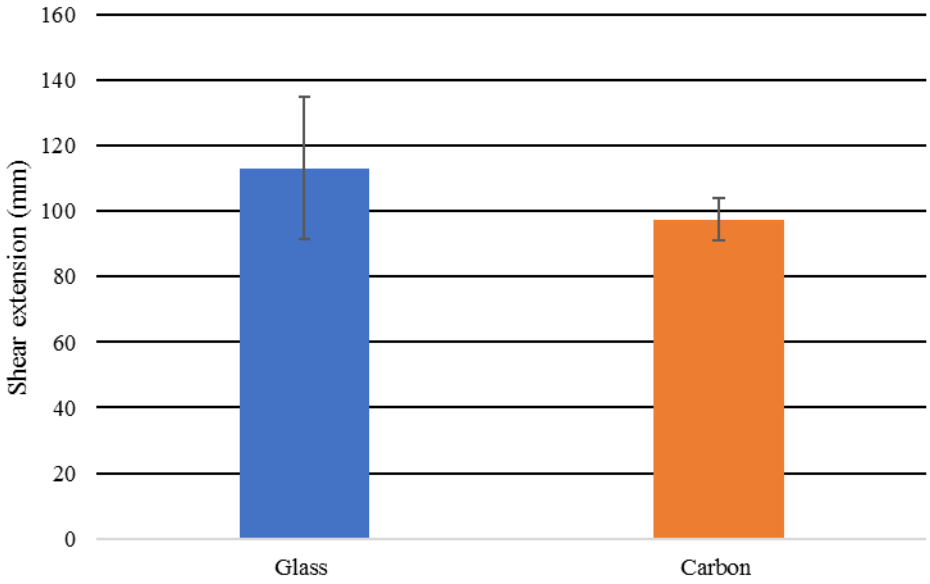

Figure 4.9. Maximum shear extension for glass and carbon fibres

Figure 4.10 ranks fabric extensions based on fabric architectures, from plain weave followed by twill weave, satin weave and woven fabrics with binder respectively. This figure elucidates the relation between fabric architecture and locking angle [38] for the fabrics tested. Fabrics with binder showed the highest variability, followed by satin weave and plain weave.

Twill weaves showed the lowest variability amongst the fabrics tested. The only group that is statistically different from the others is the first one, whereas the plain weave fabric behaves differently from the 3 other groups.

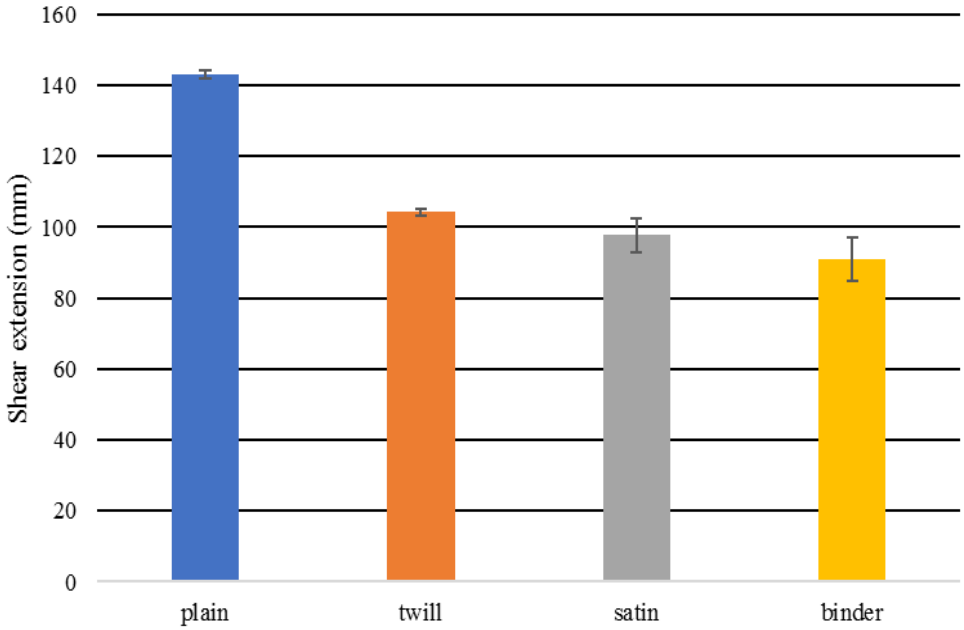

Figure 4.10. Maximum shear extension between different architectures

Figure 4.11 plots shear extension as a function of surface density. The linear regression shows a R^2 factor of 0.15, which is weak. Fabrics 102, 104, 108 and 109 seem to follow the trend more clearly. However, fabrics 101 and 103 deviate significantly from it.

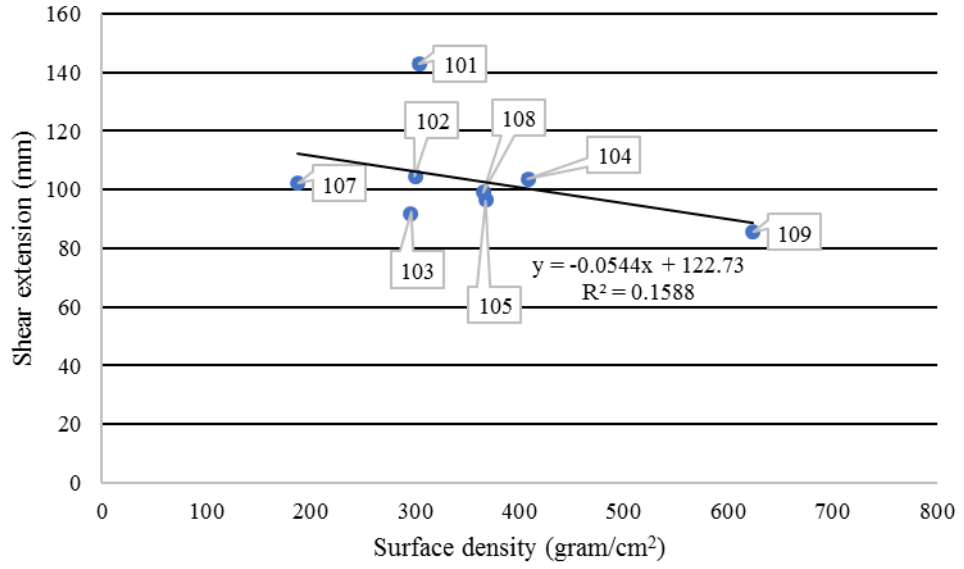

Figure 4.11. Maximum shear extension as a function of surface density

Figure 4.12 plots the data for shear extension as a function of yarn count for the tested textiles, with a R^2 of 0.06. Fabrics 102, 103, 104 and 107 are on trend but other fabrics deviate from it. It seems that fabric 101 deviates significantly due to its large shear extension.

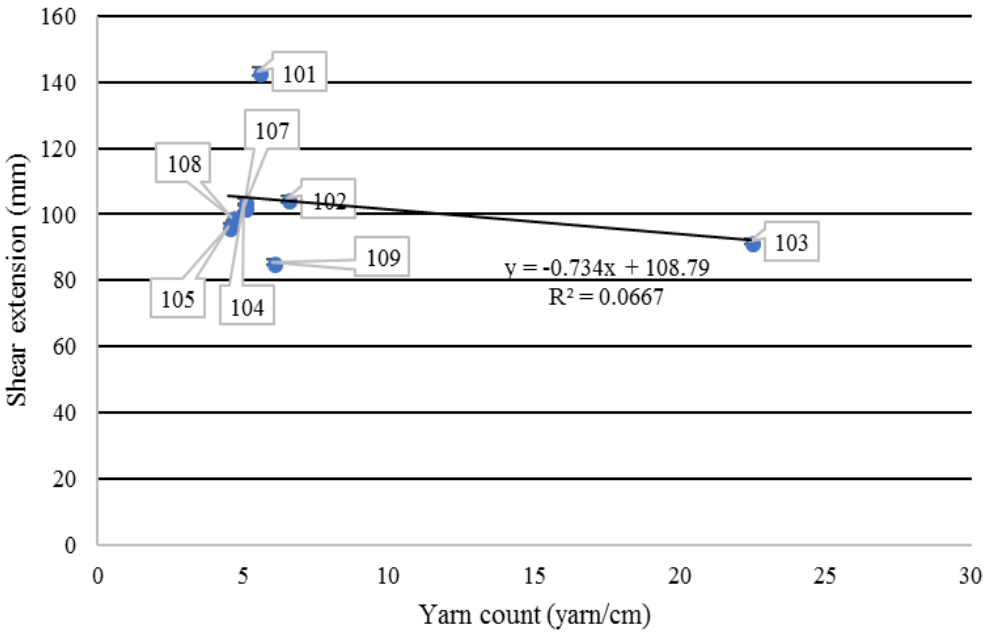

Figure 4.12. Maximum shear extension as a function of yarn count

Figure 4.13 shows a correlation with a R^2 factor of 0.89 which indicates a reasonable relation between shear extension and the cover factor. Fabrics 101, 103, 104 and 105 follow the trend noticeably, with other fabrics also in relatively good agreement with the linear trend identified. Fabric crimp as an independent variable delivers a lower R^2 factor of 0.30, as shown in Figure 4.14.

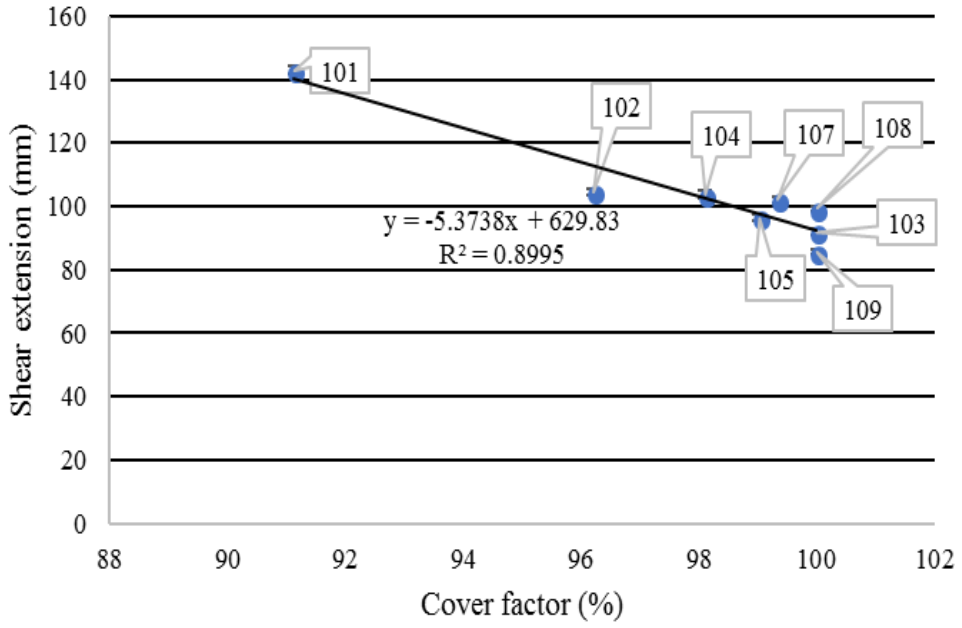

Figure 4.13. Maximum shear extension as a function of cover factor

Looking at Figure 4.14, fabrics 104, 105, 108 and 109 show a relation amongst each other, but 101, 102 103 and 107 fabrics deviate from this relation.

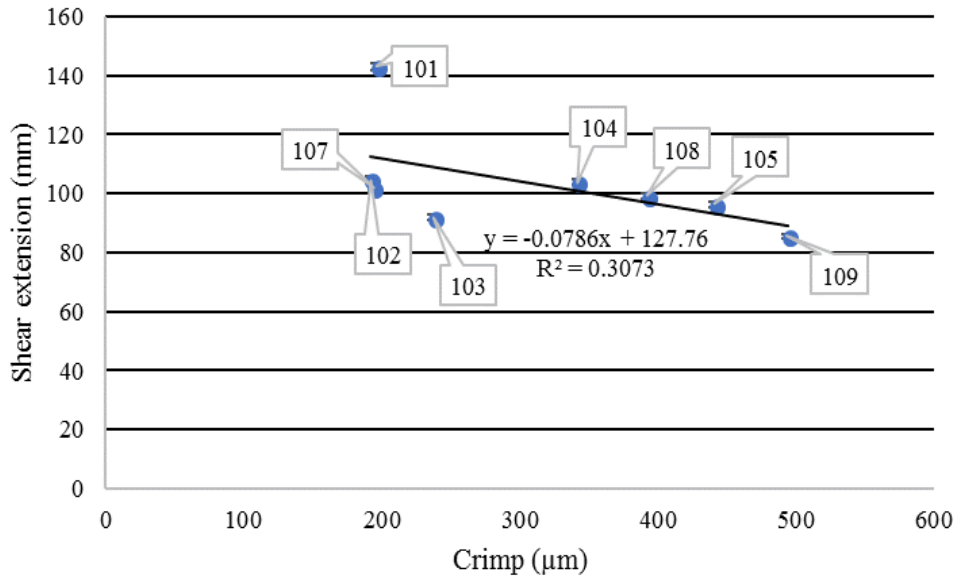

Figure 4.14. Maximum shear extension as a function of crimp

Figures 4.15 and 4.16 indicate that thickness with pressure and without pressure deliver R^2=0.21 and R^2=0.23 respectively when completed with shear maximum extension of fabrics, indicating that thickness is not a significant indicator of the propensity of a fabric to shear. It can be observed that in both figures, fabrics 102, 104, 107,108 and 109 follow a trend amongst each other and fabrics 101 and 103 deviate from it.

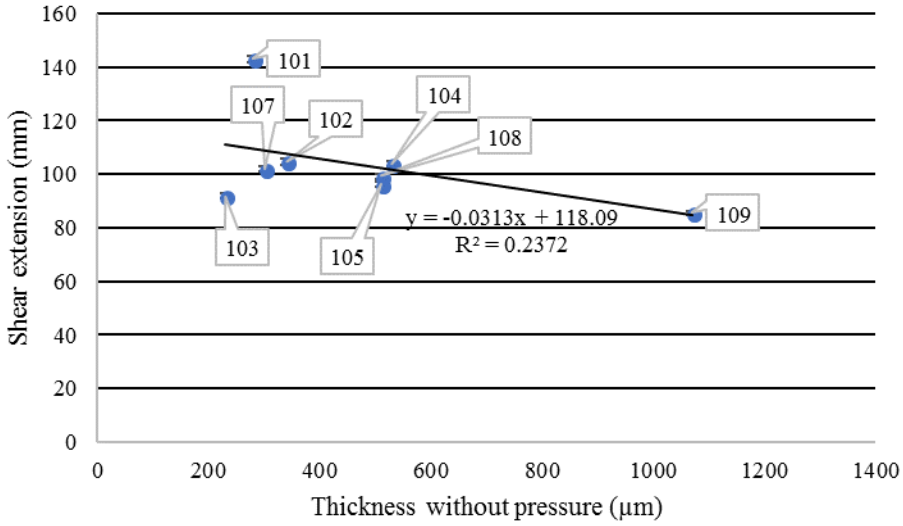

Figure 4.15. Maximum shear extension as a function of thickness without pressure

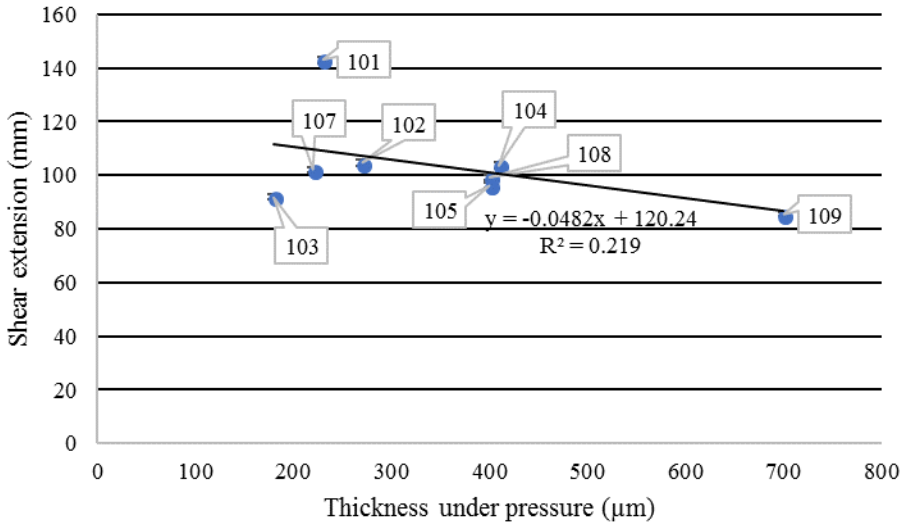

Figure 4.16. Maximum shear extension as a function of thickness under pressure

4.5 Discussion

Bias extension tests were carried out on multiple fabrics with different architectures. Shear force, which was plotted in Figure 4.1, includes yarn tension and yarn slippage friction [39]. It was observed that the cover factor has a clear effect on shear extension for the range of fabrics tested. In a study conducted by Commonwealth Scientific and Industrial Research Organization, the cover factor and shear extension were measured for plain woven and twill woven fabrics [40]. That study identified a correlation factor of 0.76 between the cover factor and the maximum extension for the textiles tested. In the present work, plain, twill, satin weaves and fabrics with binder including a 2.5-D woven fabric were tested and returned a correlation factor of 0.89.

Moreover, plain weave fabric 101 demonstrated the highest shear extension amongst other architectures. On the other hand, fabrics with binder and satin woven textiles showed the lowest shear extension.

While crimp did not show a strong relation with shear extension, it illustrated a noticeable trend between fabrics 104, 105, 108 and 109. Both thickness under and without pressure did not demonstrate a strong trend as a function of shear extension; however, fabrics 102, 104, 107, 108 and 109 were seen to have a relation amongst each other.

Higher shear extension allows the draping process to be easier and less problematic as it allows the fabric to be draped easier on double curvatures, with more reproducibility.

Chapter 5

Friction Tests

5.1 Introduction

Industrial practice shows that when draping multi-layer fabrics, friction between plies and friction of the lowest-positioned ply with the mould have an impact on the draping process. Higher friction between plies allows the stack of reinforcement layers to behave as a single ply and it reduces the slippage between plies. Lower friction between plies and the mould, on the other hand, makes handling more problematic [41]. In this chapter the results of friction tests between plies, and friction tests with aluminium plates are presented and discussed.

5.2 Apparatus and methodology

The characterization device described in Chapter 4 was used for the friction tests. Two configurations were used for measuring the friction force. One configuration aimed at measuring the friction between plies. The second configuration measured the friction between a single ply and an aluminium surface. Two layers of fabric were sandwiched between another two layers of fabric. The former group was clamped to the moving block, and the latter to the fixed block. A

plate with a mass of 10kg was positioned on top of the plate for increasing the applied friction. Each test was repeated 5 times, using a different sample each time and for each fabric. Figure 5.1 shows the friction test configuration.

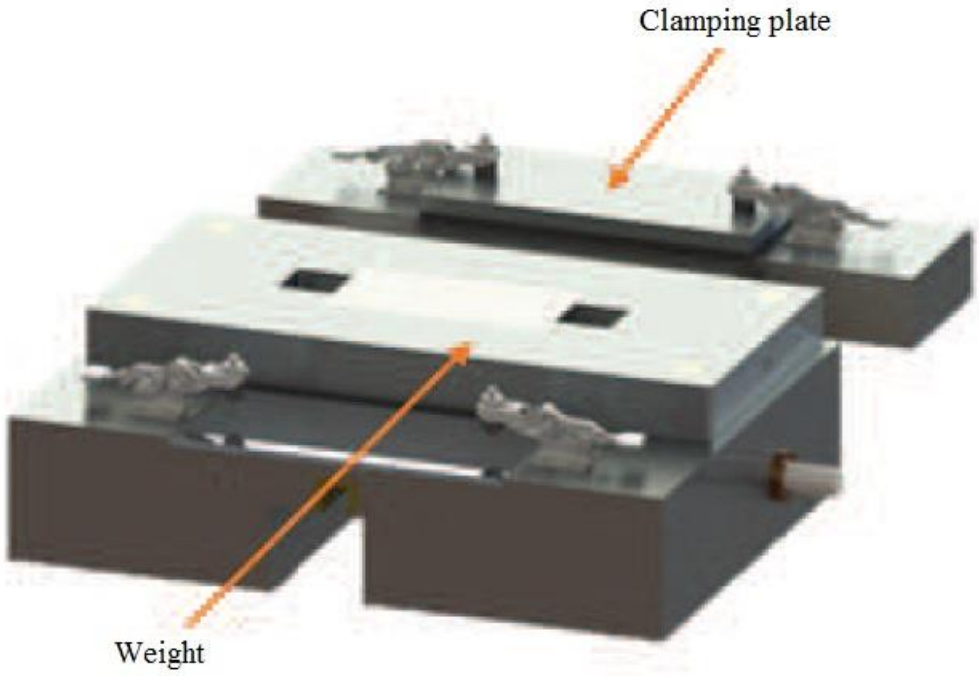

Figure 5.1. Fixed clamping plate and weight for the friction test

The linear speed used in tests was 1.3mm/s. Since the speed was consistent, the time may be converted to displacement. Figure 5.2 shows the specimen dimensions for friction tests. The direction of motion was along the long or side of the specimen.

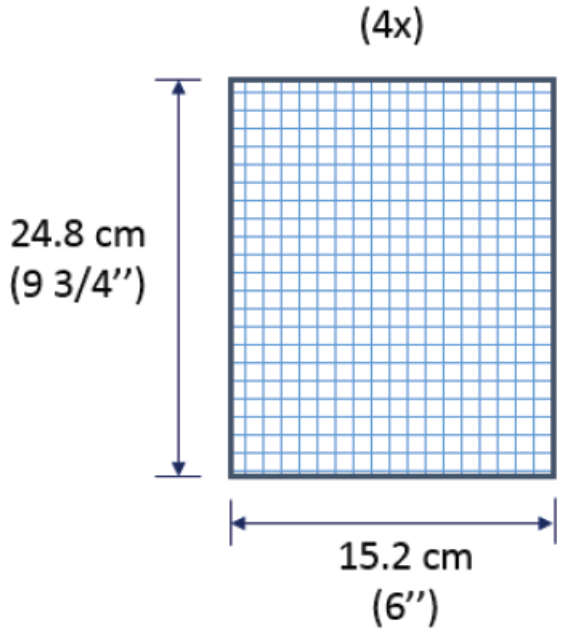

Figure 5.2. Specimen dimensions for the friction test

5.3 Friction between plies

Graphs of the friction force between plies as a function of displacement are presented below. In the graphs, axes are force (N) and displacement (mm). Furthermore, average forces for 5 friction tests performed for each fabric were calculated and compared. Fabrics 106 and 111 were not tested because they were not specified by the industrial partner, and due to limited availability. Figures 5.3 to 5.11 show the force vs displacement data for the friction between plies.

Figure 5.3 shows the data for friction between plies, for fabric 101. All five tests can be observed in the figure, showing variability in the start and at the end of tests. Figure 5.4 illustrates the data for five tests, for fabric 102 while demonstrating visible but limited variability along with an upward trend.

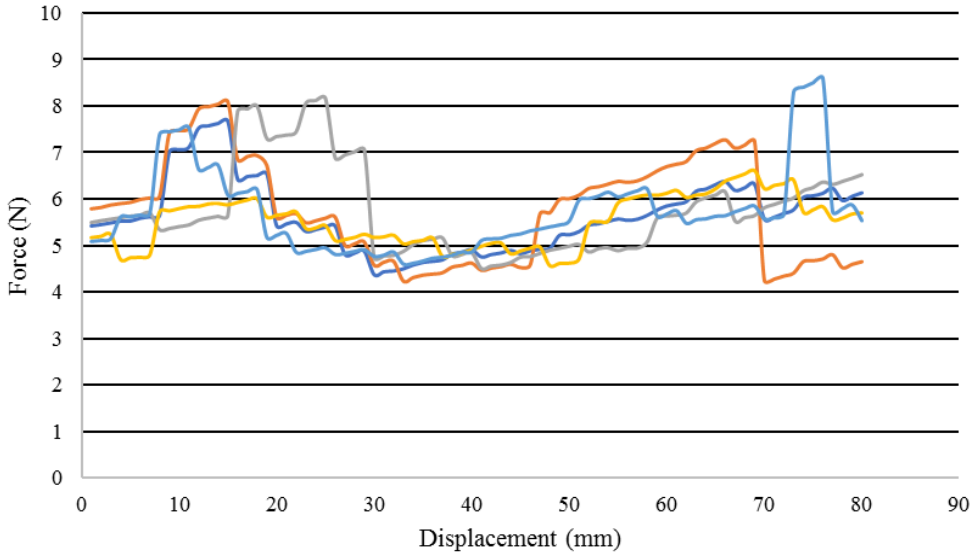

Figure 5.3. Friction between plies for fabric 101

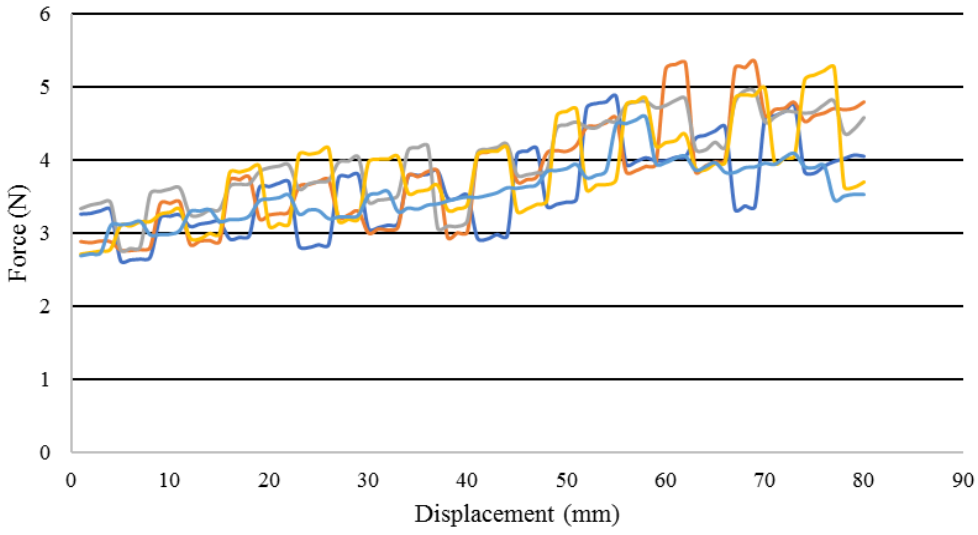

Figure 5.4. Friction between plies for fabric 102

Figure 5.5 shows the five tests results for fabric 103 while showing acceptable variability at the start of the test except for one of the repetitions and visible variability towards the end. Figure 5.6 depicts the test data for fabric 104 with substantial variability starting from the middle of the test.

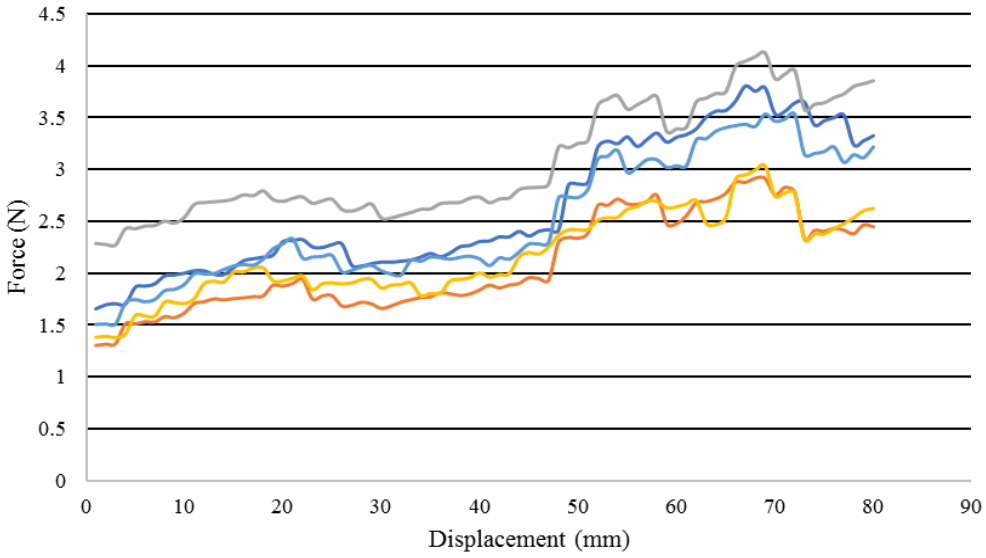

Figure 5.5. Friction between plies for fabric 103

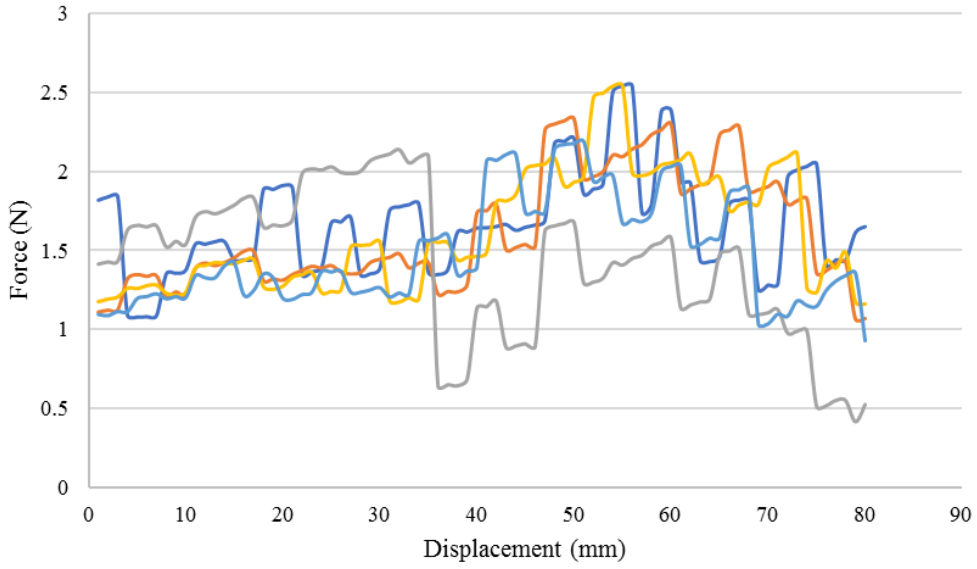

Figure 5.6. Friction between plies for fabric 104

Figure 5.7 illustrates the tests data for fabric 105 and very satisfactory reproducibility. Figure 5.8, however, shows the test results for fabric 107 while having tangible variability for the whole test duration.

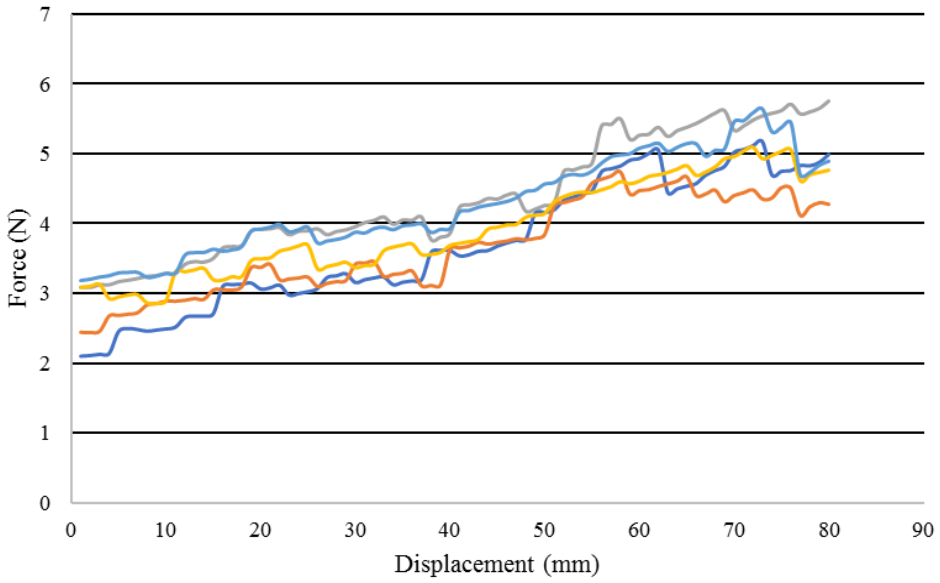

Figure 5.7. Friction between plies for fabric 105

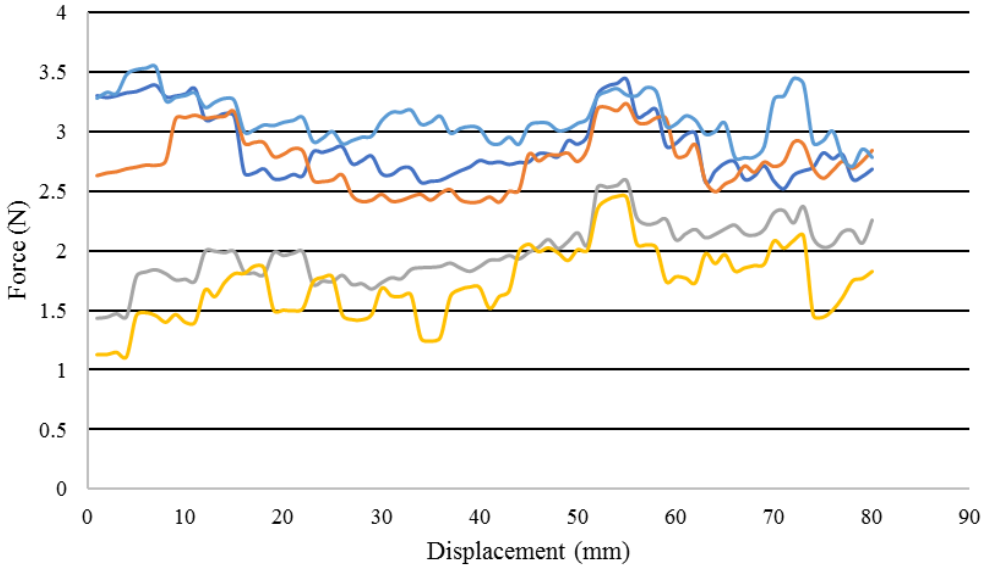

Figure 5.8. Friction between plies for fabric 107

Figure 5.9 shows the test data for fabric 108. While showing variability at the start of the test, this is minimized towards the end of the test. It should be said this fabric demonstrates low amount of friction which is not desirable in the draping process. Figure 5.10 shows test results for fabric 109 while showing a high amount of friction on average, which is an advantage for the draping process.

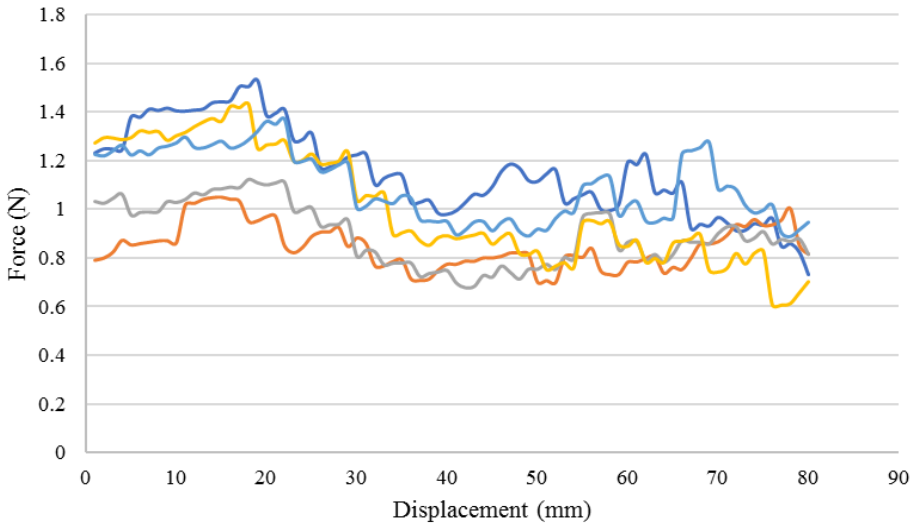

Figure 5.9. Friction between plies for fabric 108

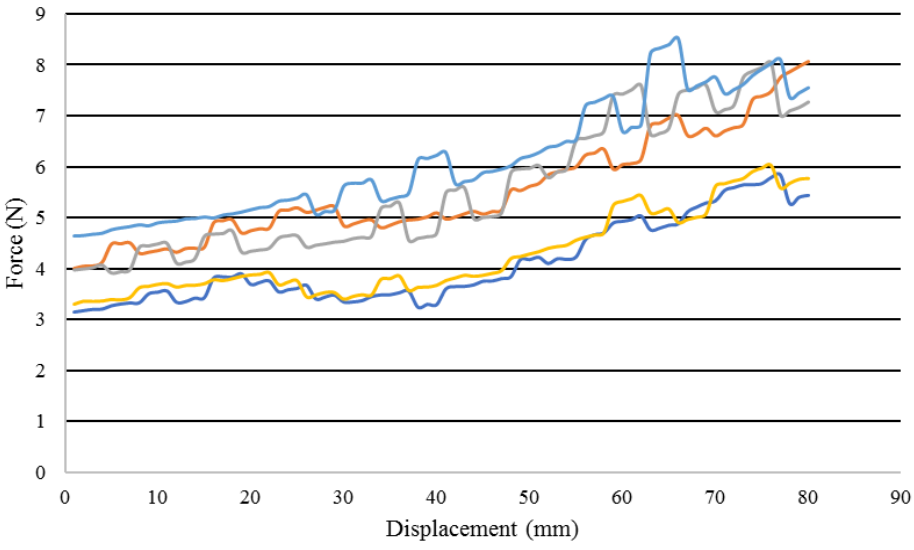

Figure 5.10. Friction between plies for fabric 109

Figure 5.11 shows the data for fabric 110 demonstrating great reproducibility throughout the test for all five repetitions. However, the amount of recorded friction is not substantial for this fabric.

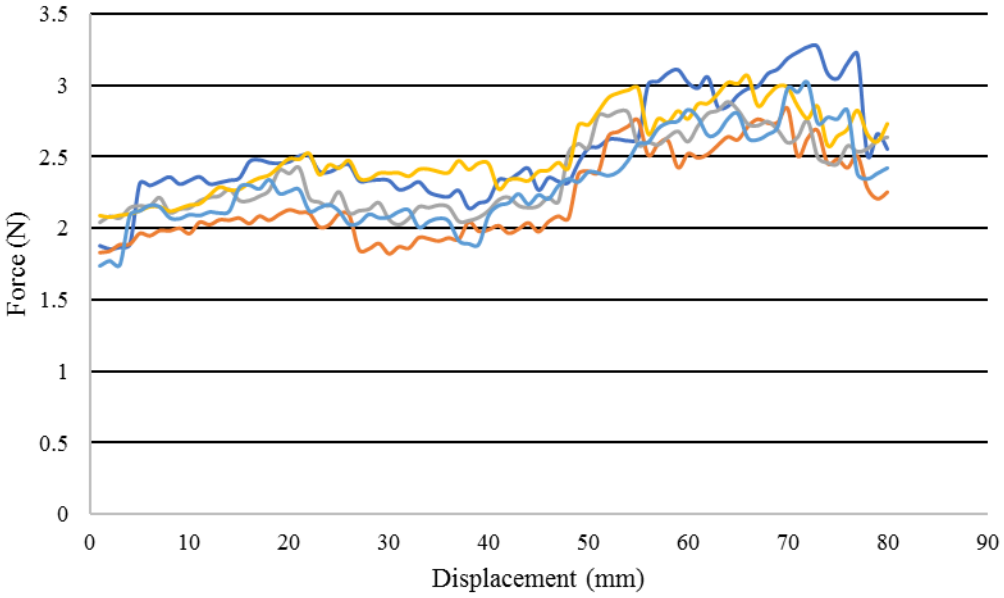

Figure 5.11. Friction between plies for fabric 110

5.4 Analysis

The average of 5 tests for each fabric was obtained and it is positioned in Figure 5.12 for comparison. This shows that fabric 101 has the highest average friction between plies, followed by fabrics 109, 105, 102, 103, 110, 107 and 104. Fabric 108 showed the lowest amount of friction. Moreover, the error bars in following figures demonstrate the standard deviation for each group.

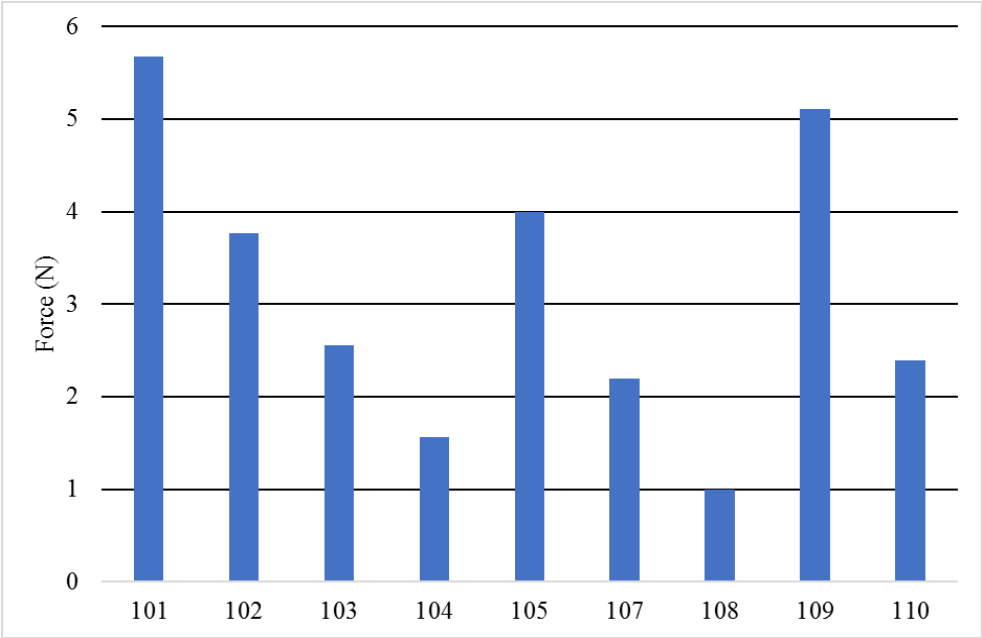

Figure 5.12. Average friction force between plies

Figure 5.13 demonstrates the impact of fabric type on intra-ply friction. It shows that glass fibre fabrics on average show higher friction between their plies. Furthermore, carbon fibre fabrics show slightly higher variability for this friction test configuration. It should be noted that differences between these 2 groups are not statistically significant as shown by the error bars.

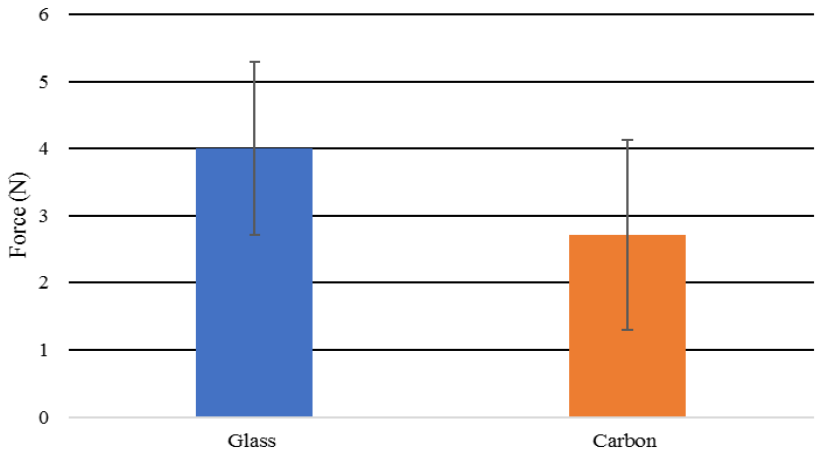

Figure 5.13. Friction force between plies for glass and carbon fibres

Figure 5.14 compares the effect of fabric architecture on inter-ply friction. Results indicate that the plain weave shows the highest friction followed by stitched fabrics and fabrics with binder, while twill and satin weaves show the lowest amount. Stitched and binder fabrics demonstrate the largest variability followed by twill and satin weave. Plain weave showed the lowest variability.

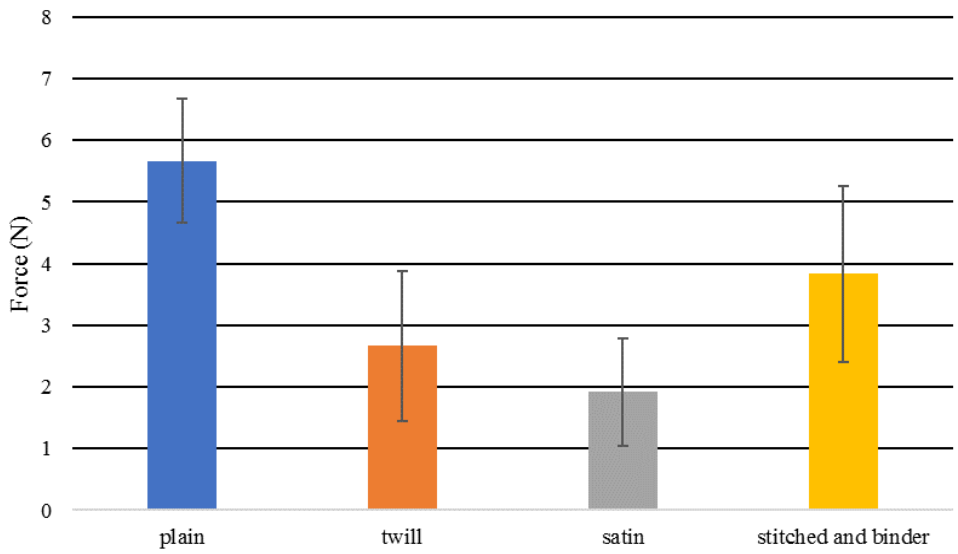

Figure 5.14. Friction force between plies between different architectures

Figures 5.15 and 5.16 plot the inter-ply friction data as a function of surface density and yarn count with R^2 factor values of 0.09 and 0.007 respectively; the data are not indicative of strong relations. However, fabrics 102, 105, 107 and 109 demonstrate a tangible relation and fabrics 103, 104 and 110 demonstrate a noticeable relation amongst each other pertaining to friction between plies and surface density.

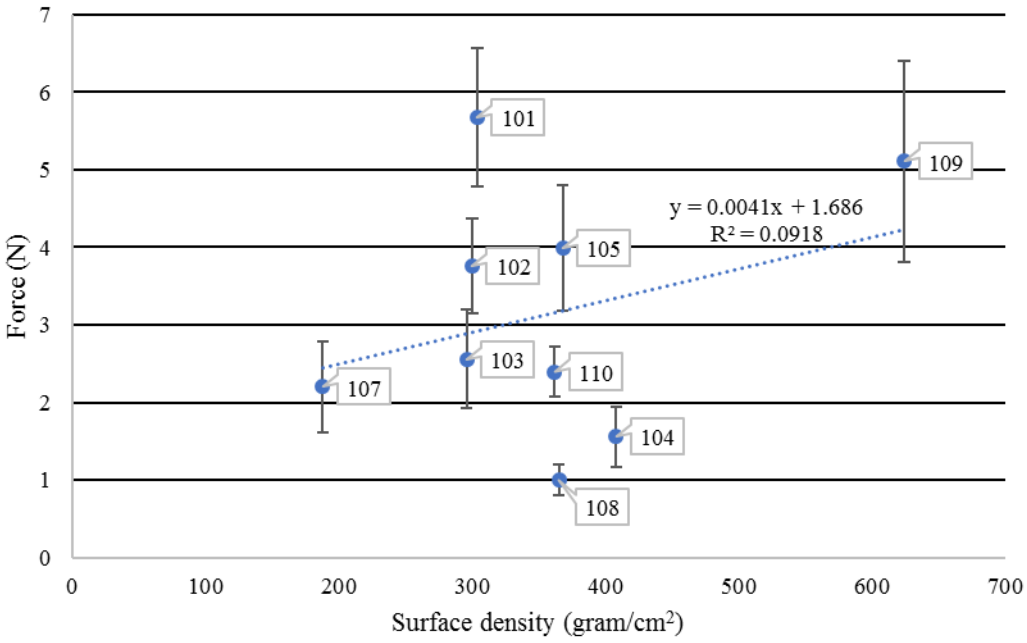

Figure 5.15. Friction force between plies as a function of surface density

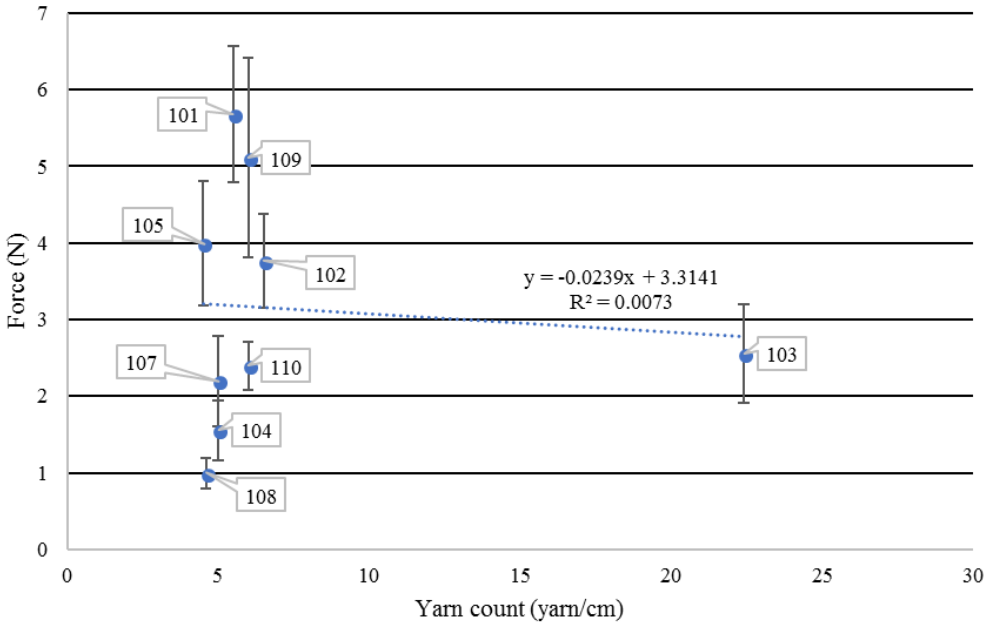

Figure 5.16. Friction force between plies as a function of yarn count

Figure 5.17 shows the friction forces as a function of the cover factor as the independent variable; R^2 is 0.34. Fabrics 101, 102 103 and 110 show a relation amongst each other with regards to cover factor. Figure 5.18 plots the friction force as a function of crimp factor, showing an R^2 factor of 0.01.

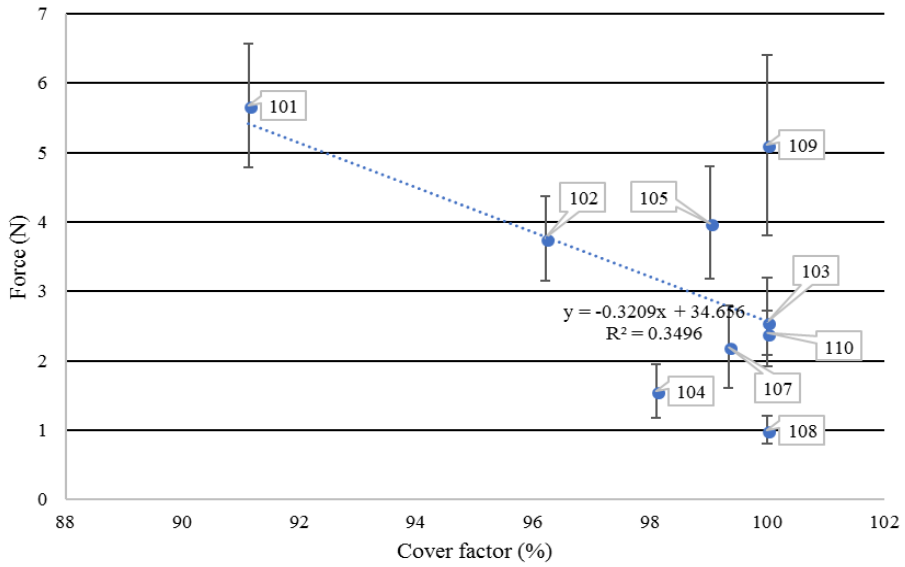

Figure 5.17. Friction force between plies as a function of cover factor

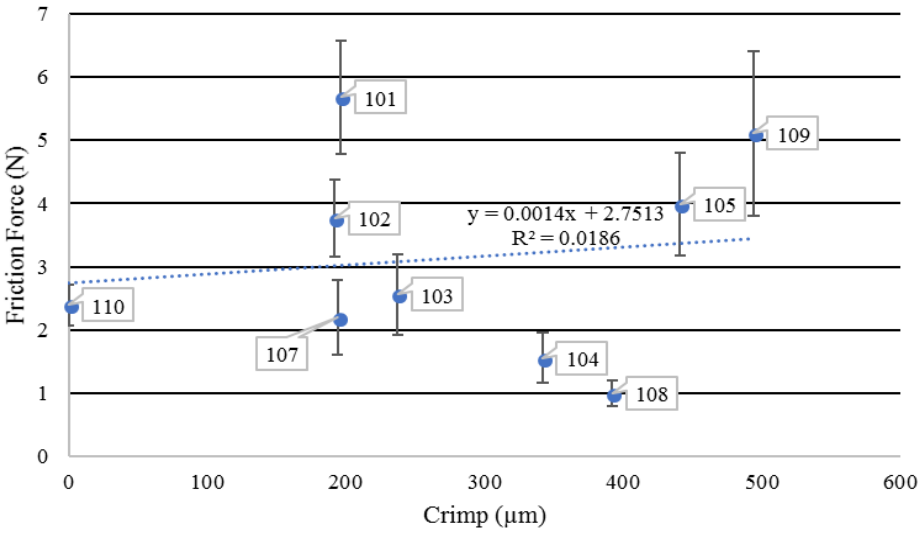

Figure 5.18. Friction force between plies as a function of crimp

Figures 5.19 and 5.20 plot the data as a function of thickness without pressure and thickness with pressure respectively. Although the R^2 factor values are 0.07 and 0.06 respectively, there seems to be a relation for fabrics 102, 105 and 109 as well as another relation between fabrics 103, 104, 107, 108 and 110 in both figures.

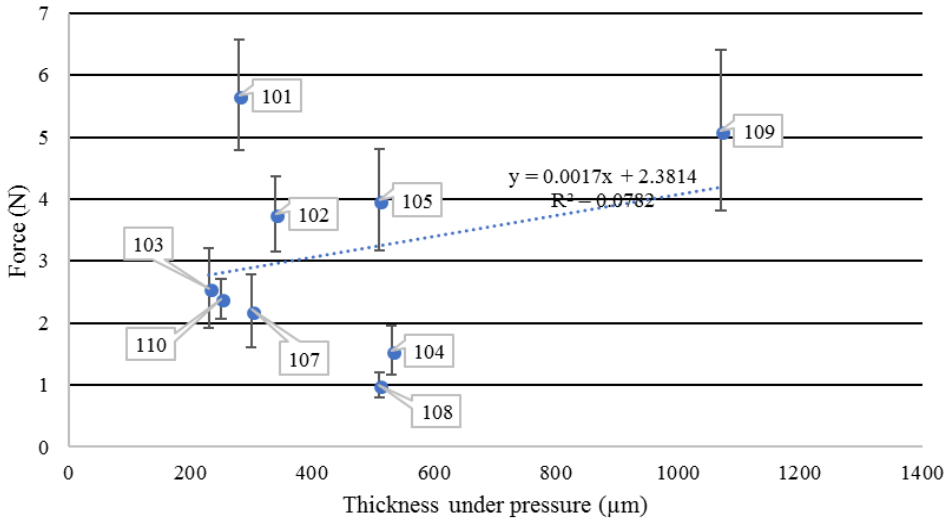

Figure 5.19. Friction force between plies as a function of thickness without pressure

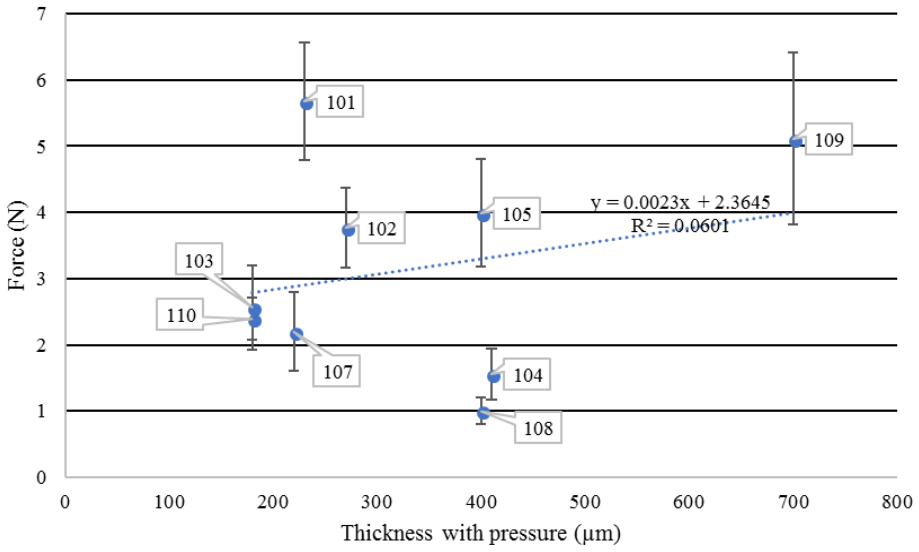

Figure 5.20. Friction force between plies as a function of thickness under pressure

5.5 Friction with aluminium

Results for this test appear as below. Here, 5 different specimens were tested for each fabric. Figures 5.21 to 5.29 show the friction force the data plotted on the graphs as a function of displacement. Figure 5.21 shows the test data for fabric 101. While the data shows reasonable reproducibility in the beginning of tests, it features noticeable variability towards the end.

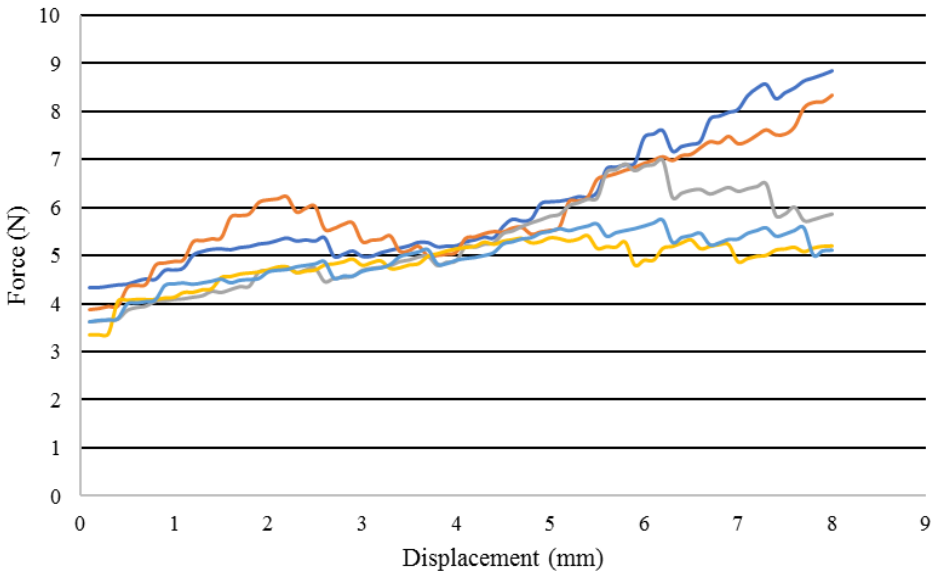

Figure 5.21. Friction with aluminium for fabric 101

Figure 5.22 shows the data for fabric 102, with initially low variability that increases towards the end of the tests. This fabric shows comparatively low friction with aluminium on average. Figure 5.23 demonstrates the results for fabric 103. The reproducibility demonstrated for this fabric is fairly reasonable for all repetitions.

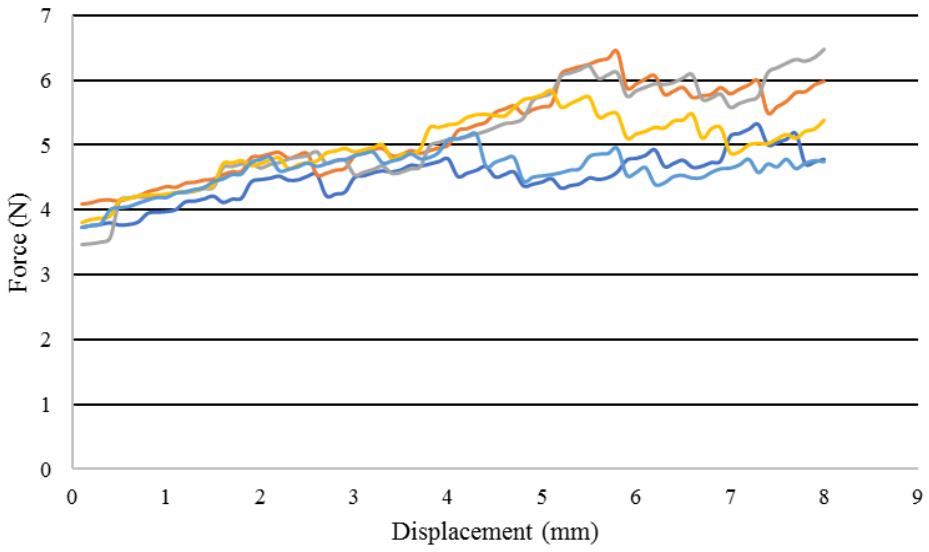

Figure 5.22. Friction with aluminium for fabric 102

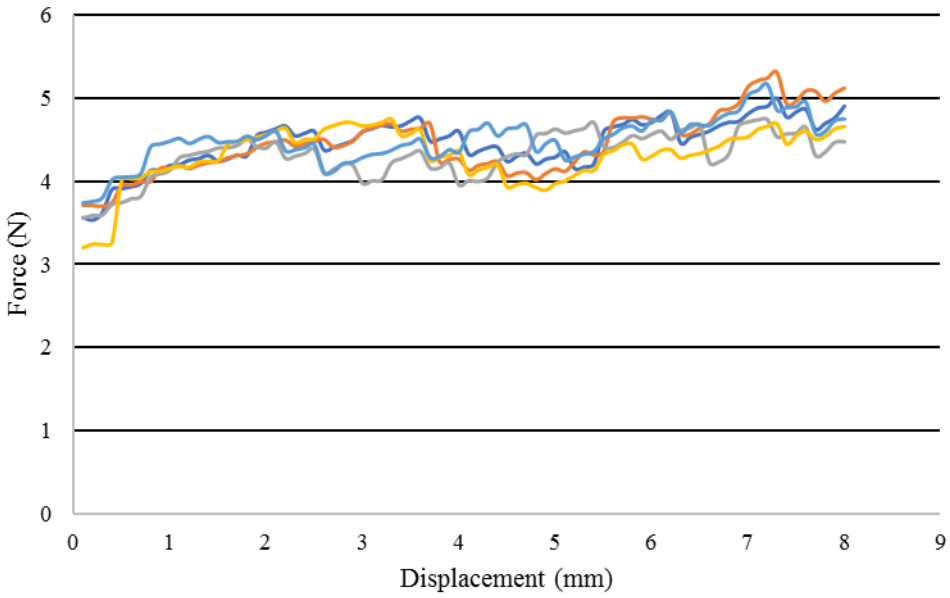

Figure 5.23. Friction with aluminium for fabric 103

Figures 5.24 and 5.25 depict the data for fabrics 104 and 105 respectively. They both show great reproducibility throughout the tests while holding an upward trend. Fabric 105 shows better reproducibility compared with fabric 104.

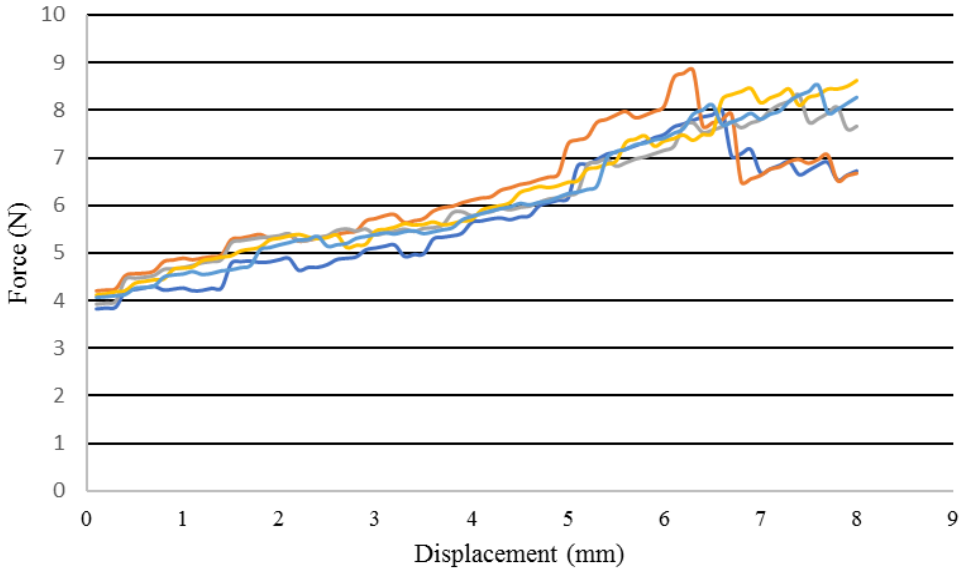

Figure 5.24. Friction with aluminium for fabric 104

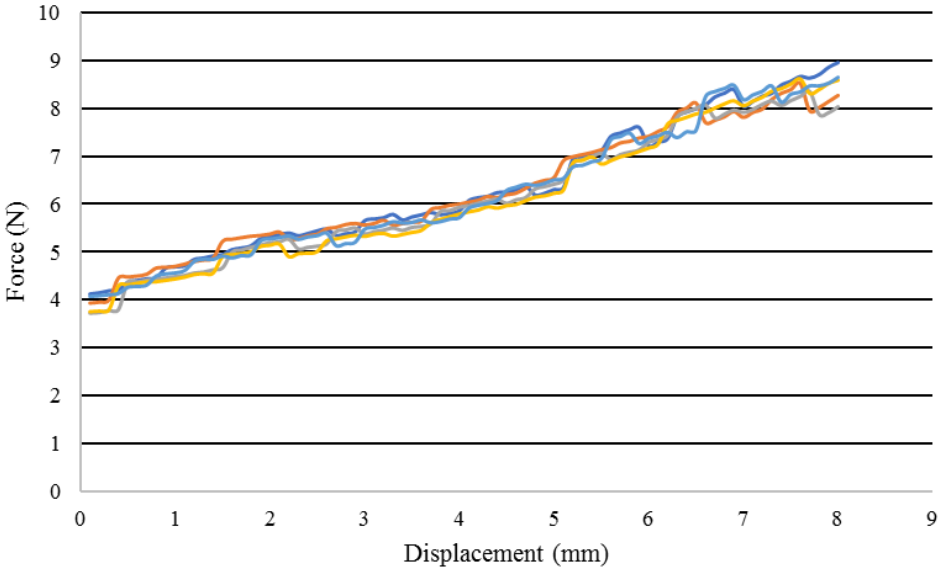

Figure 5.25. Friction with aluminium for fabric 105

Figures 5.26 and 5.27 show the data for fabrics 107 and 108 respectively. Both fabrics show low variability and a steady trend throughout the five tests.

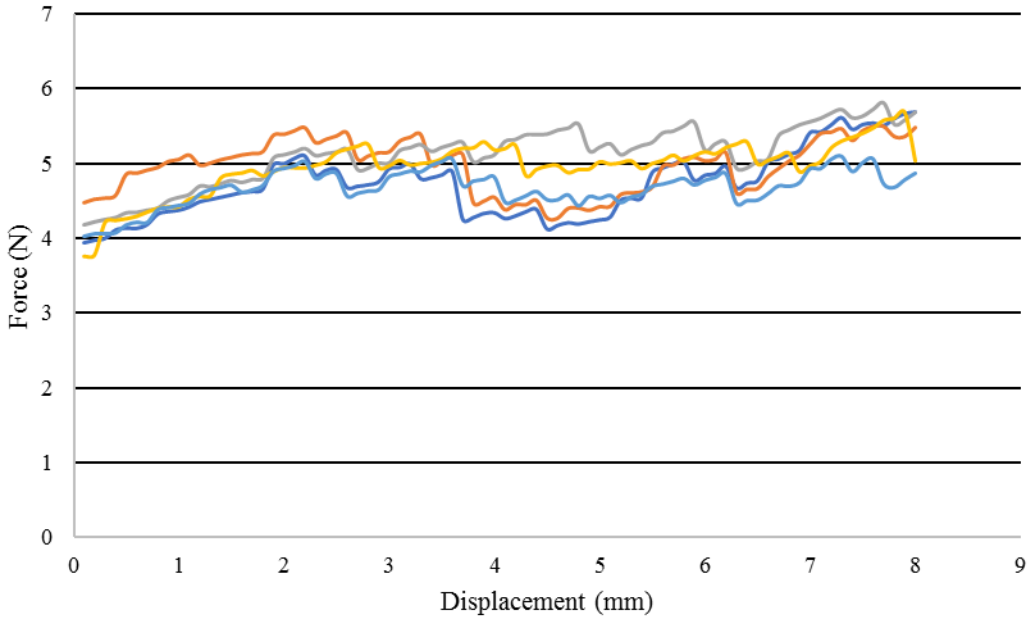

Figure 5.26. Friction with aluminium for fabric 107

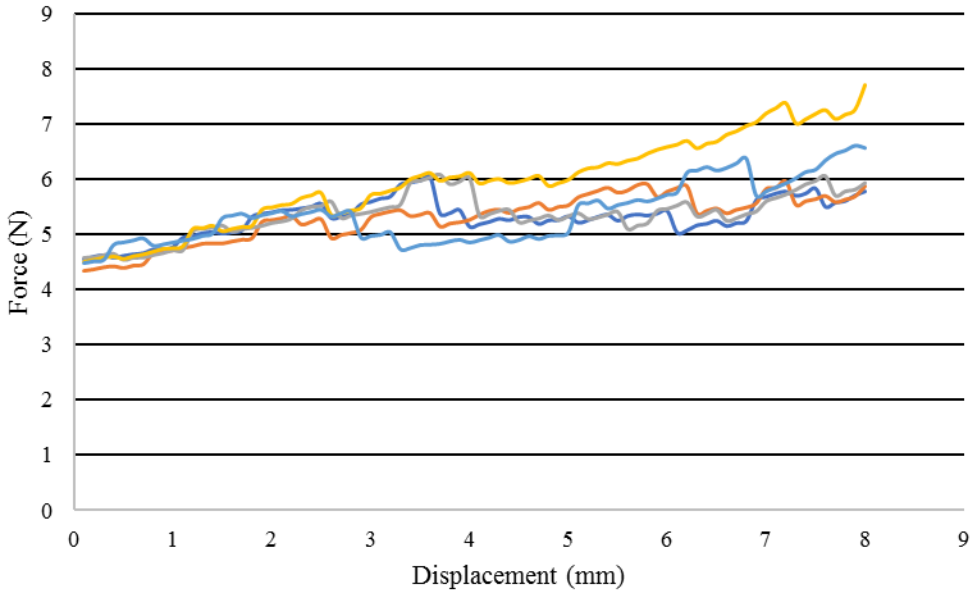

Figure 5.27. Friction with aluminium for fabric 108

Figure 5.28 shows the results of friction tests with aluminium for fabric 109. Upward trend towards the end is observed along with reasonable reproducibility. Figure 5.29, on the other hand, shows the data for fabric 110 featuring a steady trend until the middle of the test and good reproducibility.

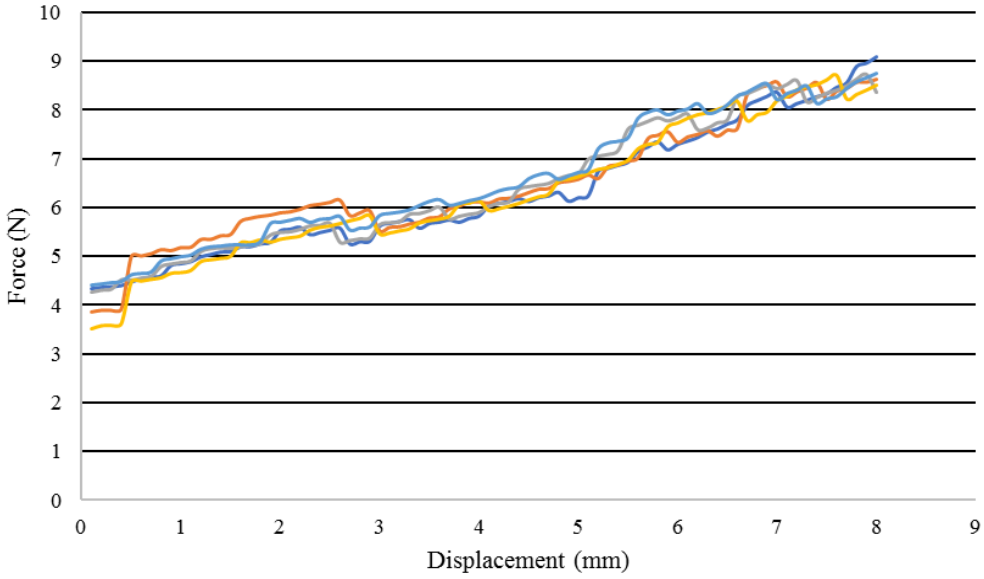

Figure 5.28. Friction with aluminium for fabric 109

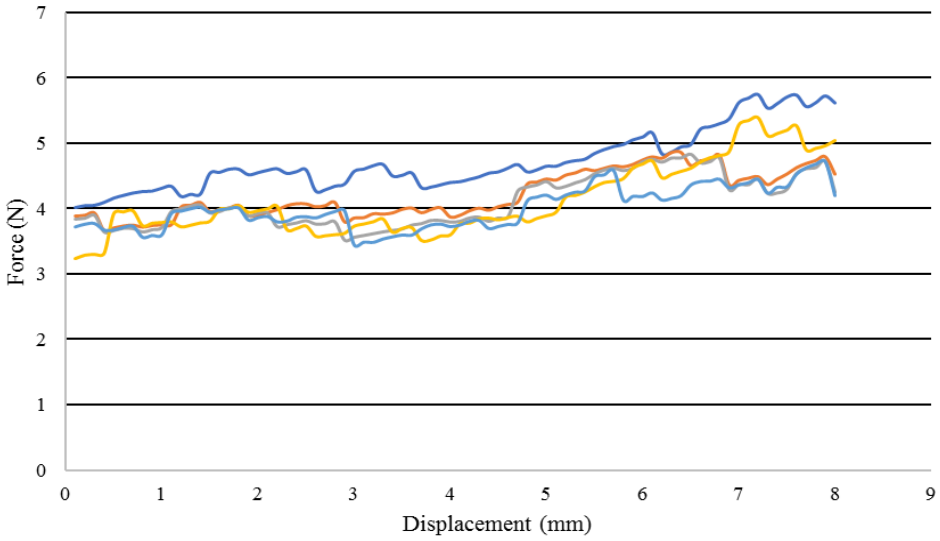

Figure 5.29. Friction with aluminium for fabric 110

5.6 Analysis

Figure 5.30 illustrates the average friction force between a ply and aluminium. These tests, fabric 109 showed the highest amount of friction with aluminium followed by fabrics 105, 104, 108, 102, 107, 103 and 110.

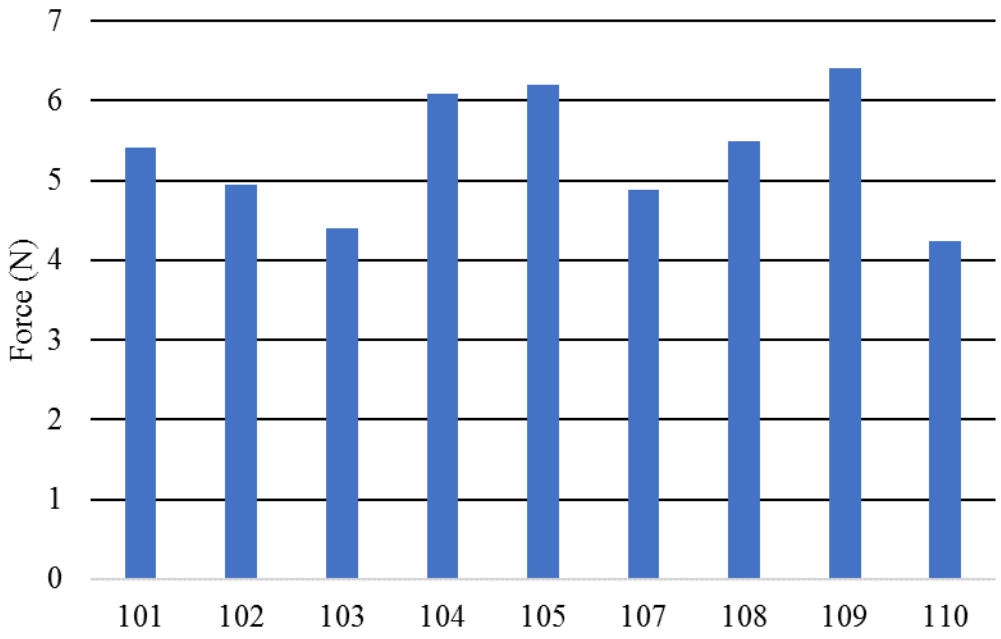

Figure 5.30. Average friction force with aluminium

Figure 5.31 demonstrates that carbon fibre fabrics show a higher average friction force with aluminium compared to glass fibre fabrics. Carbon fibre fabrics show larger variability compared to glass fibres, as seen with friction between plies.

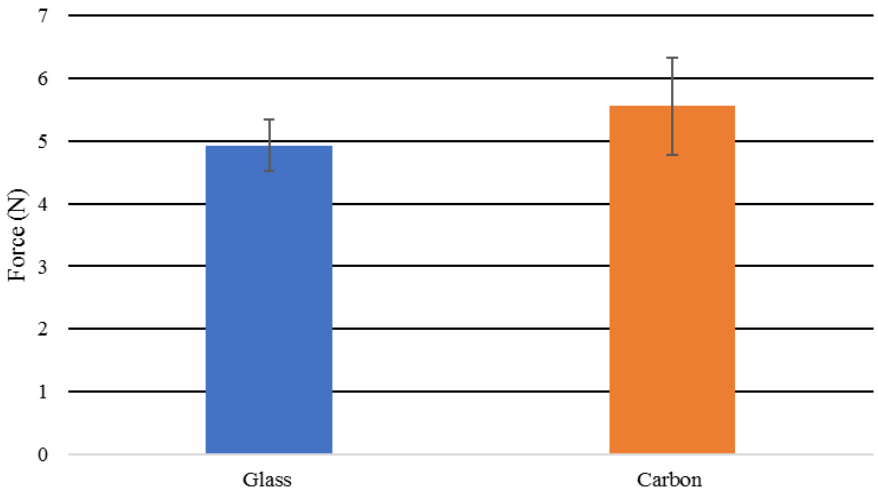

Figure 5.31. Average friction force with aluminium for glass and carbon fibre fabrics

Differences between architectures are not substantial in this case as shown in Figure 5.32. Stitched and binder fabrics show slightly higher values, followed by twill, plain and satin architectures. Stitched and binder as well as twill structured fabrics show the highest variability for friction with aluminium as seen for friction between plies. The satin architecture, on the other hand, demonstrates the lowest variability.

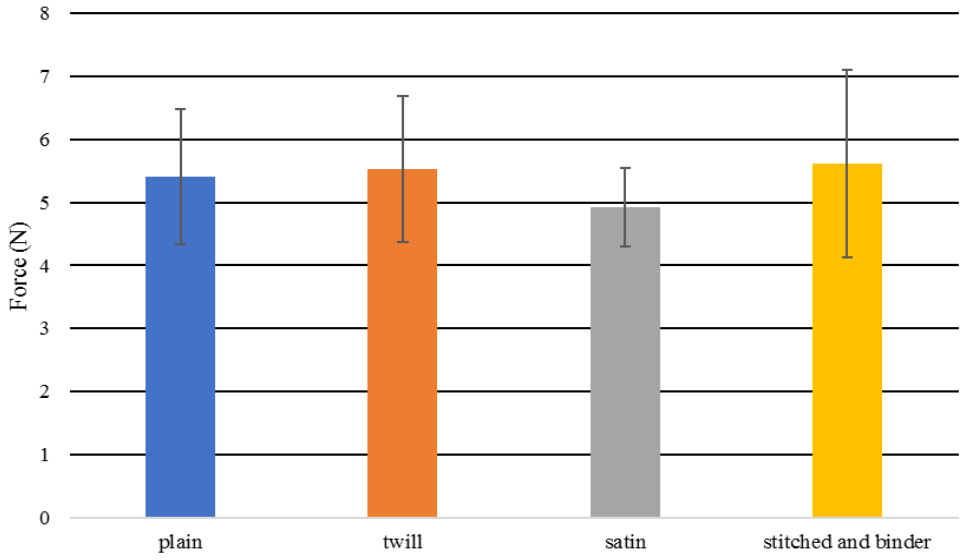

Figure 5.32. Average friction force with aluminium between different architectures

Figure 5.33 shows a linear relation with R^2 factor of 0.4 between surface density and friction with aluminium.

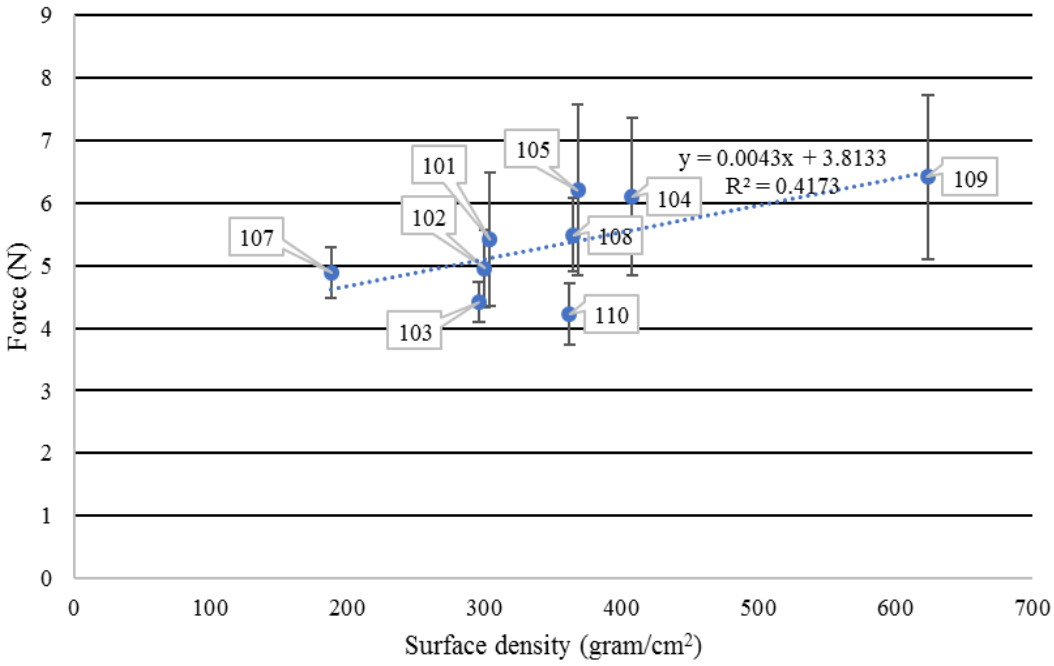

Figure 5.33. Friction force with aluminium as a function of surface density

Figure 5.34 plots the data as a function of yarn count with a R^2 factor of 0.23. Having the yarn count at the same range, fabrics might not show a reasonable trend with this parameter. The only radically different yarn count is for fabric 103 with 22.4 yarn/cm; others range from 4.5 to 6.5 yarn/cm. In this case, excluding fabric 103 would lead to a much lower R^2 value.

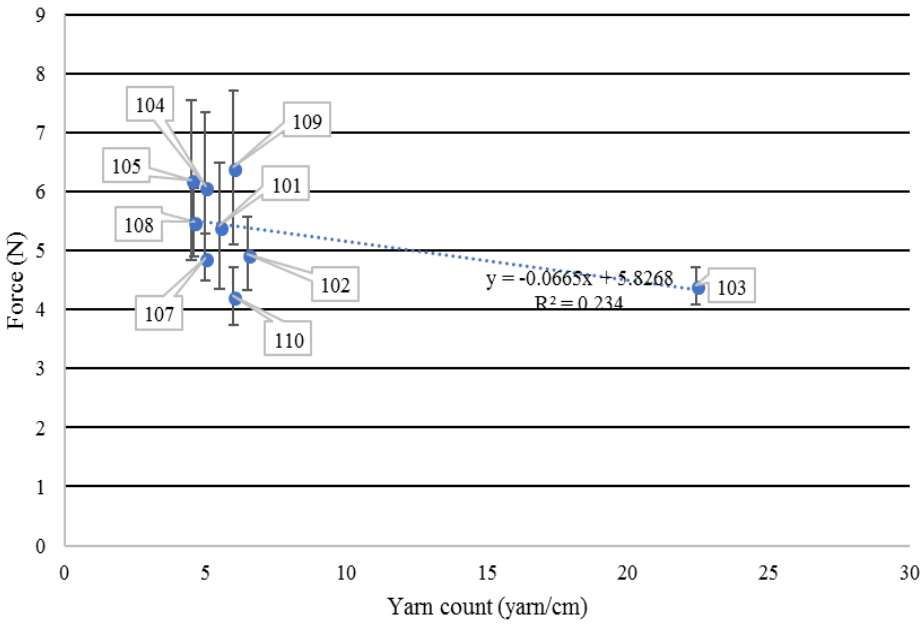

Figure 5.34. Friction force with aluminium as a function of yarn count

Figure 5.35 shows the data as a function of cover factor with a R^2 factor of 0.003. However, fabrics 102, 104, 105 and 109 show some trend amongst each other with regards to the effect of cover factor.

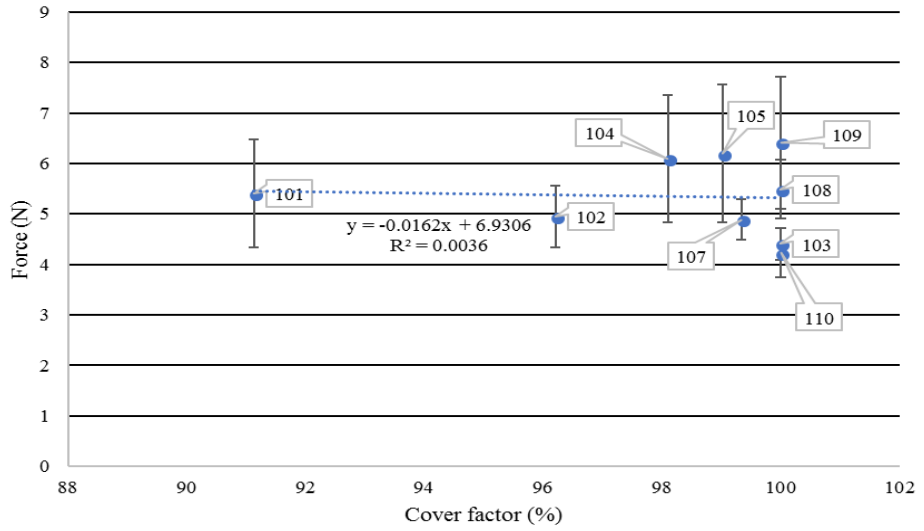

Figure 5.35. Friction force with aluminium as a function of cover factor

Figure 5.36 indicates a fairly strong relation (R^2 factor of 0.76) between crimp and friction force with aluminium. This is not surprising since crimp likely leads to higher normal forces in the textile [40].

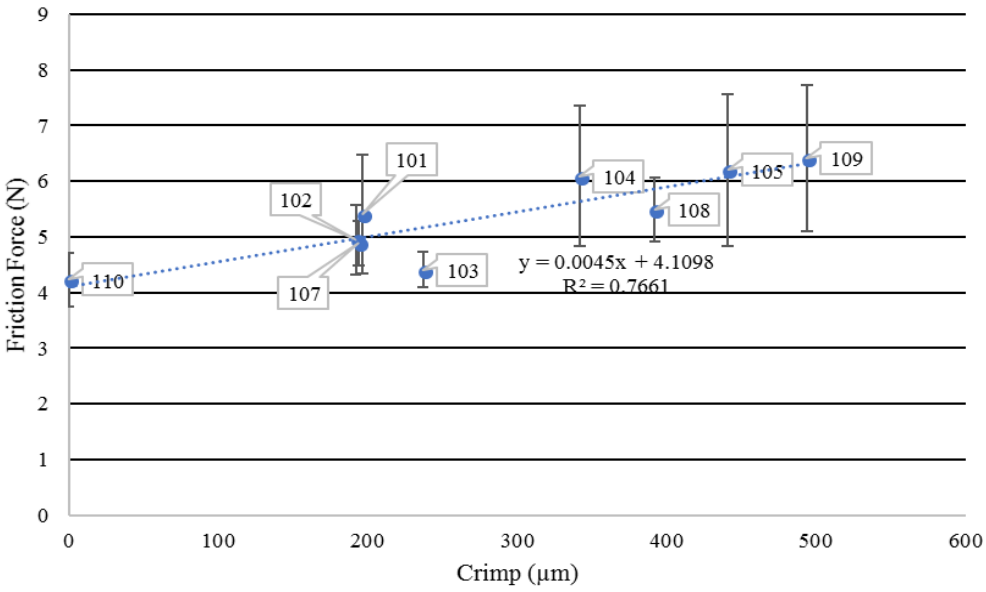

Figure 5.36.: Friction force with aluminium as a function of crimp

Figure 5.37 which plots the force as a function of thickness without pressure has the highest R^2 factor for the friction force, at around 0.73. Figure 5.38 shows similar data while having thickness with pressure as an independent variable and a R^2 factor of 0.63. In both cases, thicker fabric 109 will influence R^2 values but a trend is present nonetheless.

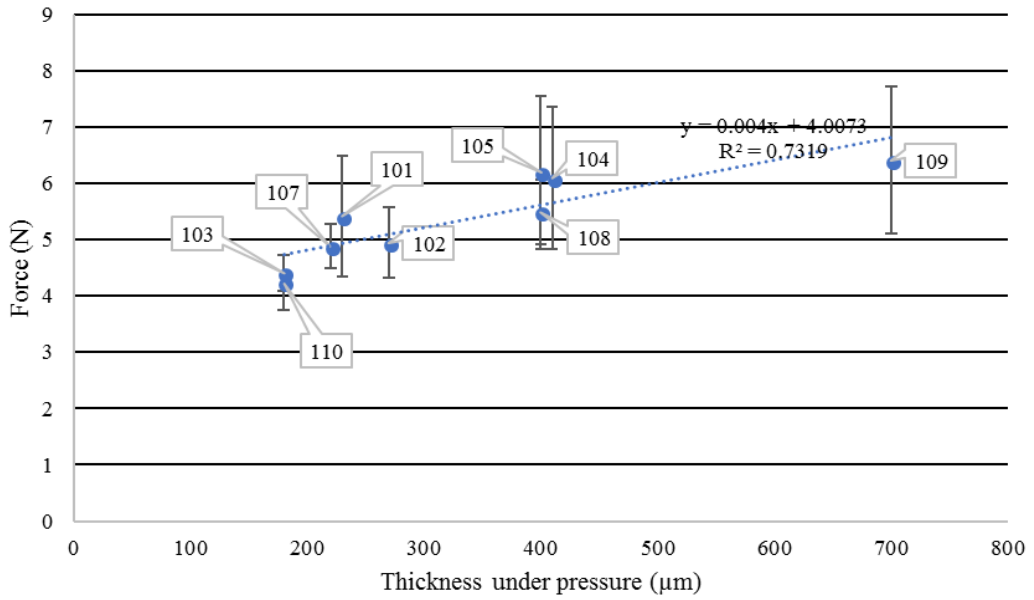

Figure 5.37. Friction force with aluminium as a function of thickness without pressure

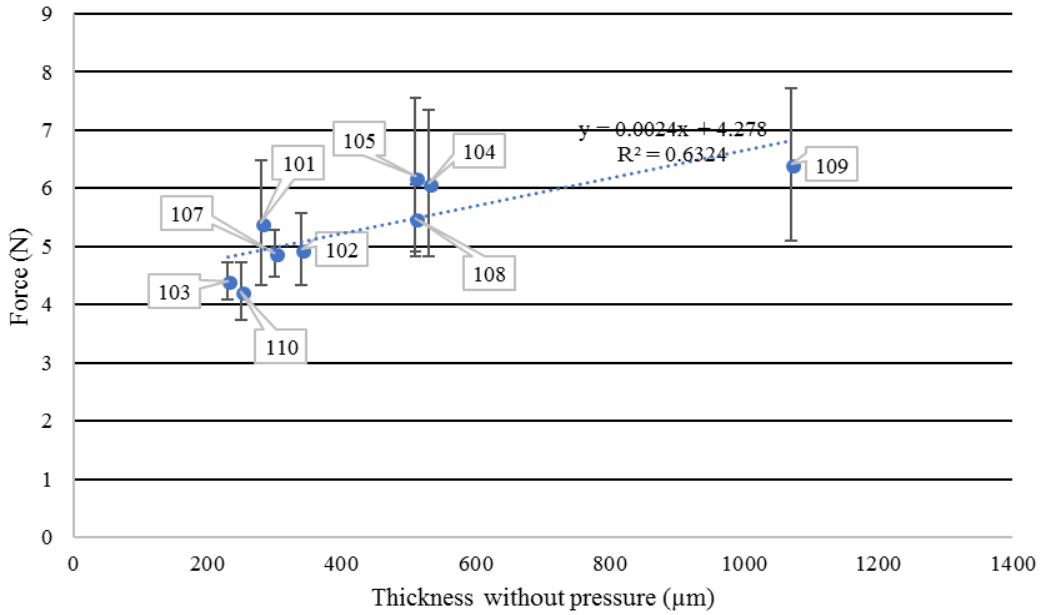

Figure 5.38. Friction force with aluminium as a function of thickness under pressure

5.7 Discussion

This chapter used two testing configurations for friction tests: friction between plies and friction between a ply and aluminium. For both cases, all analyses were conducted by looking into the relation between the friction results and fabric parameters such as fibre type, architecture, surface density, yarn count, crimp, cover factor and thickness.

Friction with aluminium results showed a higher consistency and less variability compared to friction between plies. This may be due to the extra weight that was added for maximizing friction with aluminium, as well as to the fact that there is only one ply present. Moreover, while most test results show a general steady trend, some demonstrate an ascending trend. Furthermore, while results for inter-ply friction show different forces for different fabrics, results for friction with aluminium show very similar results for different fabrics. Hence, it can be concluded that it is harder to predict the inter-ply friction force and easier to predict the friction with aluminium due to its lesser variability in results between different tests.

By looking at test results for friction with aluminium, carbon 109 and carbon 105 show the highest friction amongst fabrics. This indicates the effect of the binder on friction. Having all fibers along the longitudinal direction and thus less resistance, the non-crimp fabric (NCF) shows the lowest amount of friction with aluminium [42].

Looking at Figure 5.12, it can be concluded that fabrics 101 and 109 show the highest friction force between plies, hence these fabrics are likely to behave favourably for the preforming

process. However, fabrics 104 and 108 possess the lowest friction force between plies and consequently may prove more problematic for the preforming process.

When looking at Table 3.1 and comparing all three glass fabrics, plain weave 101 has the highest contact area followed by twill fabric 102, while 8-harness satin fabric 103 ranks the lowest. Similarly, the graph shows the same ranking for friction with these fabrics. This makes a reasonable case for the effect of contact area on friction with aluminium.

It should be mentioned that there are other fabric properties that impact friction such as fibre sizing [43], fibre count etc. which adds to the complexity of the issue and differ depending on the fibre manufacturer.

Chapter 6

Bending Tests

6.1 Introduction

The bending behaviour of fabrics is one of the key elements that affects their draping and preforming behaviour. Higher fabric stiffness results in more springback when the fabric is draped on a mould. This chapter reports the use of a standard testing method for measuring the bending stiffness in fabrics. The apparatus specification and the test procedure are presented in section 6.2, along with photos illustrating the procedure. Section 6.3 tabulates the test data and the standard deviation for each test. In Section 6.4, the analysis of bending test results is conducted as a function of fabric properties. Section 6.5 delivers a discussion on this chapter.

The cantilevered test for quantifying the bending behaviour of dry fabrics was originally introduced by Pierce. The original test consisted in measuring the overhang length of a dry fabric without use of a tilted board. The modern cantilever test was introduced afterwards as an improved version [32].

6.2 Apparatus and methodology

In the bending tests reported in this work, fabric specimens were bent under their own weight until they touched a board inclined at 41.5°. The apparatus used for the bending test consists of two 150 mm by 300 mm surfaces, one horizontal and another tilted at 41.5° from the horizontal as shown in Figure 6.1. The reason for using this angle, which is specified in the standard, is for simplifying calculations. Specimen size is 25mm by 300mm. Tests are based on their stiffness defined in standards ASTM F3260-17, ASTM D5732-95 and ASTM D1388−14 [44].

Displacing the sample toward the inclined plane was done using an aluminium plate of a similar size of 25 mm by 300 mm, which featured a rubber film on its lower surface for increasing friction between the displaced plate and the sample; this plate was positioned on top of the specimen. The measured bent length is labelled overhang length O. Bending length c is defined as half of the overhang length.

In order to measure the overhang length precisely, a 300 mm ruler was positioned next to the sample. The ruler and the sample were perfectly aligned. Hence, any length that extended past the origin of the ruler was the overhang length. The flat surface of the apparatus must be polished, so that friction with the fabric is minimized.

Figure 6.1 shows the bending rig. Figure 6.2 shows a top view of the rig, indicating its main dimensions.

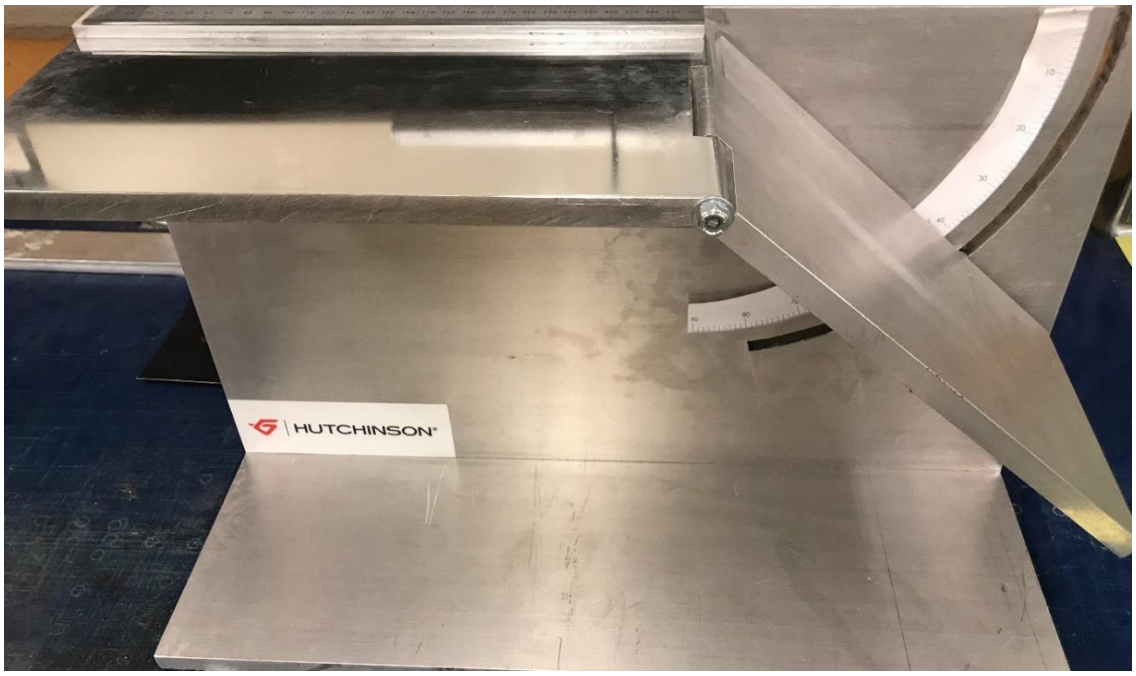

Figure 6.1. Cantilever bending test rig

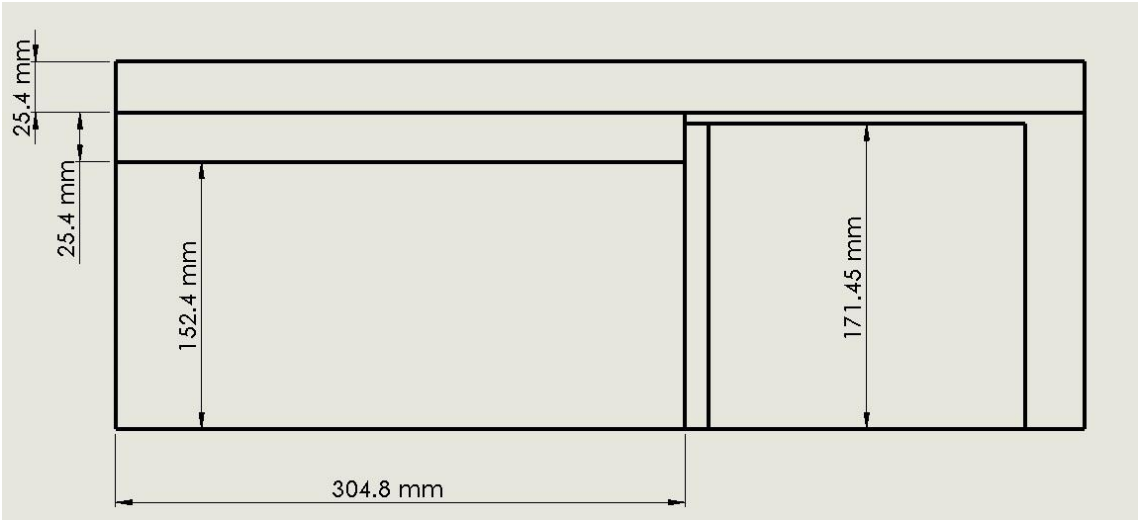

Figure 6.2. Dimensions of cantilever bending test rig

Knowing the bending length and the surface density of the fabric, the flexural stiffness *G* of the fabric can be calculated using Equation 6.1:

$$G = 9.81 \times 10^{-6}.M.c^3 \tag{6.1}$$

where *G* is the flexural stiffness ($\mu N.m$), 9.81 is the gravitational acceleration (m/s^2), *M* is the surface density (g/m^2) and *c* is the bending length (*mm*) which is calculated as *c=O/2* where *O* is the measured overhang length.

Motorized versions of such rigs exist, which move the specimens at a constant speed. In the case of manual testing, ASTM standards [45] dictate that specimens have to slide at a linear speed of 120 ± 5 % mm/min until the specimen touches the tilted board. Should the specimens twist by more than 45°, a test is deemed invalid.

Figure 6.3 shows cut specimens ready to be tested, and Figure 6.4 demonstrates the test. When characterizing a fabric, 10 strips are cut - 5 along the warp and 5 along the weft of a roll. The test is conducted 5 times on each warp sample and 5 times on each weft sample of each fabric using a different specimen. The average bending length is reported, along with the standard deviation.

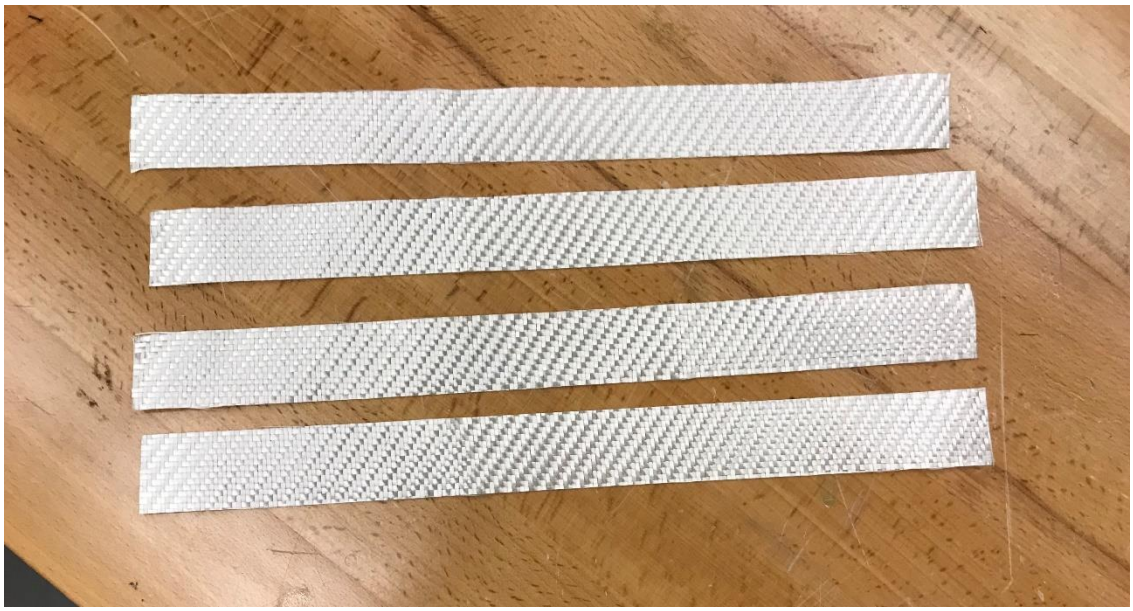

Figure 6.3. Cut specimens for the bending test

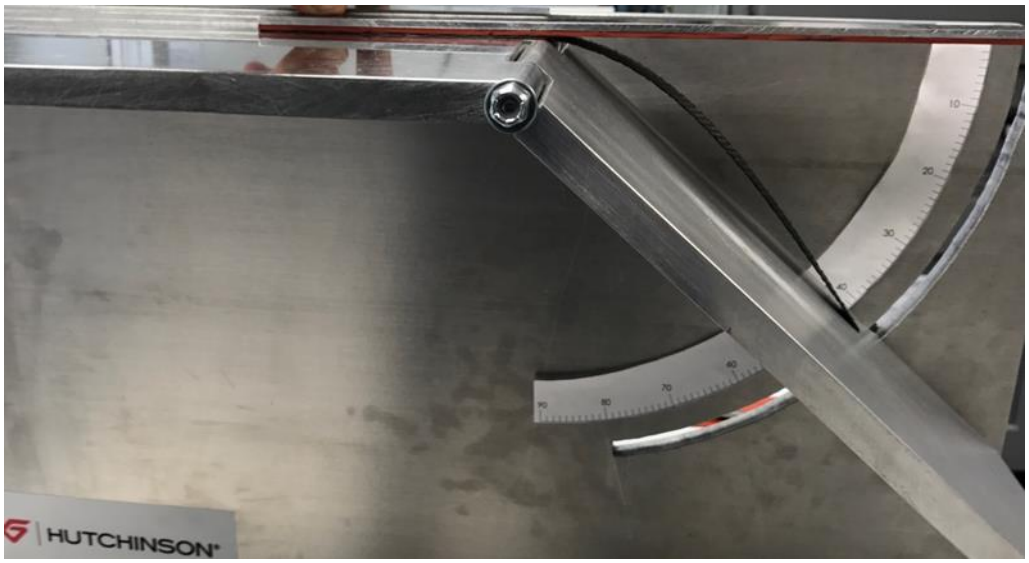

Figure 6.4. Cantilever bending test performed on a fabric

6.3 Results

Table 6.1 shows the bending length (*mm*) as well as the flexural stiffness ($\mu N.m$) for the fabrics introduced in Chapter 2 except for fabric 106 which was primarily used for developing the fraying tests discussed in Chapter 7.

Table 6.1. Flexural stiffness of fabrics

Fabric #	Fibre	Average overhang length (mm)		Average bending length (mm)		Surface density (g/m^2)	Flexural stiffness (µN.m)		Average flexural stiffness (µN.m)	Standard deviation
		Warp	Weft	Warp	Weft		Warp	Weft		
101	Glass	96.3	58.6	48.15	29.3	304	358.1	80.69	219.4	131.4
102	Glass	141		70.5		300	1099		1099	49.49
103	Glass	96.8	62.3	48.4	31.15	296	337.0	89.84	213.4	54.51
104	Carbon	150.2		75.1		408	1678		1678	45.75
105	Carbon	201.3	181.8	100.6	90.9	368	3800	2799	3300	504.0
107	Carbon	155.7		77.85		188	856.2		856.2	41.67
108	Carbon	121.7		60.85		365	817.8		817.8	50.82
109	Carbon	185.5	226.7	92.75	113.3	624	4931	9000	6965	2040
110	Carbon	153.7		76.85		362	681.2		681.2	65.21
111	Carbon	143.4		71.7		724	1106		1106	159.3

Figure 6.5 shows actual overhang length for some fabrics. From left to the right in this figure, fabrics are: plain glass 101, twill glass 102, twill carbon 104, 5-harness carbon with binder 105, and 2.5-D carbon with binder 109.

Figure 6.5. Overhang length of fabrics

Figure 6.6 illustrates the difference in flexural stiffness along the warp and weft directions [46] for plain weave glass fabric 101. Such difference was also observed with the 8-harness glass fabric 103, 5-harness carbon fabric with binder 105 as well as 2.5-D carbon fabric with binder 109. While the fabrics mentioned were stiffer along the warp, 2.5-D carbon fabric with binder 109 was stiffer along its weft direction. For other textiles tested, overhang lengths in both directions were similar.

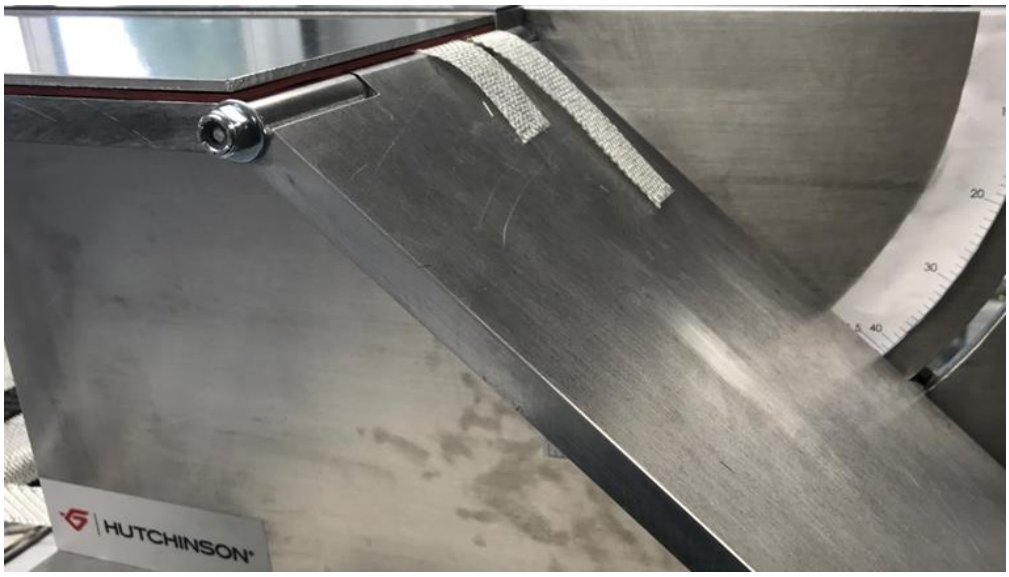

Figure 6.6. Overhang lengths along warp and weft for fabric 101

6.4 Analysis

Flexural stiffness is presented as a function of fabric type, architecture, cover factor, thickness, surface density and yarn count in Figures 6.7 to 6.14. Figure 6.7 shows that carbon fabrics on average have a higher flexural stiffness compared to glass fabrics. The figure also indicates that carbon fibre fabrics show a very large variability in flexural stiffness compared to glass fibre fabrics. This was not surprising as carbon fibres have a larger Young's modulus than glass fibres.

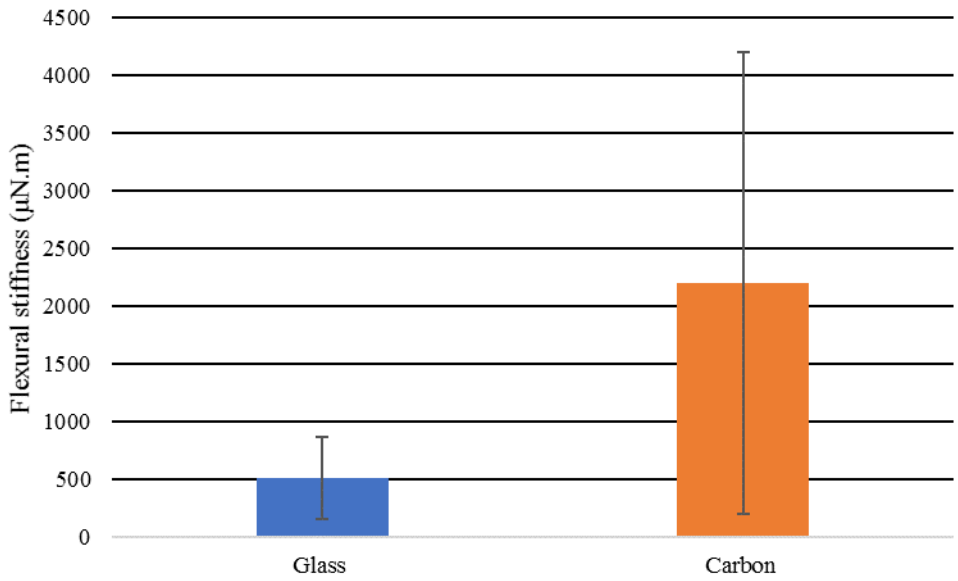

Figure 6.7. Flexural stiffness for glass and carbon fibres

Figure 6.8, on the other hand, illustrates that the plain weave structure features minimum flexural stiffness on average followed by satin weave structures. Stitched fabrics and fabrics with binder show the highest bending stiffnesses followed by twill weave structures. Stitched and binder fabrics possess the largest variability by far, followed by twill weave, satin weave and plain weave architectures.

Twill weaves and satin weaves show statistically different behaviour, as well as plain weaves and twill weaves, and also plain weaves and satin weaves. Plain weaves show flexural behaviour which is statistically different from stitched fabrics and fabrics with binders; however, twill weaves and satin weaves do not, primarily because of the very large variability associated with results for stitched fabrics and fabrics with binder.

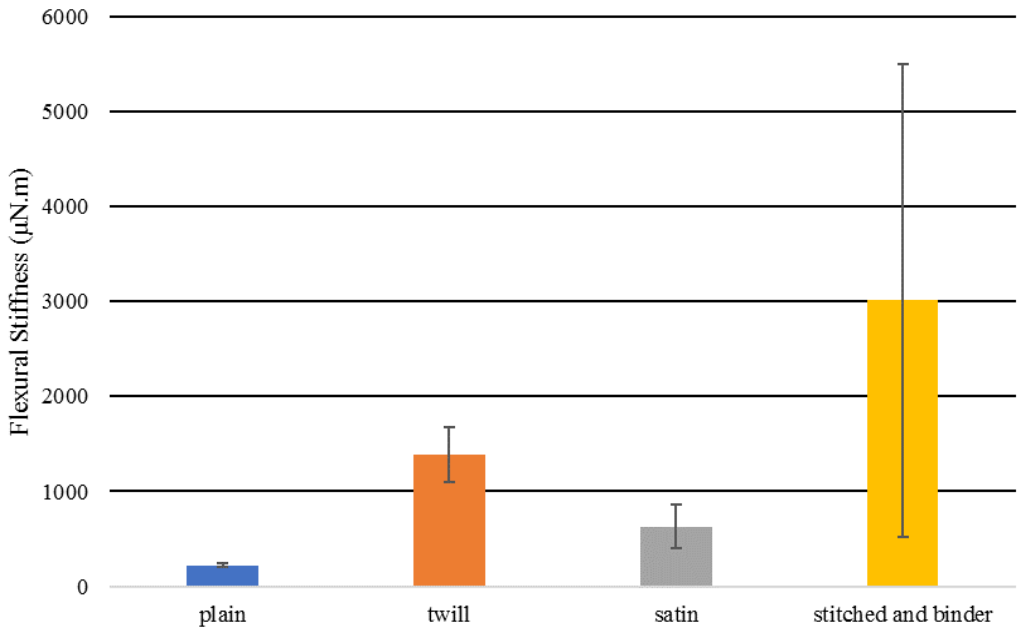

Figure 6.8. Flexural stiffness between different architectures

Figure 6.9 shows the relation between flexural stiffness and areal density, with a weak R^2 factor of 0.21. However, fabrics 102, 104, 107 and 110 seem to show a better relation amongst each other, and fabrics 101, 103, 108 and 111 seem to show another.

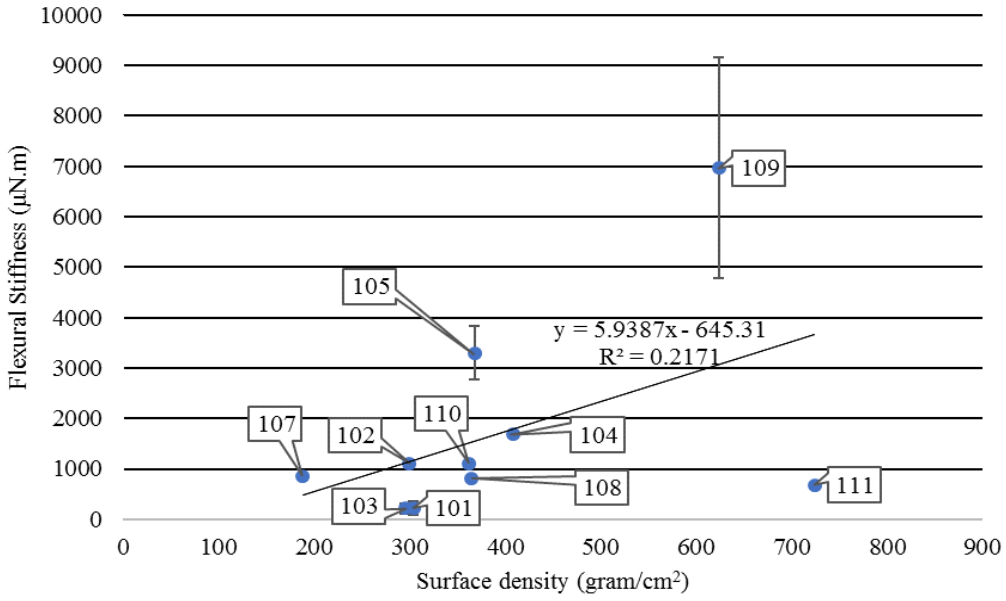

Figure 6.9. Flexural stiffness as a function of surface density

Figure 6.10 shows data for flexural stiffness as a function of yarn count with a low R^2 of 0.085. Figure 6.11 shows the data as a function of cover factor with low R^2 factor of 0.075, which indicates there is almost no relation between bending stiffness and cover factor. The most prominent deviation from fabrics is seen with fabric 109, which is a 2.5-D carbon fibre fabric with binder. Its thick structure increases the stiffness markedly.

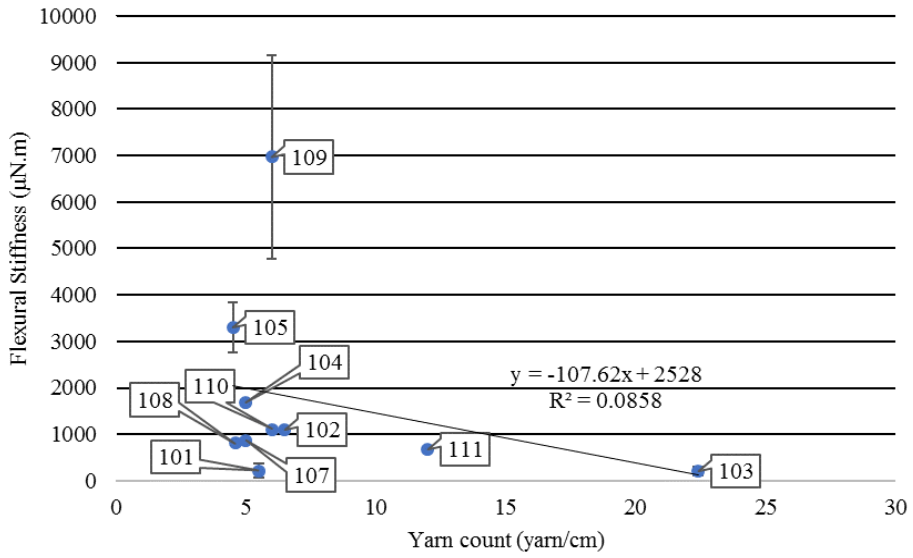

Figure 6.10. Flexural stiffness as a function of yarn count

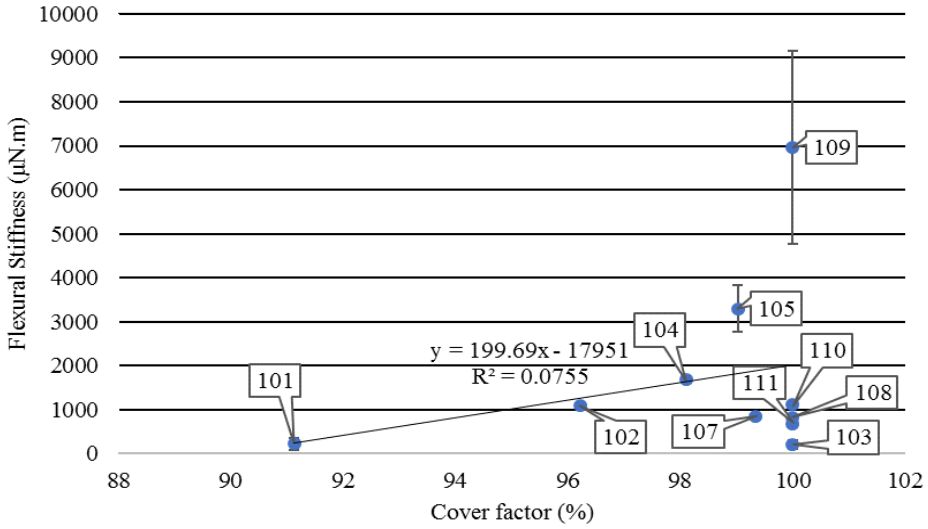

Figure 6.11. Flexural stiffness as a function of cover factor

Figure 6.12 illustrates the data as a function of crimp, with R^2 around 0.42. Fabrics 101, 103 and 108 seem to have a relation amongst each other, and fabrics 102, 105, 110 and 111 seem to constitute another. It this case also, fabric 109 is largely deviated from other fabrics due to its large stiffness.

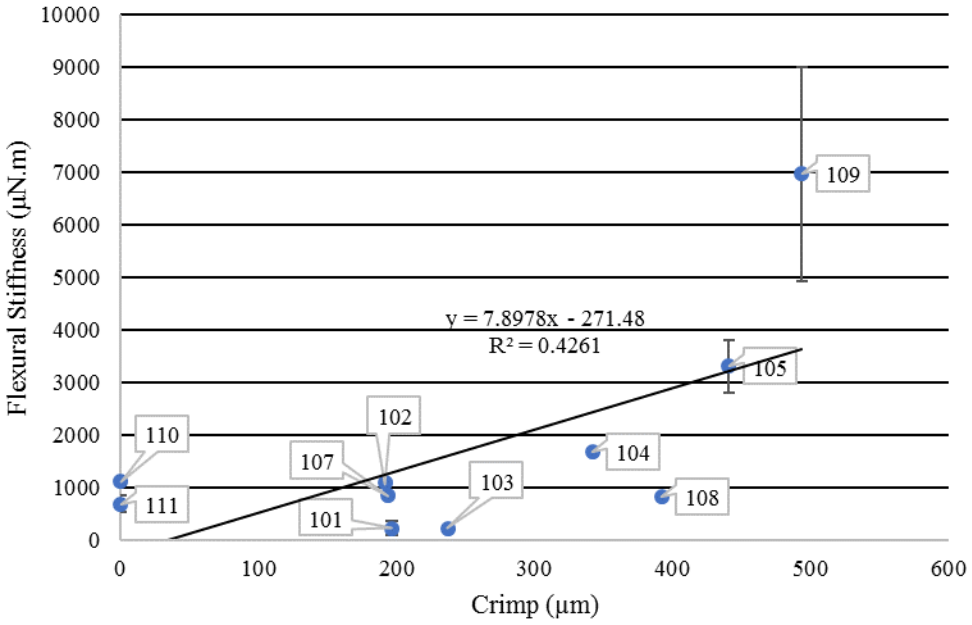

Figure 6.12. Flexural stiffness as a function of crimp

Figures 6.13 and 6.14 show flexural stiffness data as a function of thickness without pressure and with pressure respectively. Both figures demonstrate a strong trend showing a R^2 factor of 0.77 for the former and of 0.83 for the latter. These trends returned the highest values of the R^2 factor as a function of stiffness, which highlights the impact of thickness on flexural stiffness.

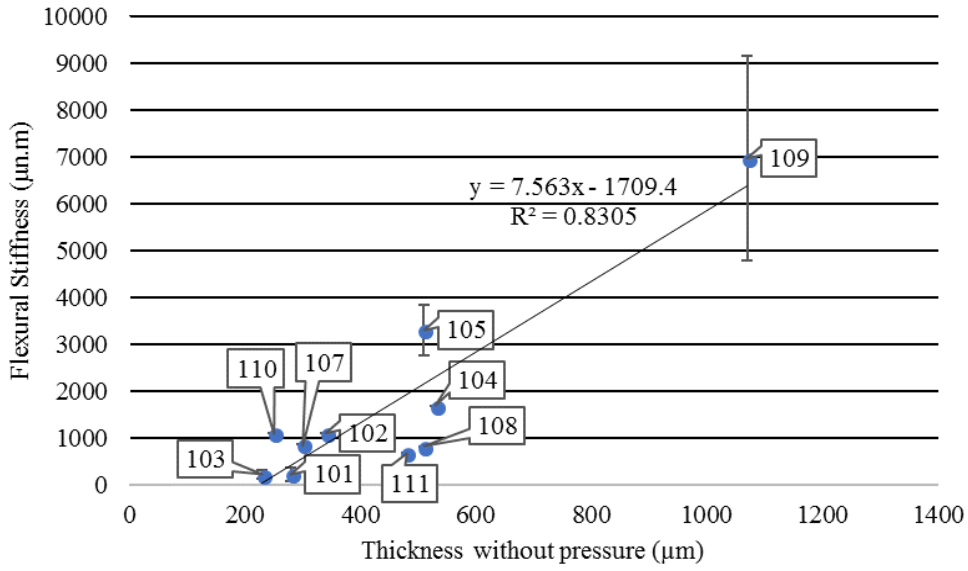

Figure 6.13. Flexural stiffness as a function of thickness without pressure

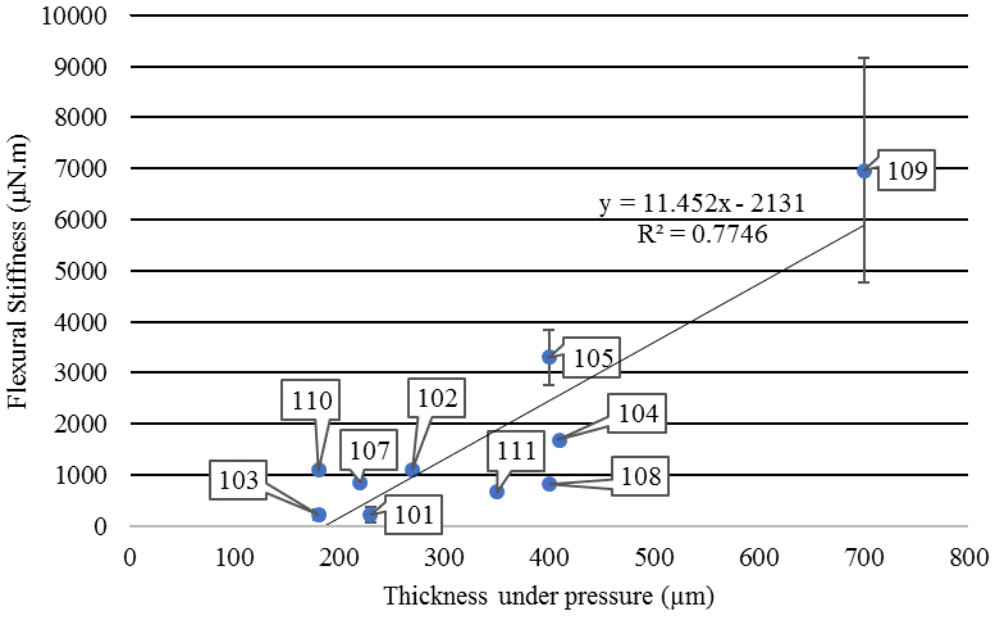

Figure 6.14. Flexural stiffness as a function of thickness under pressure

6.5 Discussion

The higher flexural stiffness is, the more difficult it is to perform draping in an industrial setting. For instance, when draped, plain glass fabric 101 will easily be bent on single-curvature moulds. 5-harness carbon fabric 105 with binder, on the other hand, requires significant manual work in order to be positioned properly, before resin infusion.

Admittedly, factors such as fabric architecture, crimp (how tight the yarns are woven onto each other), fabric's type and fabric's architecture influence the bending characteristic. However, the most influential fabric parameter in flexural stiffness found in this chapter was fabric thickness, and the R^2 factor associated with flexural stiffness and fabric thickness confirms this claim.

Table 6.1 lists flexural stiffnesses of the fabrics tested. The highest value was obtained for the 2.5-D carbon fabric 109 with binder, followed by the 5-harness carbon fabric 105 with binder. This highlights the strong impact of powder binder on flexural stiffness. Twill weave carbon fabric 104 and twill weave glass fabric 102 show comparable results. This indicates the influence of fabrics architecture on bending stiffness. The lowest values, on the other hand, were observed with the plain weave glass fabric 101 and 8-harness weave glass fabric 103.

Chapter 7

Fraying Tests

7.1 Introduction

A lack of an established standard characterization method for the fraying of dry reinforcement fabrics used in composites manufacturing precludes the use of quantitative methods for analyzing and predicting this aspect of manufacturing operations. Knowledge of the fraying characteristics of carbon and glass fabric reinforcements upon cutting and handling is important in manufacturing. Upon preforming, different fabrics behave in different ways, making it difficult to plan manufacturing efficiently; each element of the behaviour of these textiles, including fraying, demands a reproducible testing method.

When draped, industrial fabrics can show fraying around the edges. The amount of fraying varies with the fabric type, fabric architecture and mould geometry. A typical situation where fraying can occur is the darting of a fabric, which is done to facilitate the draping of a mould of complex geometry [47]. Figures 7.1 and 7.2 show two different fabrics after being cut and draped on a mould. More complex mould geometries result in higher shear and more fraying, eventually making the draping process more problematic with some fabrics.

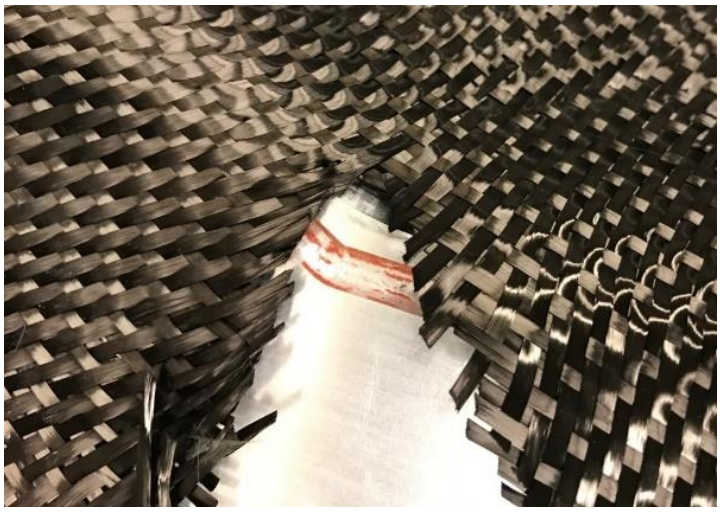

Figure 7.1. Fraying around edges after cutting and draping, carbon fibre fabric 108

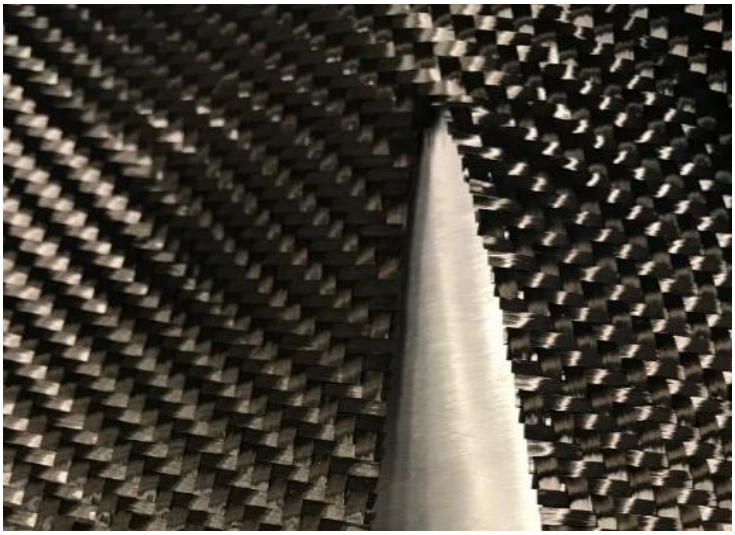

Figure 7.2. Fraying around edges after cutting and draping, carbon fibre fabric 104

Section 7.2 introduces the apparatus and methodology for this testing method including the device specifications and specimen dimensions. Section 7.3 delivers the results of the fraying test in Table 7.1, as well as in Figures 7.7 and 7.8. Section 7.4 delivers the analysis part of this test including the yarn loss as a function of fabric characteristics such as fibre type, architecture, surface density, yarn count, cover factor, crimp and thickness. Section 7.5 delivers a brief discussion for this chapter.

7.2 Apparatus and methodology

A testing rig featuring a 3.81 cm (1.5 in) diameter circular platen supported by a 0.95 cm (3/8 in) diameter rod as shown in Figure 7.3 was mounted into an adjustable speed spinner. Tests reported in this chapter were conducted at a spinning speed of 1500 RPM as measured by a digital tachometer. Circular fabric specimens measuring 15.24 cm (6 in) in diameter were secured on the platen, using double-sided General Sealants tape covering the whole surface of the circular platen. Samples were spun at the aforementioned speed for 3 seconds. Inertial forces caused some yarns to dislodge from the edges. Lost yarns were quantified using mass and area loss. Tests were run on 5 samples for each fabric. Average losses are reported in Table 7.1, along with values of the standard deviation.

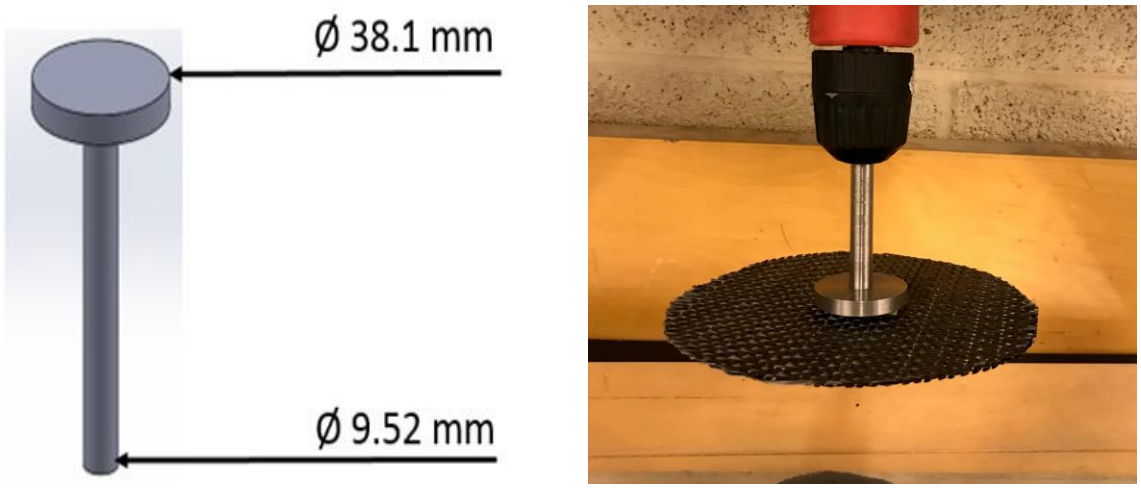

(a) (b)

Figure 7.3. Fraying test rig (a) and fabric specimen mounted on the rig (b)

The mass of each specimen was measured before and after each test, using a Smart Weight dual platform scale with 200 g capacity and ±0.001 g accuracy. Mass loss is reported as an average of 5 measurements.

The area of the specimen before the test and the non-frayed area after the test were measured using the ImageJ software. Area loss was reported as an average of 5 measurements for each fabric. Looking at the topographic images and fabric information in Chapter 3, the effects of fibre type, architecture, surface density, yarn count, cover factor, crimp and thickness are analyzed in Section 7.4.

Figures 7.4 and 7.5 show a sample of fabric 103 before and after a fraying test. Figure 7.5 shows a sample of fabric 102 after the test.

Figure 7.4. 8-harness glass fabric 103 specimen, before fraying test

Figure 7.5. 8-harness glass fabric 103, after fraying test

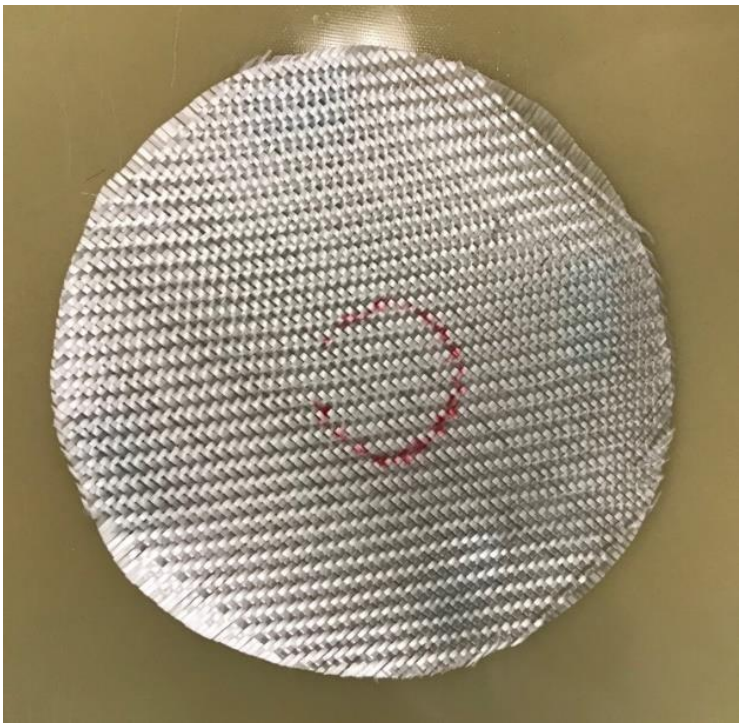

Figure 7.6. Twill glass fabric 102, after fraying test

7.3 Results

Table 7.1 lists fraying test results for mass loss, area loss and standard deviations for both measurements. fabric information such as fibre type and architecture are also mentioned. Since this test was developed at University of Ottawa, it was not conducted for all fabrics used by the industrial partner due to availability and lack of time. The test was conducted for fabrics 101 to 106.

Table 7.1. Fraying test results

Fabric number	Fibre	Architecture	Mass loss (%)	Area loss (%)	Mass loss standard deviation	Area loss standard deviation
101	Glass	Plain	43.15	77.07	2.42	4.81
102	Glass	Twill	1.39	6.04	0.22	1.25
103	Glass	8-harness satin	11.23	20.68	1.14	2.99
104	Carbon	Twill	3.03	7.20	0.53	1.36
105	Carbon	5-harness satin with binder	1.84	4.75	0.31	1.59
106	Carbon	Unidirectional Stitched	1.09	3.39	0.09	0.90

Figure 7.7 shows the results from fraying tests comparing mass loss (%) and area loss (%) for all 6 fabrics tested. This figure illustrates limited yarn loss for glass fabric 102, carbon fabric 104,

carbon fabric 105 and carbon fabric 106. On the other hand, results for glass fabric 103 show moderate amounts of yarn loss, and those for the glass fabric 101 show high yarn loss. Figure 7.8, however, shows some of the data presented in Figure 7.7, comparing mass loss (%) and area loss (%) for the four least frayed fabrics.

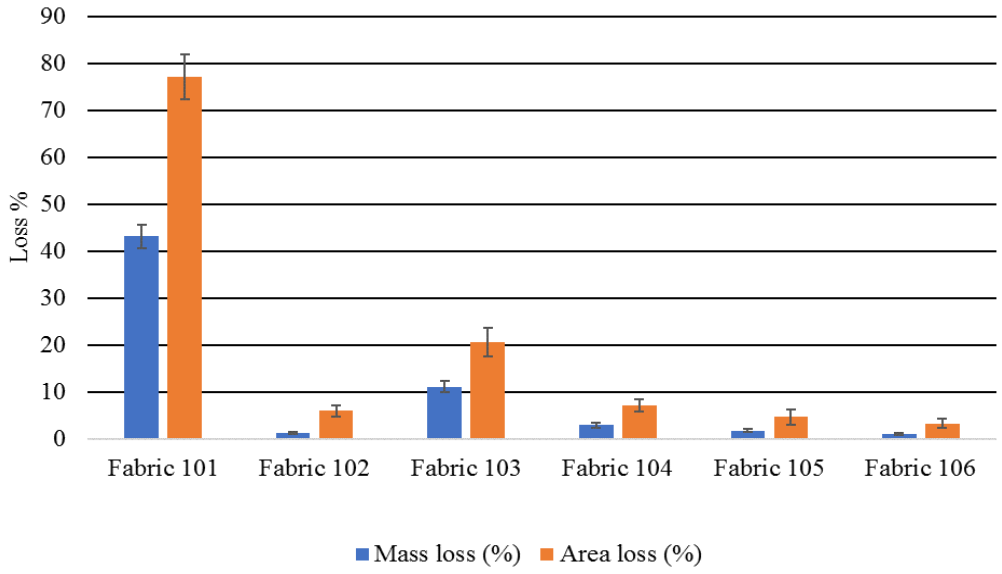

Figure 7.7. Mass loss and area loss

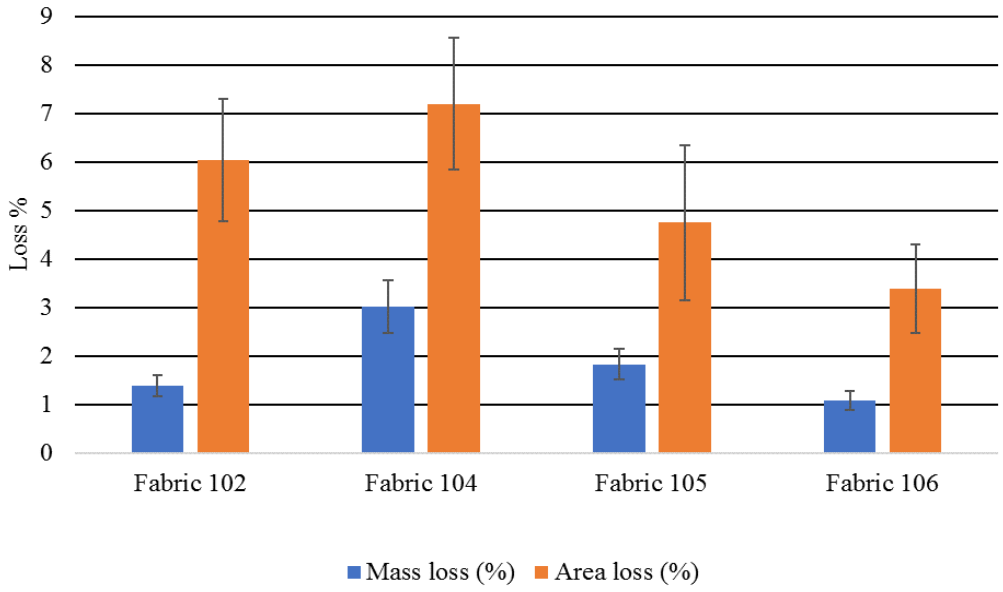

Figure 7.8. Mass loss and area loss for 4 least frayed fabrics

7.4 Analysis

Figure 7.9 shows the existing correlation between area loss (%) and mass loss (%) for fabrics tested, demonstrating a strong trend with a R^2 factor of 0.999. This validates the equivalence of the two measurement methods. However, both were used in order to investigate any existing relation as well as variability in each test. The following analyses for fabric parameters were conducted for mass loss as the mass loss was measured by a ±0.001 g accuracy scale and thus leads to be precise results.

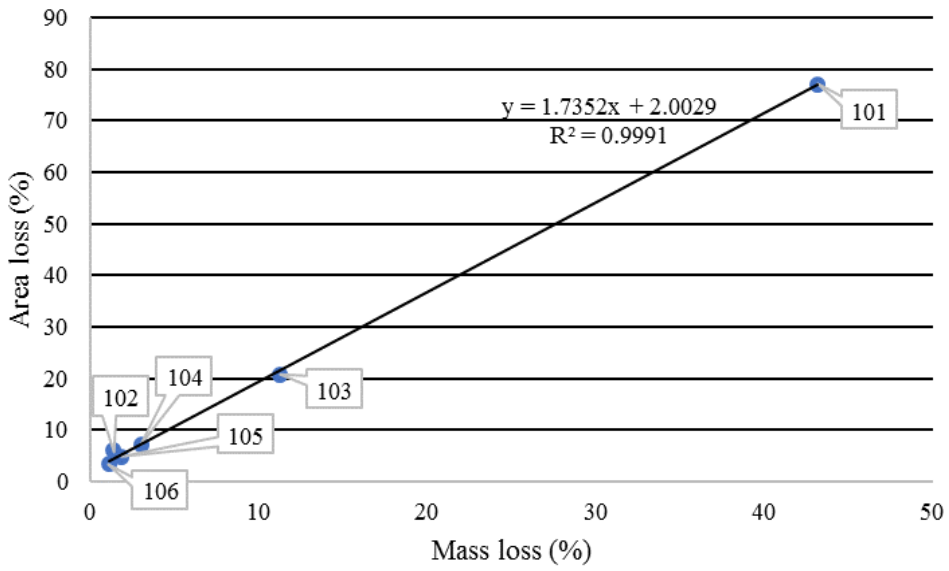

Figure 7.9. Area loss and mass loss correlation

Figures 7.10 to 7.17 show mass loss plotted as a function of fabric type, architecture, cover factor, thickness, surface density and yarn count. Figure 7.10 shows that the glass fibre fabric reinforcements tested showed higher fraying compared to carbon fibre fabrics. Glass fibre fabrics showed larger variability on mass loss that carbon fibre fabrics.

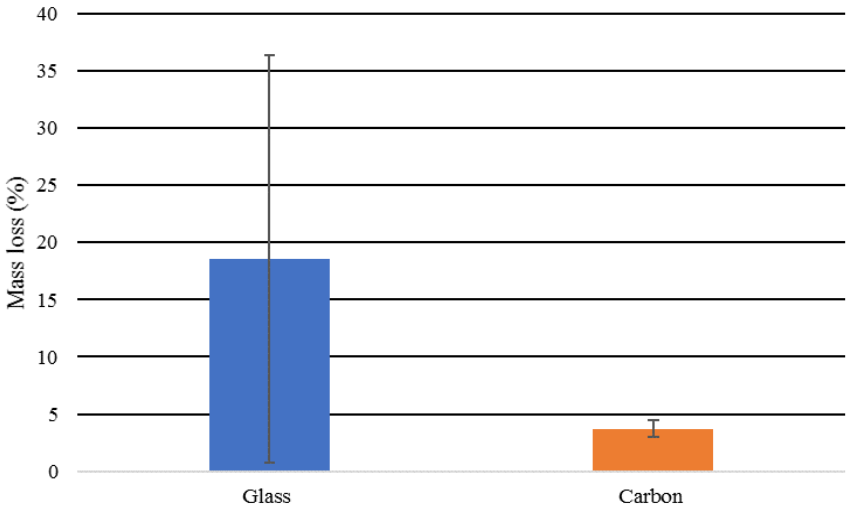

Figure 7.10. Mass loss for glass and carbon fibres

Looking at Figure 7.11, plain architecture demonstrates the largest variability followed by satin and twill. Fabrics with binder and stitching show the lowest amount. Their data are statistically different with no overlap considering their standard deviation. This demonstrates the effect of fabric architecture on mass loss results.

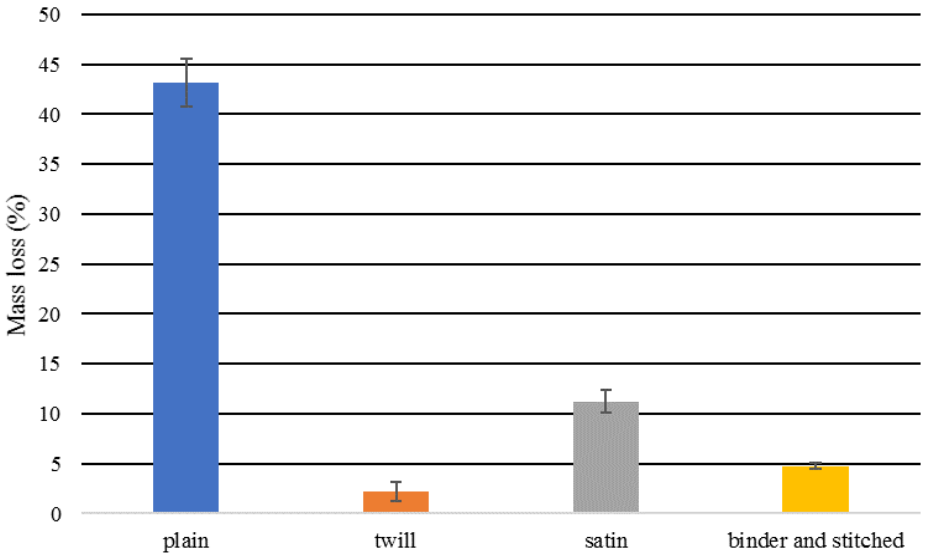

Figure 7.11. Mass loss for different architectures

Figures 7.12 and 7.13 shows R^2 factor values of 0.07 and 0.002 when plotting mass loss as a function of surface density and yarn count respectively. However, Figure 7.12 shows a relation between fabrics 103, 104 and 105, and Figure 7.13 shows a relation between fabrics 102, 104, 105 and 106. In both figures, fabric 101 has deviated largely from others due its high mass loss.

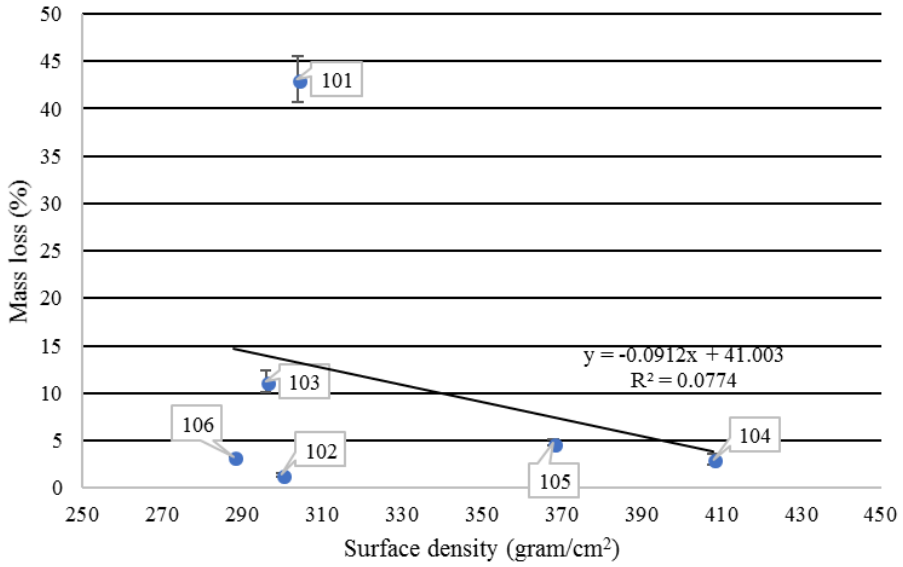

Figure 7.12. Mass loss as a function of surface density

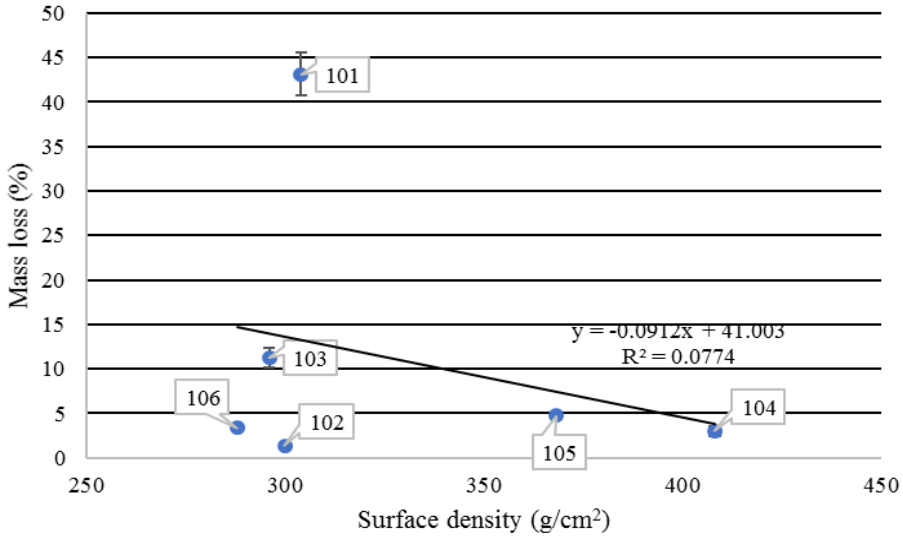

Figure 7.13. Mass loss as a function of yarn count

Figure 7.14 demonstrates mass loss and cover factor with a correlation factor of R^2= 0.68. In this case, fabrics 102 and 103 seem to deviate from the trendline. It can be observed that the plain weave glass fibre fabric 101 has lower cover factor compared to other textiles tested.

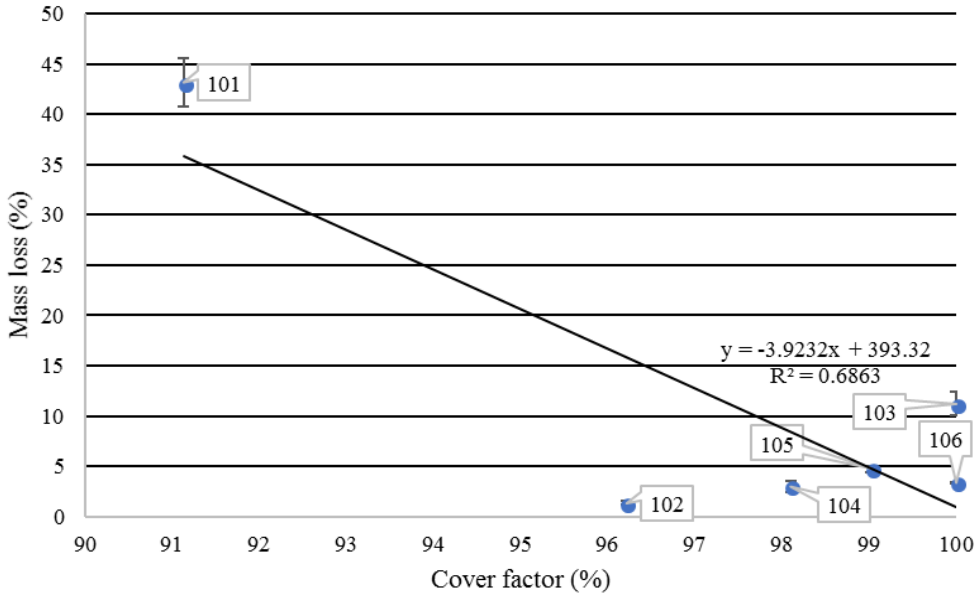

Figure 7.14. Mass loss as a function of cover factor

Figure 7.15 plots crimp as a variance of fabric mass loss. While the general R^2 factor is low, for some fabrics the analysis of fabric topography in Chapter 3 and Table 7.1 delivered information regarding each fabric crimp placing twill structured fabrics with less crimp than the 8-harness and perhaps consequently less yarn loss. Varying amounts of crimp can lead to differences in triggering of yarns sliding relatively to each other [48].

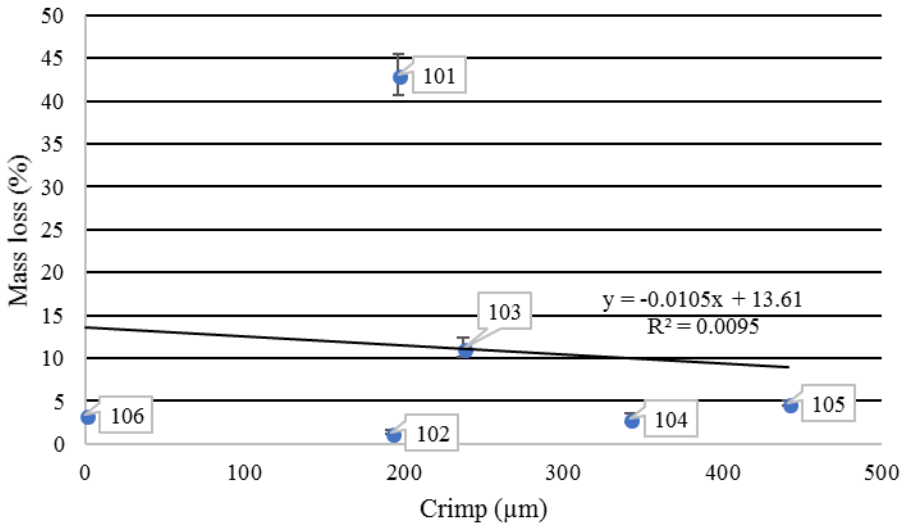

Figure 7.15. Mass loss as a function of crimp

Figures 7.16 and 7.17, finally, do not show a relation between mass loss and fabrics thicknesses. This is surprising; however, one contributing factor for lack of relation seems to be the high amount of mass loss in fabric 101.

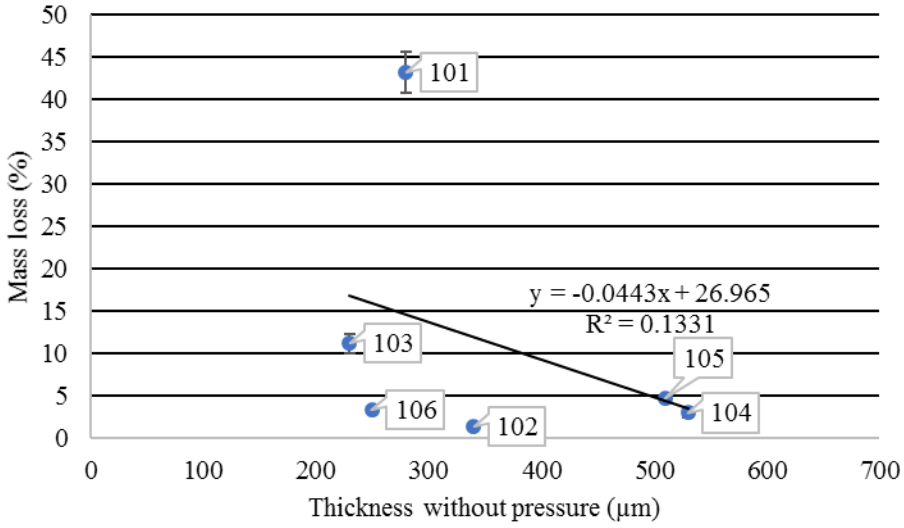

Figure 7.16. Mass loss as a function of thickness without pressure

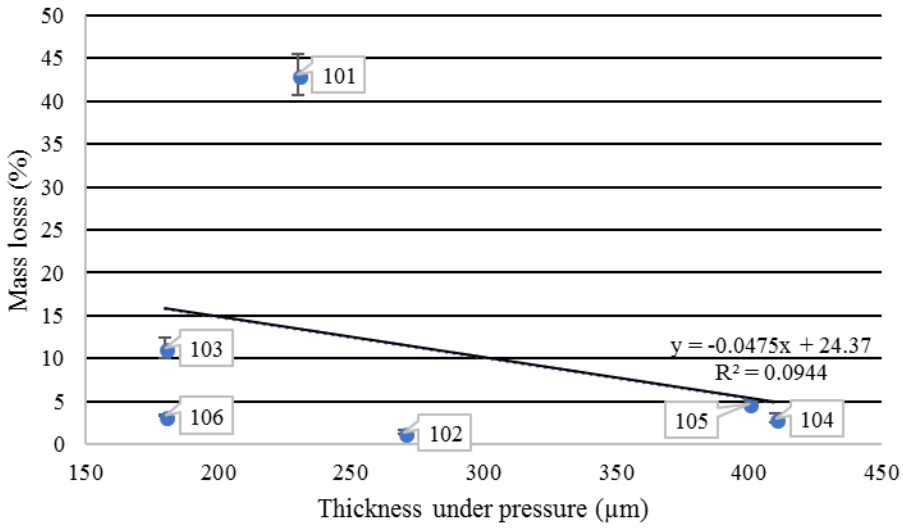

Figure 7.17. Mass loss as a function of thickness under pressure

7.5 Discussion

The highest correlation between fabric parameters and mass loss was seen when cover factor was the independent variable in Figure 7.14. This confirms the impact of cover factor in fraying of reinforcement fabrics. Surprisingly, while crimp showed a relation for some fabrics, it did not demonstrate a strong relation as an independent variable for mass loss in Figure 7.15, for the fabrics tested.

Another major finding in this chapter was the larger fraying results in glass fibre fabrics compared to carbon fabrics. It was also observed in Figure 7.11 that different architectures have statistically different amounts of mass loss.

The high amount of yarn loss seen with the plain glass fabric could be due to low inter-yarn friction, as well as to the plain weave structure itself. It can be concluded that twill fabrics show

a higher resistance to fraying. Also, the use of a binder on the fabric and the presence of stitching in fabrics prevent edge fraying efficiently.

The carbon fabric 106 used in testing had yarns extending along 45° and -45° directions with a stitch along the 0° direction. This fabric predictably returned the minimum yarn loss, confirming that stitching can be a potent solution to the occurrence of fraying in some cases [49].

This chapter introduced a reproducible testing method for measuring yarn loss in carbon and glass fabrics with minimum variability in results aiming at quantifying fraying. The impact of some fabrics attributes such as architecture, stitching and presence of a binder on yarn loss was observed and discussed. Using an automated cutting machine [50] for preparing the specimens, may lead to more accurate specimens resulting in more repeatable results.

Chapter 8

Conclusions and Recommendations

This work focused on studying elements of behaviour in textiles including shear, friction, bending and fraying at a macroscopic level, representative of draping procedures. Elements of behaviour were measured and analyzed in relation to fabric properties including fibre type, architecture, surface density, cover factor, crimp and thickness. 11 fabrics were tested in this work including plain glass, twill glass, 8-harness glass, twill carbon, 5-harness carbon, 5-harness carbon with binder, three non-crimp carbon, 4-harness carbon, and 2.5-D carbon fabrics. All fabrics used in this work except for the NCF carbon fabric 106 are Hutchinson's industrial fabrics and were cut and supplied by Hutchinson.

The objectives defined in Section 1.2 were all attained:

- Deformation modes in fibres, yarns, single ply and multi-layers were studied and discussed.
- Fabric characteristics that impact the draping process such as shear, bending, fraying and friction were defined and discussed.
- The relation between fabric parameters such as fibre type, architecture, surface density, yarn count, crimp, cover factor, surface contact area and thickness were analyzed.

- A more reproducible testing method for measuring fraying characteristic in fabrics was developed and introduced in Chapter 7.

In the shear test results, it was demonstrated that glass fabrics have larger shear extensions, and thus are easier to handle for the draping process. In terms of architecture, plain fabrics showed the highest shear extension followed by twill, satin and fabrics with binder. The cover factor had the strongest relation with the shear extension. While crimp factor did not demonstrate a strong relation, some fabrics followed a trend amongst each other.

For friction between plies results, it was observed that glass fibre fabrics on average have a higher amount of friction between their plies. It was also seen that plain weave has the highest amount of this friction followed by stitched and fabrics with binder, while twill and satin have the lowest amount. The highest correlation was seen with the cover factor as independent variable for friction between plies.

For friction with aluminium, however, carbon fabrics showed a higher average compared with glass fibre fabrics. Differences between architectures are not substantial in this case. Nonetheless, stitched and binder fabrics have the largest amount of friction by a small margin, followed by twill, plain and satin architectures. The crimp factor and the fabric thickness demonstrated the strongest correlation with this friction force.

In the bending chapter, it was demonstrated that in most fabrics the bending stiffness is higher along the warp direction compared to the weft. The only exception for this was the 2.5-D carbon fabric 109. This influences the decision making for the initial orientation of plies. It was also concluded that carbon fabrics on average have a higher flexural stiffness compared to glass

fabrics. In terms of architecture, stitched and fabrics with binder have the highest bending stiffness followed by twill, satin and plain fabrics respectively. Fabrics thicknesses showed the highest correlation with this stiffness.

In terms of fraying around the edges in the draping process, glass fibre fabrics showed much more yarn loss compared to carbon fibre fabrics. Furthermore, twill architecture showed the lowest amount of yarn loss followed by stitched and fabrics with binder, satin and plain structured textiles. Cover factor illustrated the highest correlation as a variance of mass loss measurements in fabrics.

8.1 Future work

For attaining a more accurate draping prediction, different elements of behaviour were defined, tested and analyzed for available fabrics. While considering the mould geometry and looking at the fabric elements of behaviour the complexity of the draping process can be predicted, there are cases that fabrics with high amount of fraying for instance, are virtually impossible to be draped without major obstacles. The ongoing work to tackle these problematic textiles suggests solutions such as localized binder or localized stitching where by looking at the most complex double curvature of the mould, binder or stitching is applied in order to keep the yarns together. In a similar way, fabrics with extremely high flexural stiffness can be used through some in-oven preforming processes can be used in order to simplify the draping process before the manufacturing of the composite parts.

Collecting the data from the characterizations and inputting them into a comprehensive draping predictive software which can consider all the elements of behaviour of a fabric, complexity of the mould, number of plies, and the cutting pattern is the next step for moving this work forward.

Appendix A

Graphs of shear extension tests

A1. Shear tests for fabric 102

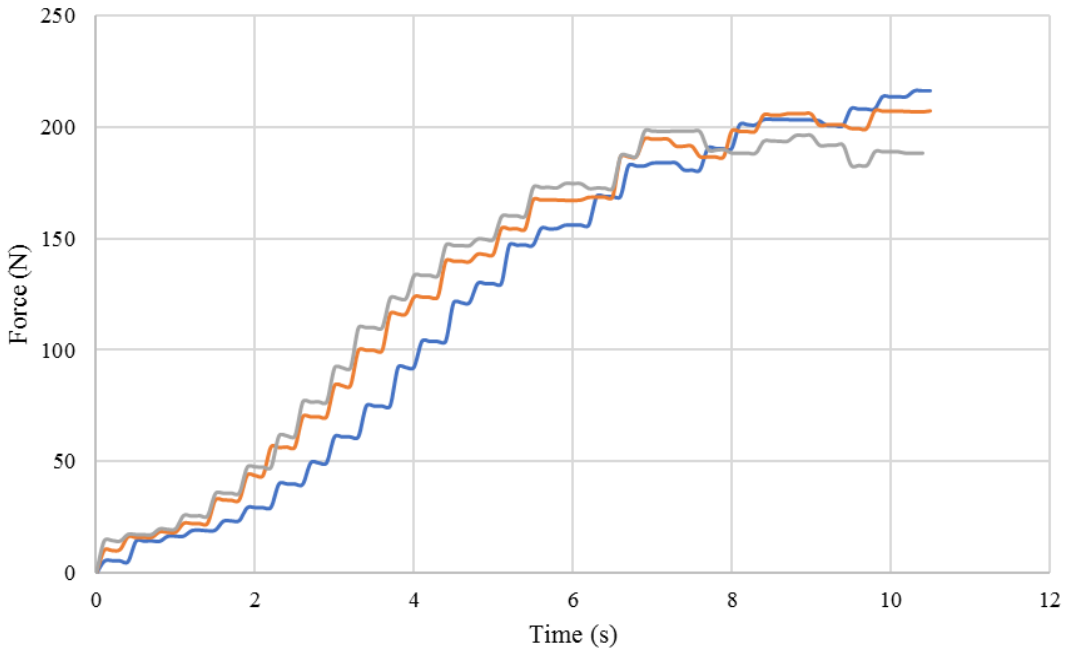

A2. Shear tests for fabric 103

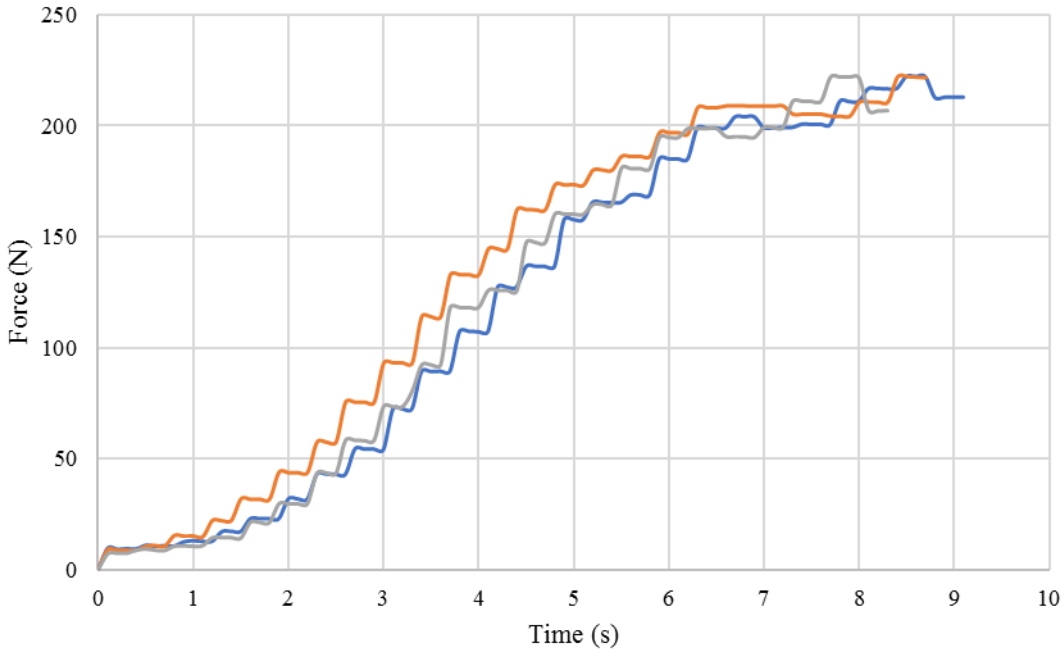

A3. Shear tests for fabric 104

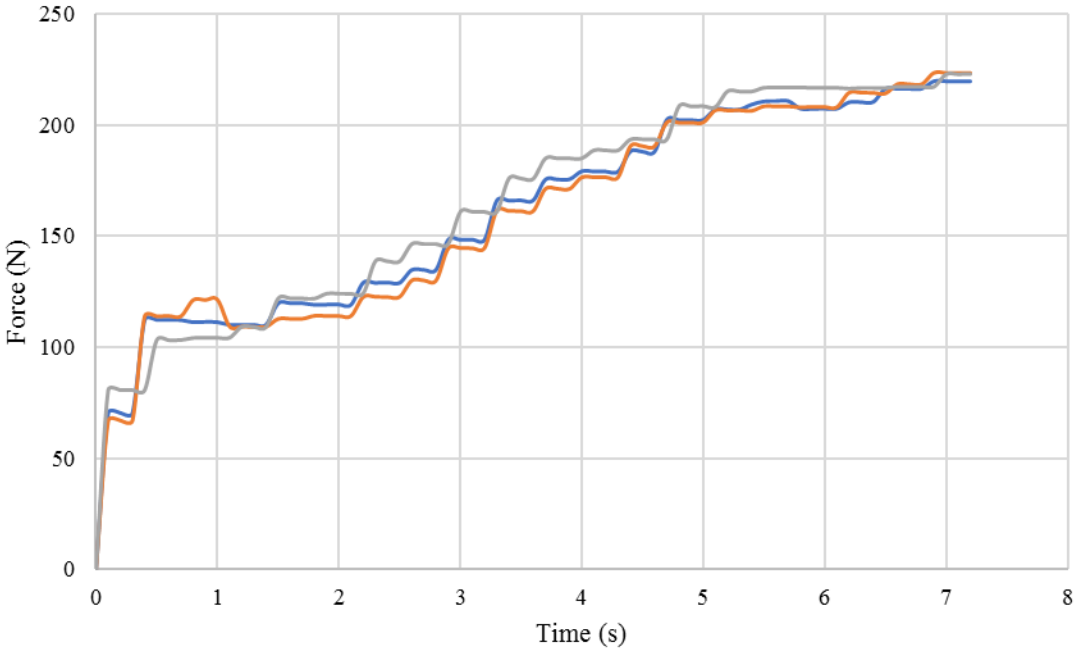

A4. Shear tests for fabric 105

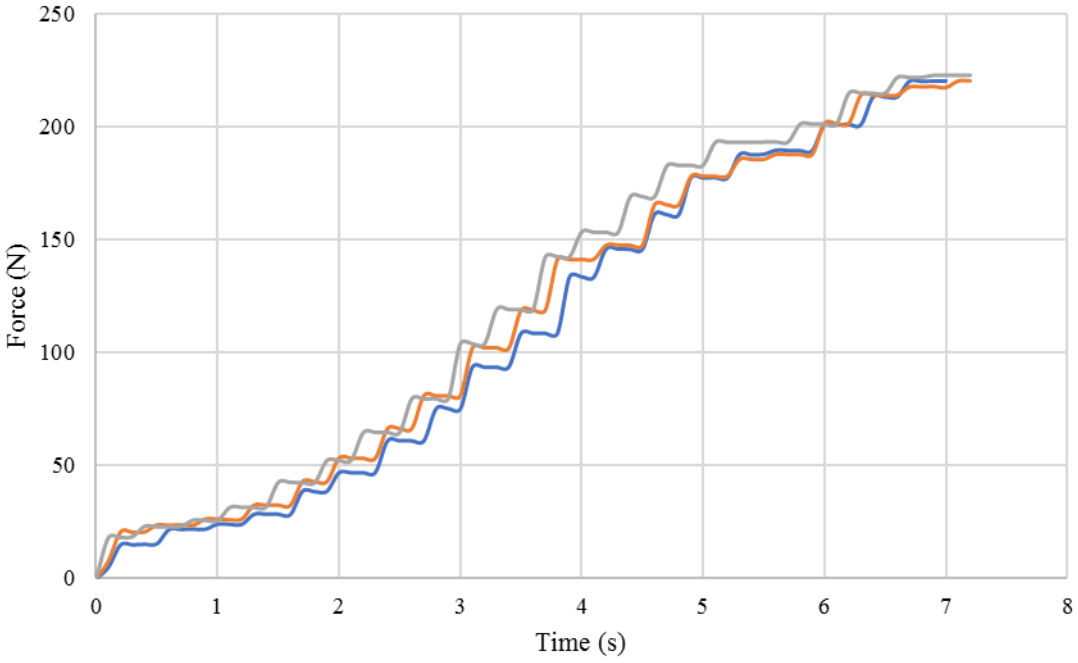

A5. Shear tests for fabric 107

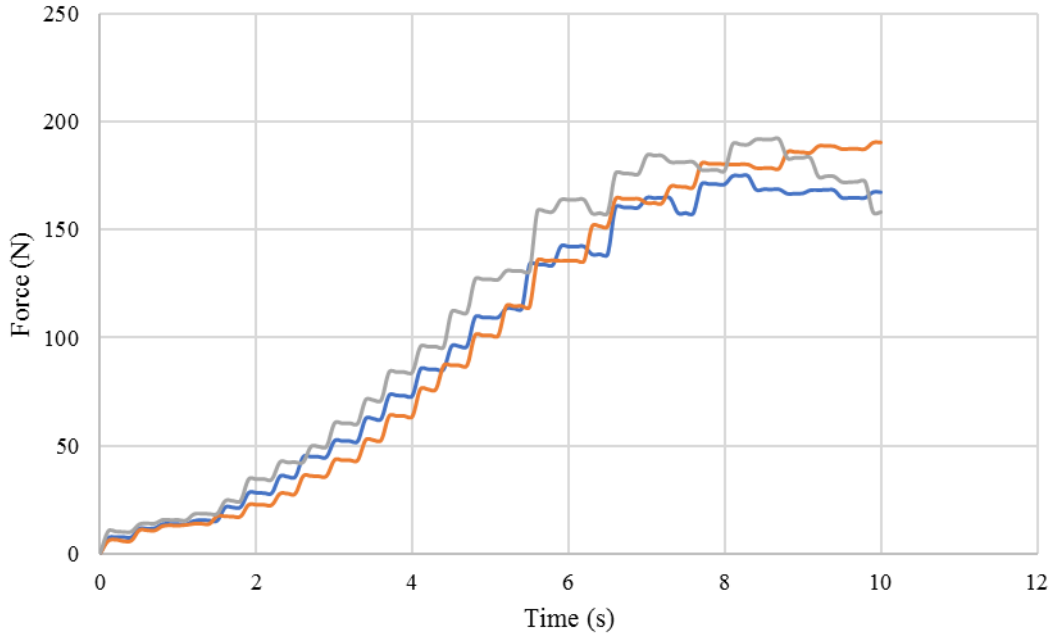

A6. Shear tests for fabric 108

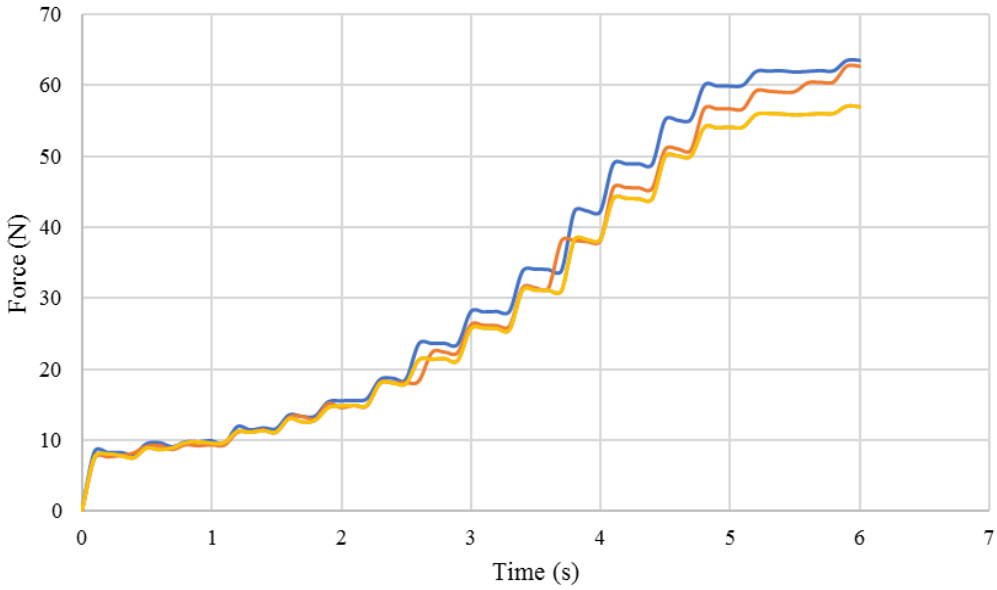

A7. Shear tests for fabric 109

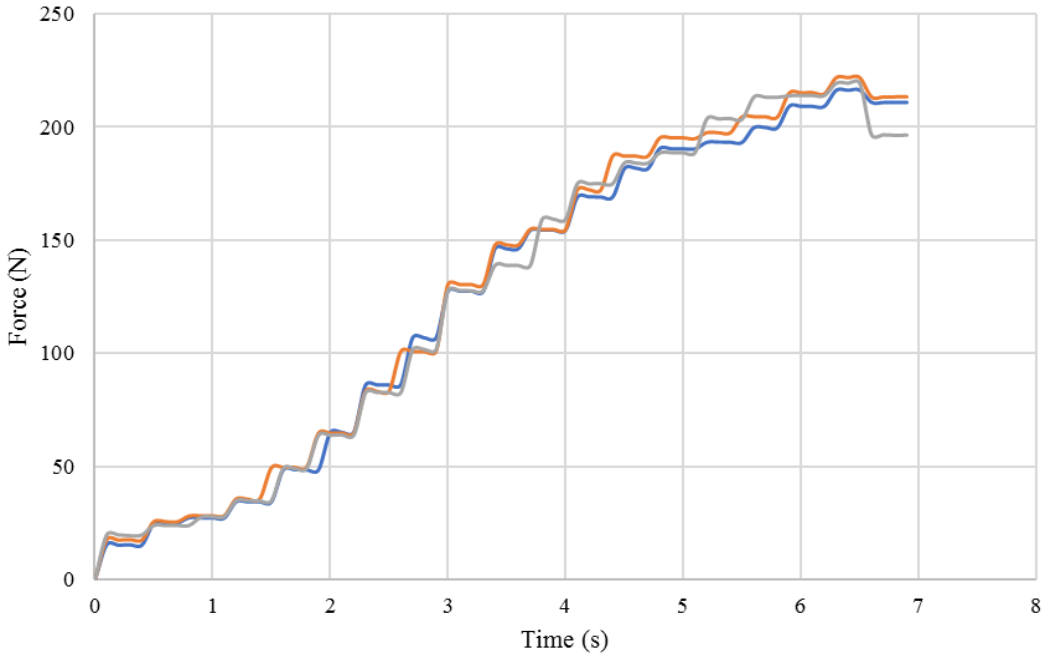

References

[1] J. van Suchtelen, “Product properties: A new application of composite materials,” *Philips Res. Rep.*, vol. 27, pp. 28–37, 1972.

[2] S. Stankovich *et al.*, “Graphene-based composite materials,” *Nature*, vol. 442, no. 7100, pp. 282–286, 2006.

[3] J. M. Bayldon and I. M. Daniel, “Flow modeling of the VARTM process including progressive saturation effects,” *Compos. Part A Appl. Sci. Manuf.*, vol. 40, no. 8, pp. 1044–1052, 2009.

[4] E. Schmachtenberg, J. Schulte Zur Heide, and J. Töpker, “Application of ultrasonics for the process control of Resin Transfer Moulding (RTM),” *Polym. Test.*, vol. 24, no. 3, pp. 330–338, 2005.

[5] B. Roeseler, B. Sarh, and M. Kismarton, “Composite Structures – The First 100 Years,” *Boeing 787 Progr. Compos. Des. Tutor.*, no. July 2007, pp. 1–41, 2009.

[6] C. Soutis, “Fibre reinforced composites in aircraft construction,” *Prog. Aerosp. Sci.*, vol. 41, no. 2, pp. 143–151, 2005.

[7] A. Charmetant, E. Vidal-Sallé, and P. Boisse, “Hyperelastic modelling for mesoscopic analyses of composite reinforcements,” *Compos. Sci. Technol.*, vol. 71, no. 14, pp. 1623–1631, 2011.

[8] F. Burnford, Nicholas, “Development of Drape Simulation Software and the Optimisation of Variable Length Textiles,” 2011.

[9] Z. Cai and T. Gutowski, “The 3-D Deformation-Behavior of a Lubricated Fiber Bundle,” *J. Compos. Mater.*, vol. 26, no. 8, pp. 1207–1237, 1992.

[10] Y. Wang, L. Zhang, and L. Cheng, “Effects of Carbon Yarn Size on the Mechanical Properties of Plain Woven C/SiC Composites,” *Int. J. Appl. Ceram. Technol.*, vol. 6, no. 4, pp. E1–E10, 2009.

[11] G. Zhou, X. Sun, and Y. Wang, “Multi-chain digital element analysis in textile mechanics,” *Compos. Sci. Technol.*, vol. 64, no. 2, pp. 239–244, 2004.

[12] N. G. Ly *et al.*, “Simple Instruments for Quality Control by Finishers and Tailors,” *Text. Res. J.*, vol. 61, no. 7, pp. 402–406, 1991.

[13] H. Barndt, F. Fortess, M. Wiener, and J. C. Furniss, “THE USE OF KES AND FAST INSTRUMENTS,” 1991.

[14] D. S. Lyle, *Focus on fabrics*. National Institute of Drycleaning, 1964.

[15] G. Pamuk and F. Ceken, “Manufacturing of weft-knitted fabric reinforced composite materials: A review,” *Mater. Manuf. Process.*, vol. 23, no. 7, pp. 635–640, 2008.

[16] L. Zhao, I. Porat, and K. Greenwood, “The computerised weaving of preforms for composites part I: The flattening of 3-dimensional preforms,” *J. Text. Inst.*, vol. 87, no. 1, pp. 183–194, 1996.

[17] R. McIlhagger, J. P. Quinn, A. T. McIlhagger, S. Wilson, D. Simpson, and W. Wenger, “The influence of binder tow density on the mechanical properties of spatially reinforced composites. Part 2 - Mechanical properties,” *Compos. Part A Appl. Sci. Manuf.*, vol. 39, no. 2, pp. 334–341, 2008.

[18] F. Boussu, I. Cristian, and S. Nauman, “General definition of 3D warp interlock fabric architecture,” *Compos. Part B Eng.*, vol. 81, pp. 171–188, 2015.

[19] J. Quinn, R. McIlhagger, and A. T. McIlhagger, “A modified system for design and analysis of 3D woven preforms,” *Compos. Part A Appl. Sci. Manuf.*, vol. 34, no. 6 SPEC., pp. 503–509, 2003.

[20] N. Gokarneshan and R. Alagirusamy, “Weaving of 3D fabrics: A critical appreciation of the developments,” *Text. Prog.*, vol. 41, no. 1, pp. 1–58, 2009.

[21] J. Launay, G. Hivet, A. V. Duong, and P. Boisse, “Experimental analysis of the influence of tensions on in plane shear behaviour of woven composite reinforcements,” *Compos. Sci. Technol.*, vol. 68, no. 2, pp. 506–515, 2008.

[22] P. Potluri and T. V. Sagar, “Compaction modelling of textile preforms for composite structures,” *Compos. Struct.*, vol. 86, no. 1–3, pp. 177–185, 2008.

[23] P. Boisse, B. Zouari, and J. L. Daniel, “Importance of in-plane shear rigidity in finite element analyses of woven fabric composite preforming,” *Compos. Part A Appl. Sci. Manuf.*, vol. 37, no. 12, pp. 2201–2212, 2006.

[24] P. Boisse, N. Hamila, E. Vidal-Sallé, and F. Dumont, “Simulation of wrinkling during textile composite reinforcement forming. Influence of tensile, in-plane shear and bending stiffnesses,” *Compos. Sci. Technol.*, vol. 71, no. 5, pp. 683–692, 2011.

[25] X. Q. Peng, J. Cao, J. Chen, P. Xue, D. S. Lussier, and L. Liu, “Experimental and numerical analysis on normalization of picture frame tests for composite materials,” *Compos. Sci. Technol.*, vol. 64, no. 1, pp. 11–21, 2004.

[26] A. S. Milani, J. A. Nemes, R. C. Abeyaratne, and G. A. Holzapfel, “A method for the approximation of non-uniform fiber misalignment in textile composites using picture frame test,” *Compos. Part A Appl. Sci. Manuf.*, vol. 38, no. 6, pp. 1493–1501, 2007.

[27] P. Harrison, M. J. Clifford, and A. C. Long, “Shear characterisation of viscous woven textile composites: A comparison between picture frame and bias extension experiments,” *Compos. Sci. Technol.*, vol. 64, no. 10–11, pp. 1453–1465, 2004.

[28] Y. Dong, J. Kong, C. Mu, C. Zhao, N. L. Thomas, and X. Lu, “Materials design towards sport textiles with low-friction and moisture-wicking dual functions,” *Mater. Des.*, vol. 88, pp. 82–87, 2015.

[29] E. Bertaux, M. Lewandowski, and S. Derler, “Relationship between Friction and Tactile Properties for Woven and Knitted Fabrics,” *Text. Res. J.*, vol. 77, no. 6, pp. 387–396, 2007.

[30] F. Van Der Weeën, “Algorithms for draping fabrics on doubly-curved surfaces,” *Int. J. Numer. Methods Eng.*, vol. 31, no. 7, pp. 1415–1426, 1991.

[31] W. R. Yu, M. Zampaloni, F. Pourboghrat, K. Chung, and T. J. Kang, “Analysis of flexible bending behavior of woven preform using non-orthogonal constitutive equation,” *Compos. Part A Appl. Sci. Manuf.*, vol. 36, no. 6, pp. 839–850, 2005.

[32] E. de Bilbao, D. Soulat, G. Hivet, and A. Gasser, “Study of bending behaviour of composite reinforcements,” *Int. J. Mater. Form.*, vol. 2, no. SUPPL. 1, pp. 205–208, 2009.

[33] Z. Dong and C. T. Sun, “Testing and modeling of yarn pull-out in plain woven

Kevlar fabrics," *Compos. Part A Appl. Sci. Manuf.*, vol. 40, no. 12, pp. 1863–1869, 2009.

[34] X. S. Zeng, V. B. C. Tan, and V. P. W. Shim, "Modelling inter-yarn friction in woven fabric armour," *Int. J. Numer. Methods Eng.*, vol. 66, no. 8, pp. 1309–1330, 2006.

[35] M. Tisza, Z. Lukacs, and G. Gal, "Integrated process simulation and die-design in sheet metal forming," *Int. J. Mater. Form.*, vol. 1, pp. 185–188, 2008.

[36] F. R. Sébastien Gagné, "Formage Sous Vide de Renforts Textiles de Carbone et de Verre pour Fabrication de Pièces Composites pour l ' Aérospatiale," University of Ottawa, 2017.

[37] K. Potter, "Bias extension measurements on cross-plied unidirectional prepreg," *Compos. - Part A Appl. Sci. Manuf.*, vol. 33, no. 1, pp. 63–73, 2002.

[38] A. C. Long, B. J. Souter, F. Robitaille, and C. D. Rudd, "Effects of fibre architecture on deformation during preform manufacture," *Adv. Compos. Lett.*, vol. 8, no. 6, pp. 333–344, 1999.

[39] B. Zhu, T. X. Yu, and X. M. Tao, "Large deformation and slippage mechanism of plain woven composite in bias extension," *Compos. Part A Appl. Sci. Manuf.*, vol. 38, no. 8, pp. 1821–1828, 2007.

[40] Y. J. Jeong and D. G. Phillips, "A study of fabric-drape behaviour with image analysis. part II: The effects of fabric structure and mechanical properties on fabric drape," *J. Text. Inst.*, vol. 89, no. 1, pp. 70–79, 1998.

[41] G. Creech and A. K. Pickett, "Meso-modelling of Non-crimp Fabric composites

for coupled drape and failure analysis," *J. Mater. Sci.*, vol. 41, no. 20, pp. 6725–6736, 2006.

[42] D. Hermann, S. S. Ramkumar, P. Seshaiyer, and S. Parameswaran, "Frictional Study of Woven Fabrics: The Relationship between the Friction and Velocity of Testing," *J. Appl. Polym. Sci.*, vol. 92, no. 4, pp. 2420–2424, 2004.

[43] Z. Dai, F. Shi, B. Zhang, M. Li, and Z. Zhang, "Effect of sizing on carbon fiber surface properties and fibers/epoxy interfacial adhesion," *Appl. Surf. Sci.*, vol. 257, no. 15, pp. 6980–6985, 2011.

[44] ASTM, "Standard Test Method for Stiffness of Nonwoven Fabrics Using the Cantilever Test 1," *Astm*, vol. 95, no. Reapproved, pp. 1–4, 2015.

[45] H. Degradable and P. Resins, "Standard Test Method for Determining the Flexural Stiffness of Medical Textiles 1," pp. 5–10, 2017.

[46] T. Hamdi, A. Ghith, and F. Fayala, "A Principal Component Analysis (PCA) method for predicting the correlation between some fabric parameters and the drape," *Autex Res. J.*, vol. 14, no. 1, pp. 22–27, 2014.

[47] N. Metaaphanon, Y. Bando, B. Y. Chen, and T. Nishita, "Simulation of tearing cloth with frayed edges," *Comput. Graph. Forum*, vol. 28, no. 7, pp. 1837–1844, 2009.

[48] S. Backert, "The Relationship Between the Structural Geometry of a Textile Fabric and Its Physical Properties: Part II: The Mechanics of Fabric Abrasion," *Text. Res. J.*, vol. 21, no. 7, pp. 453–468, 1951.

[49] K. Bilisik and M. Korkmaz, "Multilayered and Multidirectionally-stitched aramid

Woven Fabric Structures: Experimental Characterization of Ballistic Performance by Considering the Yarn Pull-out Test," *Text. Res. J.*, vol. 80, no. 16, pp. 1697–1720, 2010.

[50] A. Angerer, C. Ehinger, A. Hoffmann, W. Reif, G. Reinhart, and G. Strasser, "Automated cutting and handling of carbon fiber fabrics in aerospace industries," *2010 IEEE Int. Conf. Autom. Sci. Eng. CASE 2010*, pp. 861–866, 2010.